Dissertation

Dissection of heterogeneous hematopoietic stem cell biology in the homeostatic and disease-associated states

Esther Rodríguez Correa

2024

Inaugural dissertation

for

obtaining the doctoral degree

of the

Combined Faculty of Mathematics, Engineering and Natural Sciences

of the

Ruprecht - Karls - University

Heidelberg

Presented by

M. Sc. Esther Rodríguez Correa

Born in Madrid, Spain

Oral examination: June 12th 2024

Dissection of heterogeneous hematopoietic stem cell biology in the homeostatic and disease-associated states

Referees:

Prof. Dr. Thomas Höfer

Dr. Michael Milsom

This work is dedicated to my parents, Julio and Inma.

Summary

The hematopoietic stem cell (HSC) compartment is considered heterogeneous at both functional and molecular levels in its ability to continuously generate all mature blood cells throughout life. With age, clonal hematopoiesis can develop, where an HSC clone disproportionally contributes to the blood cell lineages. This phenomenon has been associated with an increased risk of various diseases.

In the first part of this dissertation, I utilized single cell transplantations and mathematical modeling to interrogate the functional potency of individual HSCs and their paired progeny, and assess cell-extrinsic mechanisms modulating the functionality of HSCs.

A large-scale comprehensive analysis of single HSC transplants revealed reconstitution kinetics as a novel parameter capable of predicting HSC transplantation outcomes. My data demonstrated a significant correlation between slower reconstitution kinetics and stemness, alongside a "myeloid-biased" behavior. Conversely, fast-reconstituting clones exhibited exhaustion patterns and classical "lymphoid-biased" outputs. Secondary transplantations of single daughter HSCs revealed a profound decline in functional potential compared to their parent HSC. Moreover, daughter HSC clones acquired faster reconstitution kinetics, correlating with loss of sustained myelopoiesis, and overall HSC potency.

Mathematical modeling of single cell transplantation outcomes led to the identification of cell-extrinsic feedback mechanisms regulating the activity of individual HSCs. These data highlighted that the functional outcome of a single HSC is, in part, influenced by the activity of the surrounding HSCs, unlike assumptions of intrinsic programs solely governing HSC heterogeneity. This finding was experimentally validated by altering the single cell transplantation scheme, so that the single HSC was surrounded by lymphoid-deficient *Rag2*$^{-/-}$ cells. Slow and rapid engraftment kinetics could still be detected, indicating that repopulation dynamics are mostly an intrinsic feature of the HSC clone. However, I no longer observed canonical "myeloid-biased" outcomes, denoting that, on the contrary, lineage output of single HSCs is highly dependent on that of neighboring clones.

In the second part of my dissertation, I investigated the role of *Tet2* clonal hematopoiesis of indeterminate potential (CHIP) on the evolution of hepatocellular carcinoma (HCC) with a non-alcoholic fatty liver disease (NAFLD) etiology, with the underlying hypothesis that *Tet2* CHIP is as a risk factor for this disease.

Dietary-induced HCC represents the fastest rising cancer in the western world, predominantly affecting the elderly population. This disease frequently evolves from an advanced stage of NAFLD, which is primarily characterized by chronic liver inflammation driven by infiltrating-hematopoietic cells. In this project, I employed a mouse model of *Tet2*-driven CHIP, combined with the administration of a high caloric "Western diet", able to induce liver damage and faithfully recapitulate the sequential evolution of NAFLD and HCC observed in humans.

Long-term assessment of disease progression demonstrated a synergistic effect when combining a Western diet and *Tet2* CHIP. This was evidenced by increased serum levels of the biomarkers alanine and aspartate aminotransferases (ALT, AST), higher histopathological NAFLD assessment score (NAS), and a higher incidence of transition to HCC from pre-malignant stages. Molecular characterization of Western diet liver homogenates further confirmed this synergy, revealing higher degree of fibrosis, inflammation and dysregulated metabolism in *Tet2* CHIP livers compared to wild type (WT) counterparts. To this end, a substantial part of my thesis focused on elucidating the mechanisms via which *Tet2* CHIP contributes to HCC development. A combination of functional and molecular analysis, including scRNA-seq, bulk RNA-seq and metabolomics, have revealed synergistic programs in *Tet2* CHIP Western diet mice.

Taken together, this dissertation advances the field of hematology from two angles; homeostatic and disease. It provides a comprehensive understanding on HSC heterogeneity using large-scale and fine experimental approaches and mathematical modeling. Additionally, it identifies *Tet2* CHIP as a potential risk factor for diet-induced liver cancer, offering mechanistic insights which could be exploited for therapeutic interventions.

Zusammenfassung

Das Kompartiment der hämatopoetischen Stammzellen (HSZ) gilt sowohl auf funktioneller als auch auf molekularer Ebene als heterogen in seiner Fähigkeit, während des gesamten Lebens kontinuierlich alle reifen Blutzellen zu erzeugen. Mit zunehmendem Alter kann sich eine klonale Hämatopoese entwickeln, bei der ein HSZ-Klon überproportional zu den Blutzelllinien beiträgt. Dieses Phänomen wurde mit einem erhöhten Risiko für verschiedene Krankheiten in Verbindung gebracht.

Im ersten Teil dieser Dissertation habe ich Einzelzelltransplantationen und mathematische Modellierung eingesetzt, um die funktionelle Potenz einzelner HSZ und ihrer gepaarten Nachkommen zu untersuchen und zellexterne Mechanismen zu bewerten, die die Funktionalität von HSZ modulieren.

Eine groß angelegte umfassende Analyse einzelner HSZ-Transplantationen ergab die Rekonstitutionskinetik als neuen Parameter, der die Ergebnisse von HSZ-Transplantationen vorhersagen kann. Meine Daten zeigten eine signifikante Korrelation zwischen einer langsameren Rekonstitutionskinetik und Stammzellen, sowie einem "myeloiden" Verhalten. Umgekehrt zeigten schnell rekonstituierende Klone Erschöpfungsmuster und klassische "lymphoid-lastige“ Ergebnisse. Bei der sekundären Transplantation einzelner Tochter-HSZ zeigte sich ein starker Rückgang des funktionellen Potenzials im Vergleich zu den Eltern-HSZ. Darüber hinaus wiesen die Tochter-HSZ-Klone eine schnellere Rekonstitutionskinetik auf, die mit dem Verlust einer anhaltenden Myelopoese und der allgemeinen HSZ-Potenz korrelierte.

Die mathematische Modellierung der Ergebnisse der Einzelzelltransplantation führte zur Identifizierung zellexterner Rückkopplungsmechanismen, die die Aktivität der einzelnen HSZ regulieren. Diese Daten machten deutlich, dass das funktionelle Ergebnis einer einzelnen HSZ zum Teil von der Aktivität der sie umgebenden HSZ beeinflusst wird, im Gegensatz zu der Annahme, dass intrinsische Programme allein ausschlaggebend sind. Dieser Befund wurde experimentell bestätigt, indem das Schema der Einzelzelltransplantation dahingehend geändert wurde, dass die einzelnen HSZ von lymphoid-defizienten *Rag2*$^{-/-}$ Zellen umgeben

waren. Die langsame und schnelle Einwanderungskinetik konnte immer noch festgestellt werden, was darauf hindeutet, dass die Repopulationsdynamik hauptsächlich ein intrinsisches Merkmal des HSZ-Klons ist. Allerdings beobachtete ich keine kanonischen "myeloiden" Ergebnisse mehr, was darauf hindeutet, dass die Abstammung einzelner HSZ stark von den benachbarten Klonen abhängt.

Im zweiten Teil meiner Dissertation untersuchte ich die Rolle der klonalen *Tet2*-Hämatopoese mit unbestimmtem Potenzial (CHIP) bei der Entwicklung des hepatozellulären Karzinoms (HCC) mit einer nichtalkoholischen Fettlebererkrankung (NAFLD), mit der zugrundeliegenden Hypothese, dass *Tet2* CHIP als Risikofaktor für diese Krankheit fungieren könnte.

Das ernährungsbedingte HCC ist die am schnellsten wachsende Krebserkrankung in der westlichen Welt und betrifft vor allem die ältere Bevölkerung. Diese Krankheit entwickelt sich häufig aus einem fortgeschrittenen Stadium der NAFLD, die in erster Linie durch eine chronische Leberentzündung gekennzeichnet ist, die durch infiltrierende hämatopoetische Zellen angetrieben wird. In diesem Projekt habe ich ein *Tet2* CHIP Mausmodell verwendet, das in Verbindung mit einer hochkalorischen "westlichen Diät" in der Lage ist, Leberschäden hervorzurufen und die beim Menschen beobachtete sequentielle Entwicklung von NAFLD und HCC getreu zu rekapitulieren.

Die Langzeitbeurteilung des Krankheitsverlaufs zeigte einen synergistischen Effekt bei der Kombination einer westlichen Diät und *Tet2* CHIP. Dies wurde durch erhöhte Serumspiegel der Biomarker Alanin- und Aspartat-Aminotransferasen (ALT, AST), einen höheren histopathologischen NAFLD-Bewertungsscore (NAS) und eine höhere Inzidenz des Übergangs von prämalignen Stadien zu HCC belegt. Die molekulare Charakterisierung von Leberhomogenaten aus westlicher Ernährung bestätigte diese Synergie weiter und zeigte ein höheres Maß an Fibrose, Entzündung und dysreguliertem Stoffwechsel in *Tet2* CHIP-Lebern im Vergleich zu Wild Typ (WT)-Lebern. Aus diesem Grund fokussierte sich ein wesentlicher Teil meiner Arbeit auf die Aufklärung der Mechanismen, über die *Tet2* CHIP zur Entwicklung von HCC beiträgt. Eine Kombination aus funktioneller und molekularer Analyse,

einschließlich scRNA-seq, Bulk-RNA-seq und Metabolomik, hat synergistische Programme in *Tet2* CHIP-Mäusen mit westlicher Ernährung aufgedeckt.

Insgesamt bringt diese Dissertation das Feld der Hämatologie aus zwei Blickwinkeln voran: Einerseits liefert sie ein umfassendes Verständnis der Heterogenität von HSZ mit Hilfe groß angelegter und feiner experimenteller Ansätze und mathematischer Modellierung. Darüber hinaus wird *Tet2* CHIP als potenzieller Risikofaktor für ernährungsbedingten Leberkrebs identifiziert und bietet mechanistische Erkenntnisse, die für therapeutische Interventionen genutzt werden könnten.

Contents

Table of Contents

Summary ix

Zusammenfassung xi

Contents xv

1. Introduction 1

1.1 Hematopoiesis 1

1.1.1 The hematopoietic hierarchy 1

1.2 Hematopoietic stem cells 3

1.2.1 Transplantation assays to study HSC functional potential 3

1.2.2 In vivo labelling to study HSC function under steady state conditions 4

1.2.3 Hematopoietic stem cell functional heterogeneity 5

1.2.3.1 Heterogeneous HSC self-renewal capacity 6

1.2.3.2 HSC lineage differentiation biases 6

1.2.4 Hematopoietic stem cell molecular heterogeneity 6

1.3 Clonal hematopoiesis 7

1.3.1. Tet2 clonal hematopoiesis 8

1.3.2 Clinical implications of CHIP 9

1.3.2.1 Clonal hematopoiesis-associated hematologic diseases 9

1.3.2.2 Clonal hematopoiesis-associated cardiovascular diseases 10

1.3.2.3 Clonal hematopoiesis-associated solid cancers 11

1.4 Hepatocellular carcinoma 12

1.5 Non-alcoholic fatty liver disease (NAFLD) 13

1.5.1 Mouse models of NAFLD 14

1.5.2 Roles of hematopoietic cells in NAFLD 17

2. Aims of the thesis 19

2.1 Aims project I 19

2.2 Aims project II 20

3. Results project I 22

3.1. Serial single cell transplantations to assess HSC functional heterogeneity 22

3.2. Reconstitution outcomes from primary single cell transplantations confirmed reported HSC lineage biases 23

3.3. Kinetics of reconstitution as a novel parameter to predict HSC fate 24

3.4. Daughter HSCs exhibited a significant decline in reconstitution potential compared to the parent HSC 27

3.5. Mathematical modelling of single cell transplantation outcomes 32

3.6. Lineage biases can be compromised by modulating the neighboring HSC activity 35

4. Discussion project I 40

4.1. Deconvoluting the heterogeneity within the HSC compartment 40

4.2. Reconstitution kinetics explains reported lineage biases and predicts stem cell functional potency 41

4.3. HSC heterogeneity is best explained by a continuum rather than discrete categories 43

4.4 Self-renewal compromises the functional potency of HSCs 44

4.5. Investigating the factors determining HSC functional outcomes 47

5. Results project II 50

5.1. Establishing a model to study the impact of *Tet2* clonal hematopoiesis on the evolution of non-alcoholic fatty liver disease and liver cancer 50

5.1.1 Validation of *Tet2* knock-out induction in the hematopoietic stem cell compartment 51

5.2. Exploring phenotypic synergy between *Tet2* CHIP and the Western diet 52

5.2.1. Fatty liver disease development as a result of Western diet administration 53

5.2.2. *Tet2* CHIP and the Western diet synergize in order to exacerbate the NAFLD phenotype . 54

5.2.3. *Tet2* CHIP accelerates liver cancer development in WD-treated mice 57

5.2.4. Bulk RNA-seq of NAFLD-liver homogenates revealed molecular synergy with *Tet2* CHIP 58

5.3. Understanding the mechanisms via which *Tet2* CHIP exacerbates NAFLD and promotes HCC 64

5.3.1 Systemic analysis revealed distinct hematopoietic alterations due to the WD or *Tet2* CHIP 64

5.3.2 Local analysis of liver-infiltrating hematopoietic cells 66

5.3.2.1 Similar degree of liver immune infiltration in WD mice with or without *Tet2* CHIP 66

5.3.2.2 Molecular characterization of liver-infiltrating hematopoietic cells using bulk and single cell approaches 70

5.3.2.3. Phenotypic analysis at 3-months suggested no clear acceleration of the NAFLD phenotype 75

5.3.2.4. *Tet2* CHIP and WD induced a metabolomic reprogramming in liver-infiltrating hematopoietic cells 77

6. Discussion project II 81

6.1. Clonal hematopoiesis as a risk factor for non-hematologic diseases 81

6.2. Selecting an optimal model to investigate the impact of *Tet2* CHIP on liver disease 82

6.3. Heterogeneity in disease progression in mice treated with a Western diet 85

6.4. Exploring the mechanisms via which *Tet2* CHIP contributes to NAFLD-HCC progression 87

6.5 Identifying biomarkers for NAFLD-HCC 90

7. Materials and Methods 92

7.1 Animal experiments 92

7.2 Treatments 92

7.2.1 Tamoxifen 92

7.2.2 Diet 93

7.3 Bone marrow transplantations 93

7.3.1 Body irradiation and transplantation 93

7.3.2 Single cell transplantations (Project I) 93

7.3.3 Bulk bone marrow transplantations (Project II) 94

7.4 Sample collection 94

7.4.1 Blood 94

7.4.2 Serum 95

7.4.3 Bone marrow 95

7.4.4 Liver 95

7.5 Histology 96

7.6 EchoMRI 96

7.7 Flow Cytometry 96

7.7.1 Isolation of murine LT-HSC cells via FACS 96

7.7.2 Isolation of liver-infiltrating immune cells by FACS 98

7.7.3 Isolation of liver-infiltrating immune cells by FACS for bulk RNA sequencing 98

7.7.4 Isolation of liver-infiltrating immune cells by FACS for scRNA sequencing 98

7.7.5 Isolation of liver-infiltrating immune cells by FACS for low input metabolomics 98

7.7.6 Antibody-based staining of peripheral blood cells 99

7.7.7 Antibody-based staining of bone marrow cells 100

7.7.8 Flow cytometry analysis 100

7.8 In vitro single HSC expansion and colony PCR 100

7.9 RNA-sequencing 102

7.9.1 Bulk RNA-sequencing of liver-infiltrating hematopoietic cells 102

7.9.2 Bulk RNA-sequencing of liver homogenates 102

7.9.3 Single cell RNA-sequencing of liver-infiltrating hematopoietic cells 103

7.10 Data visualization and statistical analysis 103

References 112

List of Figures 122

List of Tables **125**

List of Abbreviations **126**

Conference Talks and Poster Presentations **129**

Conference talks **129**

Poster presentations **129**

Manuscripts **130**

Contributions **131**

Acknowledgments **133**

1

Introduction

1.1 Hematopoiesis

Hematopoiesis, the intricate and highly regulated process by which blood cells are formed, is essential to ensure organismal homeostasis[1]. The blood system has a high regenerative potential. In human adults, over 10^{10} blood cells are produced per day in steady state conditions[2]. This continuous process begins in the bone marrow, and gives rise to three distinct classes of hematopoietic cells: red blood cells (RBCs) or erythrocytes, which are responsible for the transport of oxygen and nutrients throughout the body; white blood cells (WBCs) or leukocytes, which form the immune system and are responsible for fighting infections and external agents; and platelets (PLTs) or thrombocytes, which mediate coagulation responses and blood vessel homeostasis upon injuries. Within the white blood cells, two lineages have been identified: myeloid and lymphoid, responsible for the innate and adaptive immune responses, respectively. The process of blood production is highly organized in several differentiation steps, elucidated by various models.

1.1.1 The hematopoietic hierarchy

The classical model of hematopoiesis has a tree-like hierarchical shape (**Figure 1.1A**), consisting of a series of differentiation branching points that ultimately produce all mature blood cell types[3]. Hematopoietic stem cells (HSCs) sit at the very top of this hierarchy, maintaining the continuous production of the whole system. Within this compartment, two populations with variable functional potential have been identified: long-term (LT)-HSCs and short-term (ST)-HSCs. Downstream the stem cell compartment, multipotent progenitors (MPPs) are located[4]. MPPs can be further subdivided into a range of progenitors with specific

differentiation potential (MPP2, MPP3, MPP4, MPP5). Nevertheless, MPPs retain their multipotent nature, akin to HSCs, collectively constituting the hematopoietic stem and progenitor cell compartment (HSPCs).

Subsequently, MPPs can give rise to committed progenitors, which are restricted to the production of specific hematopoietic cell types, thus are considered oligopotent. Common myeloid progenitors (CMPs)[5] serve as a branching point of lineage commitment, giving rise to megakaryocyte-erythroid progenitors (MEPs) or granulocyte-monocyte progenitors (GMPs)[6]. Similarly, lymphoid-myeloid common progenitors (LMPPs) differentiate into common lymphoid progenitors (CLPs)[7] or GMPs. This step-wise differentiation process ends in the production of all mature blood cells such as erythrocytes, platelets, granulocytes, monocytes, T-lymphocytes and B-lymphocytes.

Alternative models of hematopoiesis have been proposed in recent years. One of them is the early split model (**Figure 1.1B**), in which lineage commitment occurs earlier in the hierarchy, specifically at the MPP level[8]. More recently, there has been proposed a continuum Waddington-like model (**Figure 1.1C**), in which HSCs gradually acquire transcriptomic changes to define lineage commitment, challenging the traditional concept of discrete differentiation states[9].

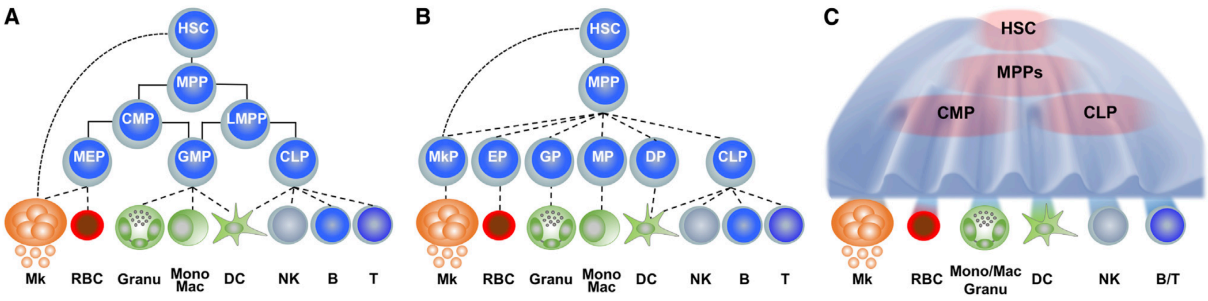


Figure 1.1 Models of hematopoiesis. A) Classic model of hematopoiesis. Tree-like hierarchy assuming discrete states of differentiation. **B)** Early split model of hematopoiesis. Lineage commitment takes place at the MPP level. **C)** Continuum Waddington-like model of hematopoiesis. HSCs gradually acquire transcriptional changes to determined their lineage commitment, instead of passing through a series of discrete and stable differentiation stages. Mk= Megakaryocyte, RBC= Red blood cell, Granu= Granulocyte, Mono= Monocyte, Mac= Macrophage, DC= Dendritic cell, NK= NK cell, B= B cell, T= T cell

Image taken from Haas et al. [10]; Reprinted with permission from Elsevier through copyright.com

1.2 Hematopoietic stem cells

Hematopoietic stem cells (HSCs), which reside at the apex of the hematopoietic hierarchy, are responsible for the long-life maintenance of hematopoiesis. There are two distinct abilities which define this cell type, one is the self-renewal capacity to divide and generate identical HSCs without differentiation[11,12]. Secondly, HSCs possess multipotent capacity to generate each cell type of the blood system. These characteristics diminish as cells progress down the hematopoietic hierarchy and commit to specific lineages through the process of differentiation. The purification of HSCs from the murine bone marrow (BM) was initiated in 1988, facilitated by the development of monoclonal antibodies and technologies of multicolor fluorescence-activated cell sorting (FACS). The isolation of HSCs relies on the expression of cell surface markers. While individual markers may not be exclusive to stem cells, their combination enables the enrichment of a highly pure HSC population. Several cell surface combinations have been proposed over the past years, typically involving the initial negative selection for mature cell lineage markers (CD4, CD8, B220, Gr1, CD11b, Ter119), and positive selection for Sca1 and c-Kit, known to enrich for stem and progenitor-like populations. Additional markers have been included in the purification schemes, such as $CD34^{-}CD135^{-}$[13], the two SLAM markers $CD150^{+}CD48^{-}$ cells[14] or the Hoechst-effluxing side population (SP)[15]. More recently, high endothelial protein C receptor (EPCR) expression has been associated to functionally potent HSCs[16]. In our lab, we use the SLAM markers to enrich for mouse HSC, and further subdivide ST-HSC and LT-HSCs based on the high or low expression of the CD34 marker respectively, occasionally including EPCR when aiming to enrich for potent stem cells.

1.2.1 Transplantation assays to study HSC functional potential

The competitive repopulation assay is the gold standard method to study HSC functional potential[17]. This assay serves as a tool to systematically interrogate the self-renewal and multipotent properties from a source of HSCs of interest competing against a known set of competitor cells, typically sourced from the entire bone marrow of a congenic mouse[18]. Together, cells of interest and competitor cells are transplanted into lethally irradiated recipient mice, which exhibit impaired endogenous hematopoiesis. In this way, only functional HSCs would enable the reconstitution of the whole hematopoietic system and

ensure the long-term survival of the recipient mice. A more stringent approach to assess HSC functionality is serial transplantations. In this method, the source of HSCs undergoes sequential transplantations into irradiated recipient mice, hence allowing the assessment of functional self-renewal divisions needed to sustain healthy hematopoiesis[19]. To assess the functional potency of HSCs at the single cell level, clonal transplantations are needed. In the 1996, it was shown for the first time that a single multipotent HSC was able to regenerate the entire blood system and exhibited inherent self-renewal potential[20] (**Figure 1.2A**). In addition to single cell transplantation studies where one HSC is interrogated at a time in recipient mice, genetic barcoding technologies have emerged as an alternative approach for clonal analysis of multiple HSCs simultaneously in the same recipient mouse[21–23]. Genetic barcoding consists of the labelling of single HSCs with unique and heritable DNA tags, that can be transferred to mature progeny. These recombinant tags are stably integrated through lentiviral or retroviral systems. Post-labelling, tagged HSCs are transplanted into lethally irradiated mice, facilitating the simultaneous analysis of diverse clonally-derived hematopoietic systems based on the distribution of the genetic tags.

1.2.2 In vivo labelling to study HSC function under steady state conditions

Although transplantation approaches are ideal to assess the potential of HSCs, it is broadly recognized that the outcomes following transplantation might not faithfully represent the actual behavior of HSCs during unperturbed hematopoiesis, in the absence of conditioning-induced stress to regenerate the hematopoietic system. Therefore, in vivo tracing methods have been developed, involving the specific labelling of HSCs in situ, commonly through the use of transgenic or knock-in reporter mouse strains[24–27] (**Figure 1.2B**). In these models, the selective expression of particular enzymes, such as Cre or Sleeping Beauty recombinases within the HSC population, induce the labelling of HSCs with fluorescent reporters or genetic barcodes, either at a bulk or single cell level. As HSCs differentiate into mature progeny, the label is passed down, facilitating clonal lineage tracing within the living organism. Recent publications have combined genetic lineage tracing methods with single-cell transcriptome profiling. Notable examples include PolyloxExpress[28], a method that labels individual HSCs with unique DNA barcodes transcribed as mRNA. Another innovative approach is CARLIN

(CRISPR array repair lineage tracing)[29] and its more refined versions, which involve the expression of barcodes through CRISPR/Cas9-mediated mutagenesis. These cutting-edge methodologies not only provide insights into the clonal dynamics of HSCs but also offer a glimpse into the molecular attributes governing their behavior.

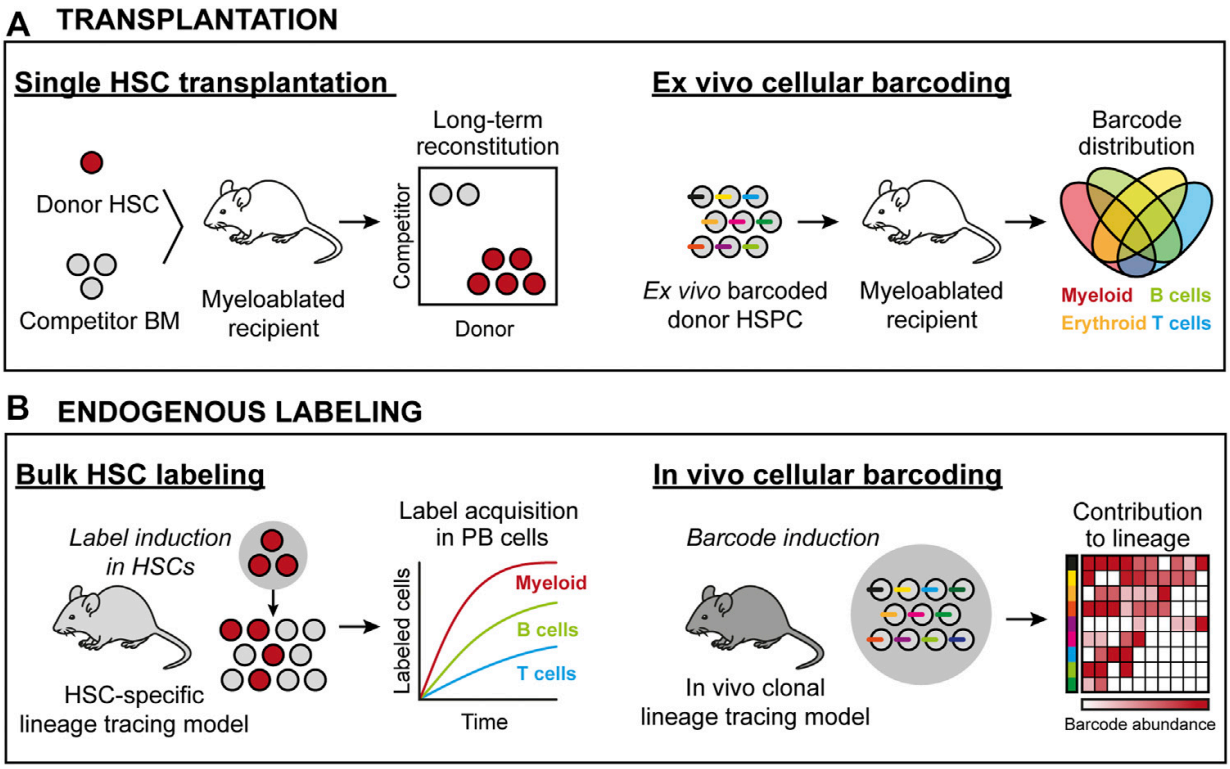


Figure 1.2. Approaches to study HSC functionality. A) Transplantation as a tool to assess the potency of HSCs, either through single cell transplantations, or in barcoding settings where multiple HSCs are interrogated simultaneously. **B)** Assays to interrogate the function of HSCs in native hematopoiesis. In vivo tracking of in situ labeled HSCs using fluorescent reporters or unique barcodes which are transmitted down the hematopoietic progeny.

Image taken from Anna Konturek-Ciesla, A & David Bryder[30]. Reprinted with permission from copyright owners Konturek-Ciesla and Bryder.

1.2.3 Hematopoietic stem cell functional heterogeneity

In the classical model of hematopoiesis, the HSC population has been considered homogenous, sharing self-renewal and multipotent properties. However, recent studies have revealed high functional heterogeneity within the HSC pool, and the presence of HSC subsets exhibiting a spectrum of behaviors in terms of self-renewal, differentiation, and proliferation properties.

1.2.3.1 Heterogeneous HSC self-renewal capacity

Initial transplantation studies of variable immunophenotypically defined populations have demonstrated profound differences in their capacity to sustain hematopoiesis over time. These studies led to the categorization of HSCs into distinct functional subsets[4]: long-term HSCs, which can sustain hematopoiesis for > 3~4 months, short-term HSCs, with exhibit transient reconstitution (mostly < 1 month), and MPPs, which lack self-renewal potential. Moreover, single cell transplantation and barcoding experiments have shown that even within the most potent LT-HSC compartment, the degree to which each HSC sustains the system can vary[31–34].

1.2.3.2 HSC lineage differentiation biases

As seen for the self-renewal potential, the ability to differentiate into different hematopoietic lineages is variable when transplanting populations of various immunophenotypes. Large-scale transplantations of single HSCs revealed myeloid and lymphoid biases in the majority of the interrogated cells, with only rare instances of achieving a "balanced" multilineage output[31–34] (**Figure 1.3**). These findings challenge the classical hematopoiesis model, wherein HSCs are presumed to be multipotent and homogenous. More recent studies not only propose myeloid and lymphoid biases, but unraveled a more complex heterogeneity within the HSC pool in terms of lineage commitment. This includes the identification of platelet-biased HSCs with notable self-renewal capacity and clones predominantly generating platelets and red blood cells[35,36]. Barcoding experiments involving the transplantation of multiple HSCs have substantiated these findings[25]. Notably, HSC lineage biases have also been reported under native conditions, suggesting that this may be an intricate feature of HSCs.

1.2.4 Hematopoietic stem cell molecular heterogeneity

Single cell RNA sequencing technologies have been critical in understanding the heterogeneity and dynamics of hematopoiesis. These studies have questioned the classical model of hematopoiesis, showing that HSCs gradually acquire transcriptional changes shaping their differentiation trajectory to different hematopoietic lineages, suggesting a

continuum of differentiation rather than discrete stages[9,37,38]. The concept of lineage bias has also been reported at the molecular level, with the identification of HSCs expressing megakaryocytic genes, such as the von Willebrand factor (Vwf) marker[39]. This finding aligns with the observation of megakaryocytic-biased HSCs in transplantation and native hematopoiesis studies[25,35,36]. More recent studies have highlighted the importance of epigenetic programming in HSC lineage decisions[40].

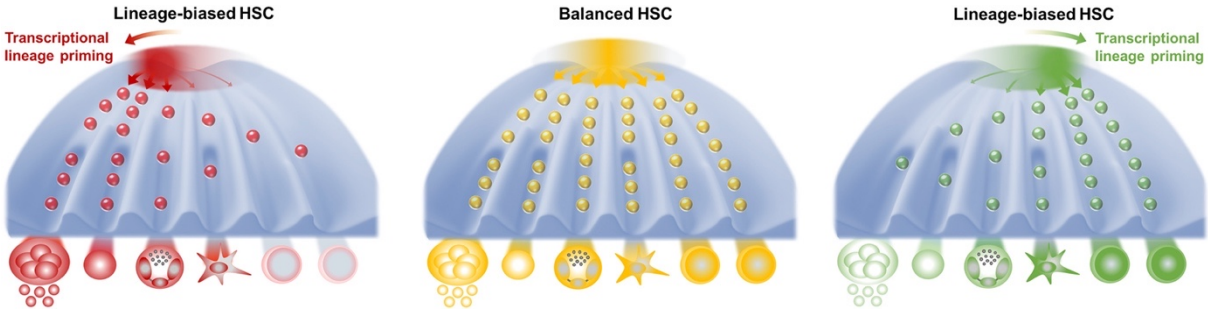


Figure 1.3. HSC lineage biases. A continuous Waddington-like model of hematopoiesis, where HSCs located at the top of the hierarchy can exhibit three distinct features: balanced contribution towards the production of myeloid and lymphoid lineages, or skewed production of one of the arms of the hematopoietic system, determined by a transcriptional lineage priming.

Image taken from Haas et al.[10] Reprinted with permission from Elsevier through s100.copyright.com.

1.3 Clonal hematopoiesis

One of the main drivers of HSC heterogeneity stems from the continuous and gradual accumulation of somatic mutations during the aging process, particularly due to replication errors[41]. The majority are neutral mutations that have no harmful or beneficial effect to the cells. But occasionally, these mutations can confer advantageous effects, leading to their proliferation and increased overall population fitness[42]. Specifically, somatic mutations in HSCs inducing enhanced proliferation and survival result in the clonal expansion of mutant hematopoietic cells. This phenomenon is termed clonal hematopoiesis (CH). When these mutations occur in genes linked to hematologic malignancies among seemingly healthy individuals without apparent hematologic symptoms, the condition is termed clonal hematopoiesis of indeterminate potential (CHIP) or age-related clonal hematopoiesis (ARCH)[43–45] (**Figure 1.4A**). Conventionally, CHIP was defined with the criterion that mutations should be present in at least 2% of peripheral blood cells (variant allele frequency VAF>2%)[46]. Whole-exome sequencing data from peripheral-blood cells of individuals selected without

consideration of hematological parameters revealed a significant increase in the frequency of CHIP with age[44] (**Figure 1.4B**). Another notable observation from these studies is that CHIP frequently arises from mutations in a specific group of genes (**Figure 1.4C**). Somatic mutations in genes responsible for epigenetic remodeling, such as DNA methylation/demethylation (*DNMT3A, TET2*) or histone modifications (*ASXL1*, *EZH2*) are common drivers of CHIP, others include *JAK2*, *TP53*, and *SF3B1*.

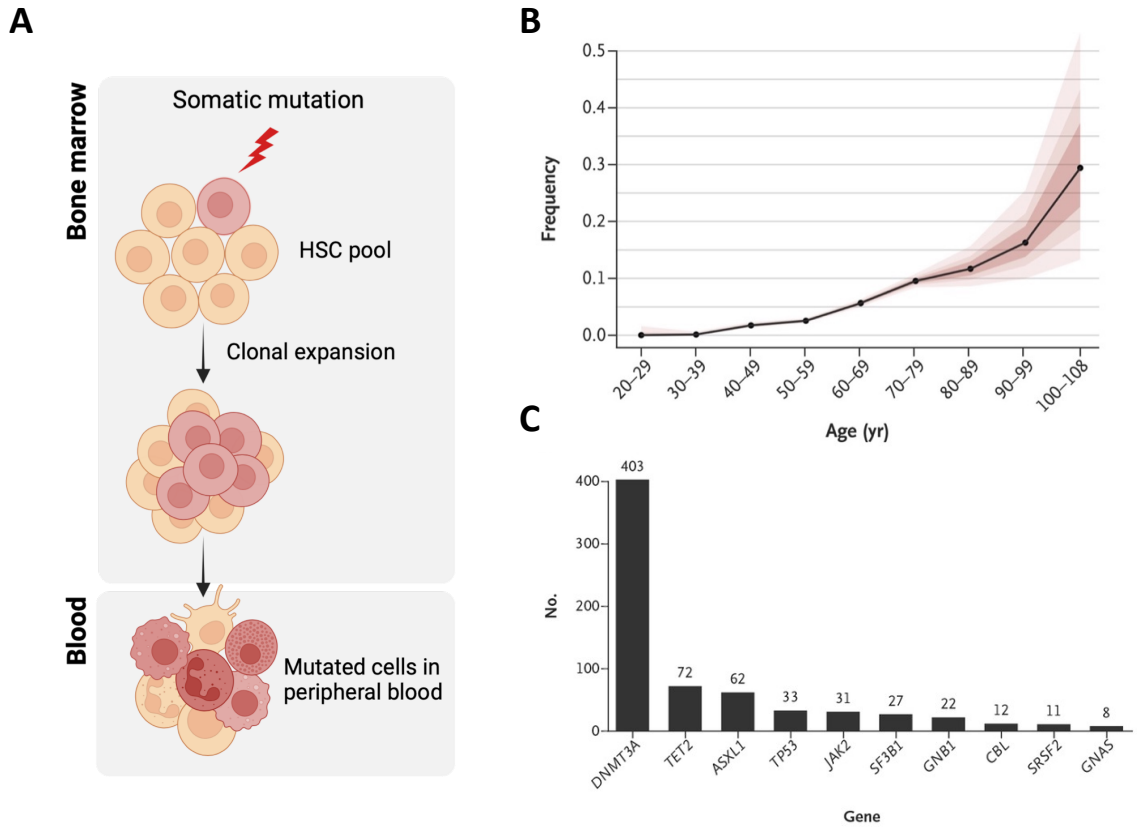


Figure 1.4. Clonal hematopoiesis of indeterminate potential (CHIP). A) Scheme describing the process of clonal hematopoiesis. **B)** Frequency of observed CHIP in individuals across different ages. **C)** Most commonly mutated genes in CHIP.

B and C images taken from Jaiswal et al.[44] Reprinted with permission from Massachusetts Medical Society through s100.copyright.com. Image A created using Biorender.

1.3.1. Tet2 clonal hematopoiesis

Ten-eleven translocation-2 (TET2) is one of the enzymes of the TET family, involved in DNA demethylation through the enzymatic conversion of 5mC to 5-hydroxymethylcytosine (5hmC)[47]. *TET2* is reported as the second most frequently mutated gene in CHIP, as well as a

prevalent mutant gene in patients with hematologic malignancies, reported in 10-20% of patients with myelodysplastic syndromes/myeloproliferative neoplasms (MDS/MPN), 40-50% with chronic myelomonocytic leukemia and 10-20% with acute myeloid leukemia (AML)[48,49]. A number of in vitro and in vivo mouse studies have elucidated the biological implications of *Tet2* mutations in HSCs, showing that *Tet2* mutant HSCs acquire enhanced self-renewal capacity and a differentiation bias towards the myeloid lineage[50,51]. The impact of *Tet2* deficiency in peripheral blood cells is not fully explored, as initial studies were mainly focus on understanding the consequences on stem cell biology. Nevertheless, recent studies have shown that TET2 function is also relevant in mature cells, and its deletion is associated with the acquisition of a pro-inflammatory phenotype due to enhanced production of cytokines such as IL1β and IL6[52,53].

1.3.2 Clinical implications of CHIP

Several population studies based on exon-sequencing have reported that individuals with CHIP have an increased risk for all-cause mortality[43,44]. In particular, CHIP has been linked to the development of hematological, and more recent, non-hematological diseases.

1.3.2.1 Clonal hematopoiesis-associated hematologic diseases

The occurrence of CHIP has been linked to an approximately 10-fold rise in the relative risk of developing hematological malignancies, especially myeloid malignancies such as AML[43,44]. Analyses of population-based cohorts revealed a correlation between the size of the mutant clone or VAF and the risk of disease development. Remarkably, mutations in genes such as *TP53*, *JAK2*, *SF3B1*, *SRSF2*, and *U2AF1* were significantly enriched in individuals progressing to hematological malignancies[54]. The connection between CHIP and blood cancers extends to therapy-related secondary AML (sAML) and MDS, where cytotoxic treatments for solid cancers exert a selection pressure favoring the clonal expansion of mutant HSCs with enhanced fitness, thereby increasing the risk of transformation (**Figure 1.5**). In this context, mutations in DNA damage response genes, notably *TP53* and *PPM1D*, were found to be more prevalent[55,56].

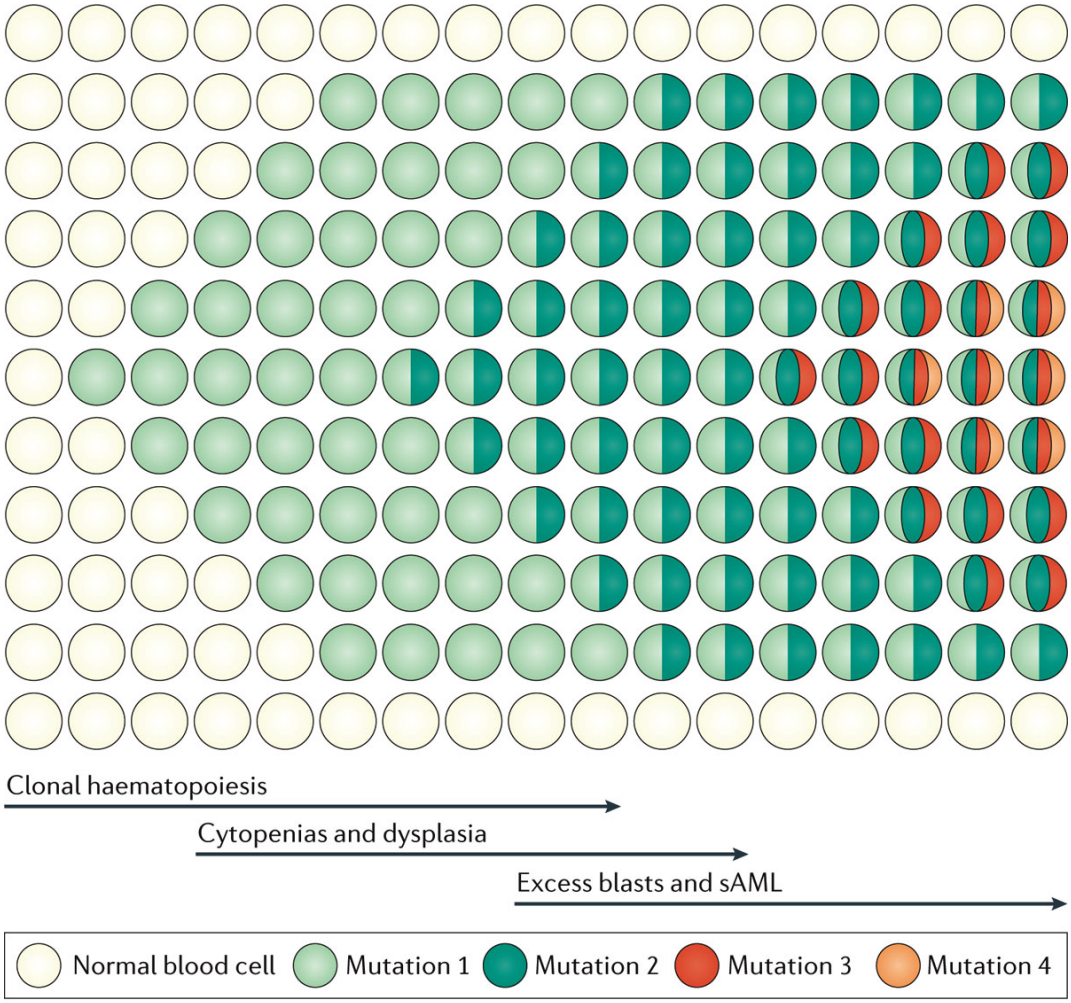


Figure 1.5. Association between CHIP and the development of hematological malignancies.
Image taken from Sperling et al. [57], Reprinted with permission from Springer Nature through s100.copyright.com.

1.3.2.2 Clonal hematopoiesis-associated cardiovascular diseases

Even though HSCs are the cells in which the initial mutation "hit" occurs, eventually mutant cells are also found in the peripheral blood. Importantly, these blood cells circulating in the periphery frequently infiltrate organs, which leaves the possibility that mutant mature blood cells could also enhance the development of non-hematologic diseases. First studies examining the effect of CHIP on non-hematological diseases confirmed this association, especially with regard to cardiovascular diseases (**Figure 1.6**). Risk of ischemic stroke and coronary heart disease has been shown to be more than doubled in individuals with CHIP[44,54], making CHIP a recognized risk factor for cardiovascular conditions, surpassing the impact of well-known factors such as smoking. Furthermore, carriers of CHIP exhibit a 4-fold higher

risk of early-onset myocardial infarction. As for blood cancers, the risk was associated with the size of the mutant clone[53]. The precise mechanism via which mutant hematopoietic cells exacerbate cardiovascular diseases remains unclear. Recent investigations employing mouse models of *Tet2* clonal hematopoiesis have established a causal relationship between CHIP and atherosclerosis, manifested by an enlargement of atherosclerotic lesions[52,53]. Mechanistically, this increased disease severity was attributed to an enhanced inflammatory phenotype in heart-infiltrating mutant macrophages, a phenomenon also observed in the context of congestive heart failure[58]. Moreover, *Jak2* mutations induce the activation of neutrophils, prompting the formation of neutrophil extracellular nets (NETs), potentially triggering thrombosis and contributing to adverse cardiovascular outcomes. Collectively, these examples generate strong evidence supporting a correlation between CHIP and cardiovascular diseases[59].

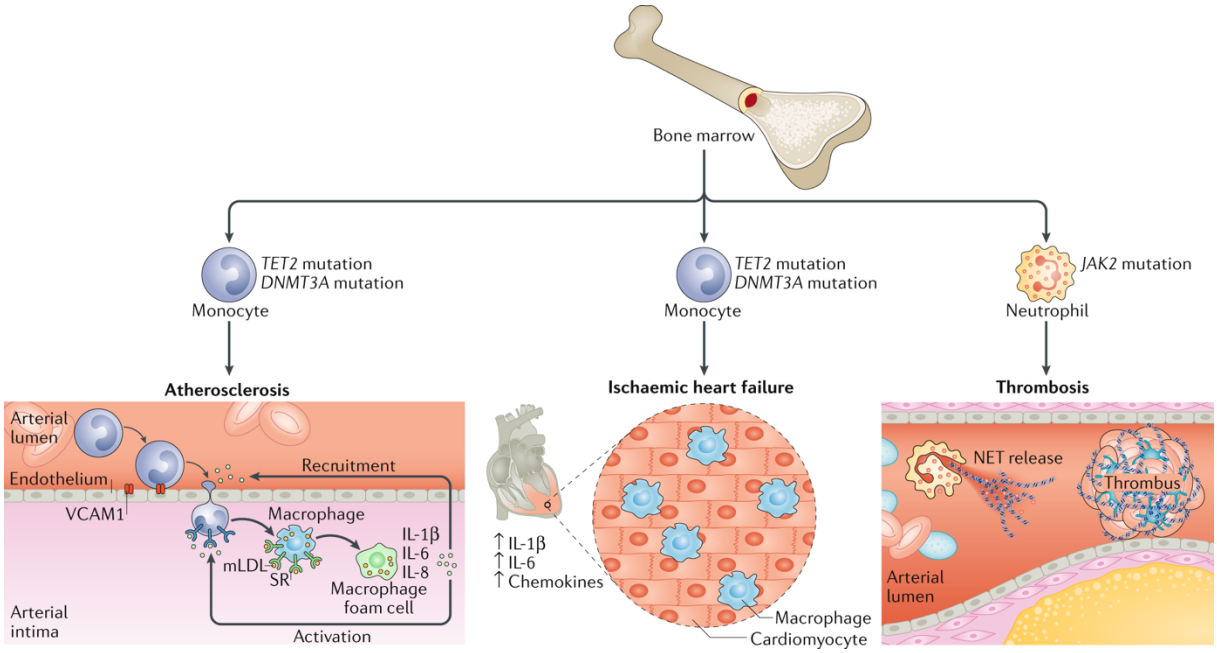


Figure 1.6. Associations between CHIP and cardiovascular diseases.
Image taken from Jaiswal, S. & Libby, P [60]. Reprinted with permission from Springer Nature through s100.copyright.com.

1.3.2.3 Clonal hematopoiesis-associated solid cancers

New studies have started to investigate the association between clonal hematopoiesis and the risk for developing solid cancer. Analysis of a cohort of 8,810 cancer patients from the Memorial Sloan Kettering (MSK) revealed a CHIP prevalence of 30%[56,61]. Notably, CHIP appeared to be associated to specific types of solid cancers. In particular, CHIP was present frequently in thyroid and ovarian cancer patients, whereas melanoma, prostate cancer,

colorectal cancer, and renal cell carcinomas had lower incidence of CHIP. Follow up studies such as the UK Biobank with information from 200,453 individuals showed correlative data between CHIP and the development of lung cancer, kidney cancer, lymphoma, and sarcoma[62]. Another indication supporting the association between CHIP and solid cancer development was the discovery of CHIP mutant immune cells as part of the tumor microenvironment in biopsies from breast cancer patients[63]. In vivo studies with transgenic mouse models of CHIP have provided additional evidence connecting *Tet2* deletion in hematopoietic cells to increased progression to lung carcinoma[64]. Nonetheless, *Tet2* CHIP appears to have an antitumorigenic effect in a melanoma model[65]. More recently, *DNMT3A* CHIP studies have shown an association to colitis-induced colon cancer progression[66,67].

1.4 Hepatocellular carcinoma

Liver cancer stands as the seventh most prevalent cancer globally, and the fourth primary cause for cancer related mortality (**Figure 1.7**). Hepatocellular carcinoma (HCC) represents the most common type of liver cancer, accounting for 80% of cases[68]. Almost all hepatocellular cancers are driven by a setting of chronic liver disease, which can have different aetiologies. Hepatitis B (HBV) and C (HCV) infections contribute to 80% of HCC cases[69]. Nowadays the prevalence of virus-induced HCC has significantly declined due to the development of HBV vaccine and anti-viral HBV and HCV treatments[70,71]. On the contrary, the incidence of HCC attributed to dietary and sedentary lifestyle has significantly increased in developed countries over the past years[72]. Excessive alcohol consumption is also considered a common risk factor for HCC, affecting approximately 15-30% of patients[68]. Another rising risk factor for HCC, especially in developed countries, is non-alcoholic fatty liver disease (NAFLD), affecting approximately 25% of the global population[73]. This condition primarily results from caloric excess and a sedentary lifestyle, leading to obesity and metabolic syndrome.

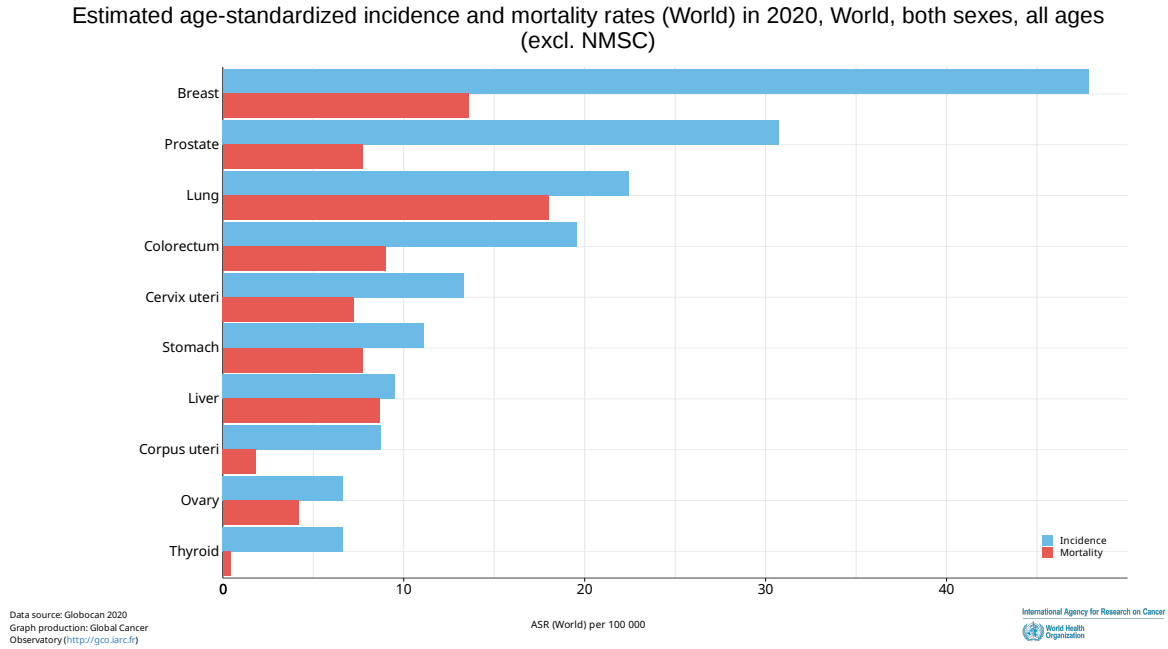


Figure 1.7. Incidence and mortality rates of highest ranked cancer types. Liver cancer is s 7th most prevalent cancer entity globally, and the 4th leading cause for cancer-related mortality.
Data are from the GLOBOCAN 2020 database, collated by the International Agency for Research on Cancer and hosted by the Global Cancer Observatory.

1.5 Non-alcoholic fatty liver disease (NAFLD)

NAFLD encompasses a range of liver conditions, ranging from non-alcoholic fatty liver (NAFL) characterized by simple steatosis, to nonalcoholic steatohepatitis (NASH), featuring chronic inflammation and hepatocyte injury (**Figure 1.8**). The progression of NAFLD can lead to fibrosis, cirrhosis, and eventually hepatocellular carcinoma[74]. The development of NAFLD-induced HCC involves a step-wise process initiated by hepatic steatosis, or abnormal lipid overload of hepatocytes. This lipid dysregulation, known as lipotoxicity[75], induces the formation of reactive oxygen species (ROS) resulting in elevated cellular oxidative stress. Subsequent metabolic reprogramming and inflammation[76] mark the transition to NASH, diagnosed when inflammation and hepatocyte injury become evident. Chronic inflammation and liver damage stimulate the activation of regenerative pathways and the proliferation of hepatic stellate cells (HSCs), responsible for the remodeling of the extracellular matrix (ECM)[77]. This excessive production of hepatic ECM results in increased fibrosis, which is considered a critical risk factor for cirrhosis and HCC development[78]. Within this environment of continuous liver regeneration, hepatocytes acquire proliferation and survival advantages, which increases the risk for transformation and HCC progression.

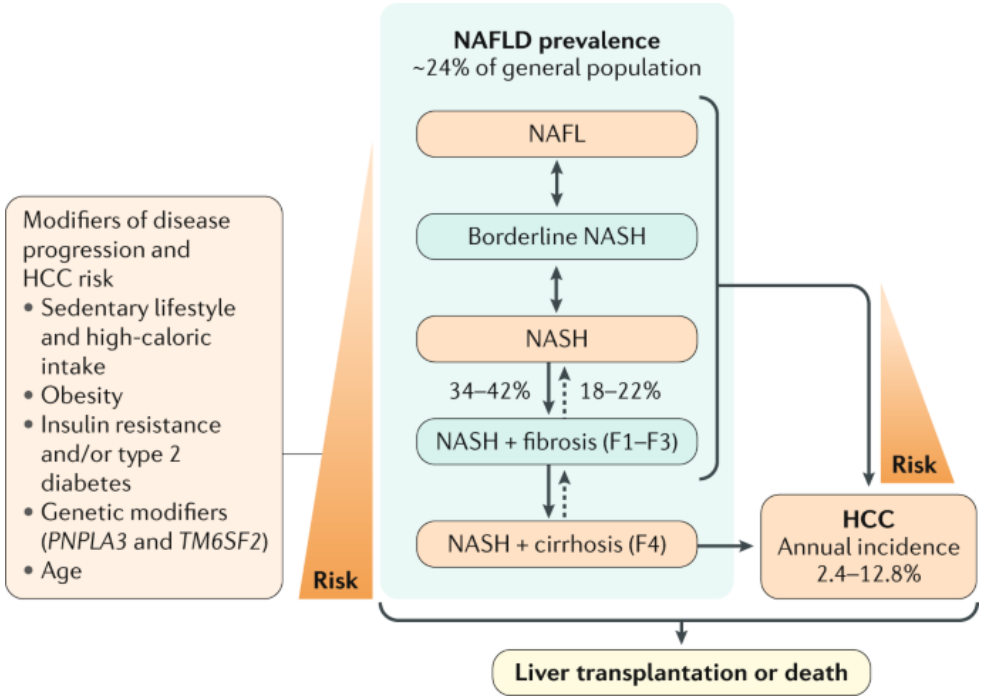


Figure 1.8. Stages of non-alcoholic fatty liver disease. NAFLD, a multifactorial disease ranging from non-alcoholic fatty liver (NAFL) to steatohepatitis (NASH), cirrhosis and ultimately HCC.
Image taken from Anstee, Q. M. et al. [74]. Reprinted with permission from Springer Nature through s100.copyright.com.

1.5.1 Mouse models of NAFLD

Understanding the pathogenesis of NASH-HCC relies on the development of preclinical models able to mimic the pathophysiology and the sequential evolution of NAFLD-driven HCC observed in humans (**Table 1.1**). Indeed, many of the so far reported models do not recapitulate the evolution of the human disease, or are unable to induce the final progression to HCC[79]. Dietary models have been extensively used, alone or in combination with toxins or genetic modifications. High fat diet (HFD) can trigger hepatic steatosis, however no inflammation nor hepatic injury[80]. Western diet (WD), supplemented with cholesterol and sucrose in addition to fat, reach a higher degree of liver damage, but still far from human phenotypes[81]. More severe phenotypes are observed when diets are methionine and choline deficient (MCD) or only choline deficient (CD)[82]. However, these diets do not recapitulate the stages of the human disease, and do not trigger HCC. Combination of HFD and CD results in a better preclinical model reaching the HCC stage[83]. However, this model exhibits a very low penetrance of the disease, with only 25% of mice developing HCC. More recent diets combine

HFD or WD with the administration of fructose[84]. This combination represents the most accurate model of human NAFLD-HCC, passing through all stages of the disease.

Other models combine the administration of a diet together with toxins, such as streptozotocin (STZ), a drug targeting pancreatic insulin-producing β cells to induce type 1 diabetes. Even though this treatment regimen induces a very fast evolution of the liver disease, mice stay lean and develop type I diabetes[85]. Diethylnitrosamine (DEN) + HFD is an alternative induction model, but it does not mimic NASH-driven HCC[86]. Genetic models have been also implemented in combination with diets. Obesity mouse models such as leptin (ob/ob)- and leptin-receptor (db/db)-deficient mice do not reach the stage of NASH nor HCC[87]. SREBP-1c transgenic mice, PTEN, PPAR-α, AOX, and MAT1A deficient mice, and the agouti (KK-Ay/a) mouse have been also used to model NASH-HCC. MUP-uPA transgenic mice exhibit elevated levels of urokinase plasminogen activator (uPA), inducing oxidative stress in hepatocytes[80,88]. HFD-fed MUP-uPA mice can develop NASH and a high proportion of them HCC. Finally, the B6/129 mouse strain fed with a WD containing high-fructose-sucrose solution (WD-SW diet), known as the DIAMOND mice, is also a good model of NAFLD, with a significantly high penetrance of HCC (90%)[89].

Table 1.1 Preclinical models of NASH-induced HCC. Abbreviations: ✓✓: marked expression; ✓: modest expression; X: no expression; ?: not assessed; HFD: high-fat diet; WD: Western Diet; MCD: methionine-and-choline deficient diet; CD: choline-deficient diet; STAM: streptozotocin+HFD-treated mice; DEN: diethylnitrosamine; ob/ob: leptin-deficient mice; db/db: leptin-receptor-deficient mice; SREBP1c Tg: sterol regulatory element-binding protein 1c transgenic mice; Agouti: KK-Ay-a mice; PTEN ko: phosphatase and tensin homologue deleted on chromosome 10 knockout mice; PPARα ko: peroxisome proliferator-activated receptor α knockout mice; AOX ko: acetyl-CoA oxidase deficient mice; MATA1 ko: methionine adenosyl transferase 1A knockout mice; MUP-uPA Tg: mice expressing transiently high amounts of urokinase plasminogen activator in hepatocytes; DIAMOND: isogenic BL6/129 hybrid strain fed an obesogenic WD supplemented by high fructose and sucrose.
Table taken from Febbraio, M. A et al. [79]. Reprinted with permission from Elsevier through s100.copyright.com.

	Obesity	**Insulin Resistance**	**Steatosis**	**Inflammation/ ER Stress**	**NASH**	**Fibrosis**	**p62 Accumulation**	**HCC**
Diet Models								
HFD	✓✓	✓✓	✓✓	✓	×	×	×	×
WD	✓✓	✓✓	✓✓	✓	×	×	×	×
MCD	×	×	✓✓	✓	✓✓	✓✓	?	×
CD	×	×	✓✓	✓	✓✓	✓✓	?	×
HFD/fructose	✓✓	✓✓	✓✓	✓✓	✓✓	✓✓	?	✓✓
CD HFD	✓✓	✓✓	✓✓	✓✓	✓✓	✓	?	✓
Toxins/Diet-Based Models								
STAM	×	✓✓	✓✓	✓✓	✓✓	✓	?	✓✓
HFD/DEN	✓✓	✓✓	✓✓	✓✓	×	×	✓✓	✓✓
CD HFD/DEN	✓✓	✓✓	✓✓	✓✓	×	×	?	✓✓
Genetic/Diet Models								
ob/ob	✓✓	✓✓	✓✓	✓	×	×	?	×
db/db	✓✓	✓✓	✓✓	✓	×	×	?	×
SREBP1c Tg	×	✓✓	✓✓	✓✓	✓✓	✓✓	?	✓
Agouti	✓✓	✓✓	✓✓	✓	×	×	?	×
PTEN ko	×	✓✓	✓✓	✓✓	✓✓	✓✓	?	✓
PPARα ko	×	×	×	✓✓	✓✓	✓✓	?	✓
AOX ko	×	×	×	✓✓	✓✓	×	?	✓
MAT1A ko	×	×	×	✓✓	✓✓	×	?	✓
MUP-uPA Tg	✓✓	✓✓	✓✓	✓✓	✓✓	✓✓	✓✓	✓✓
DIAMOND	✓✓	✓✓	✓✓	✓✓	✓✓	✓✓	?	✓✓

1.5.2 Roles of hematopoietic cells in NAFLD

The liver is considered an important immunological organ, containing several cell types from the innate and adaptive immune systems. Some of these cell types are resident, such as Kupffer cells, and others infiltrate in situations of organismal stress. Throughout the progression of NAFLD-driven HCC, the liver immune composition is reshaped, and these cells participate in the induction of chronic inflammation, fibrosis and hepatic injury, therefore being critical drivers of NAFLD-HCC[90]. A complex crosstalk between the immune cells and the hepatocytes governs the step-wise process of this disease (**Figure 1.9**). Neutrophils are known to infiltrate the liver, and induce liver damage via the production of ROS, cytokines, and neutrophil extracellular traps (NETs)[91,92]. In early stages of the disease, monocytes infiltrate the liver to differentiate into monocyte-derived macrophages[93]. This massive infiltration replaces embryonically-derived Kupffer cells, which die due to the toxicity induced by excessive lipid accumulation[94]. Nevertheless, infiltrating monocytes display different molecular programs to the resident Kupffer cells, especially with regards to their pro-inflammatory phenotype[94]. Dendritic cells (DCs) also accumulate in NASH livers, contributing to local inflammatory responses, although their precise role remains poorly understood[95]. Recent studies underscore the importance of platelets in NASH development, engaging in early inflammatory responses and activating other immune cell types[96]. Indeed, anti-platelet therapy was shown to reduce signs of NASH pathology[97,98]. In terms of the lymphoid arm, B cells are also increased in livers of NASH patients[99]. Preclinical models have revealed their pro-inflammatory role, and B-cell depletion has been able to ameliorate hepatic fibrosis[99]. Specific subsets of $CD4^+$ and $CD8^+$ T cells are also relevant drivers of chronic inflammation in NASH[83]. Specifically, $CD8^+$ T cells expressing exhaustion ($PD1^+$, $CXCR6^+$) and activation markers (Granzymes) are highly enriched in NASH human and mouse livers, specifically at the more advanced stages of the pathology[100].

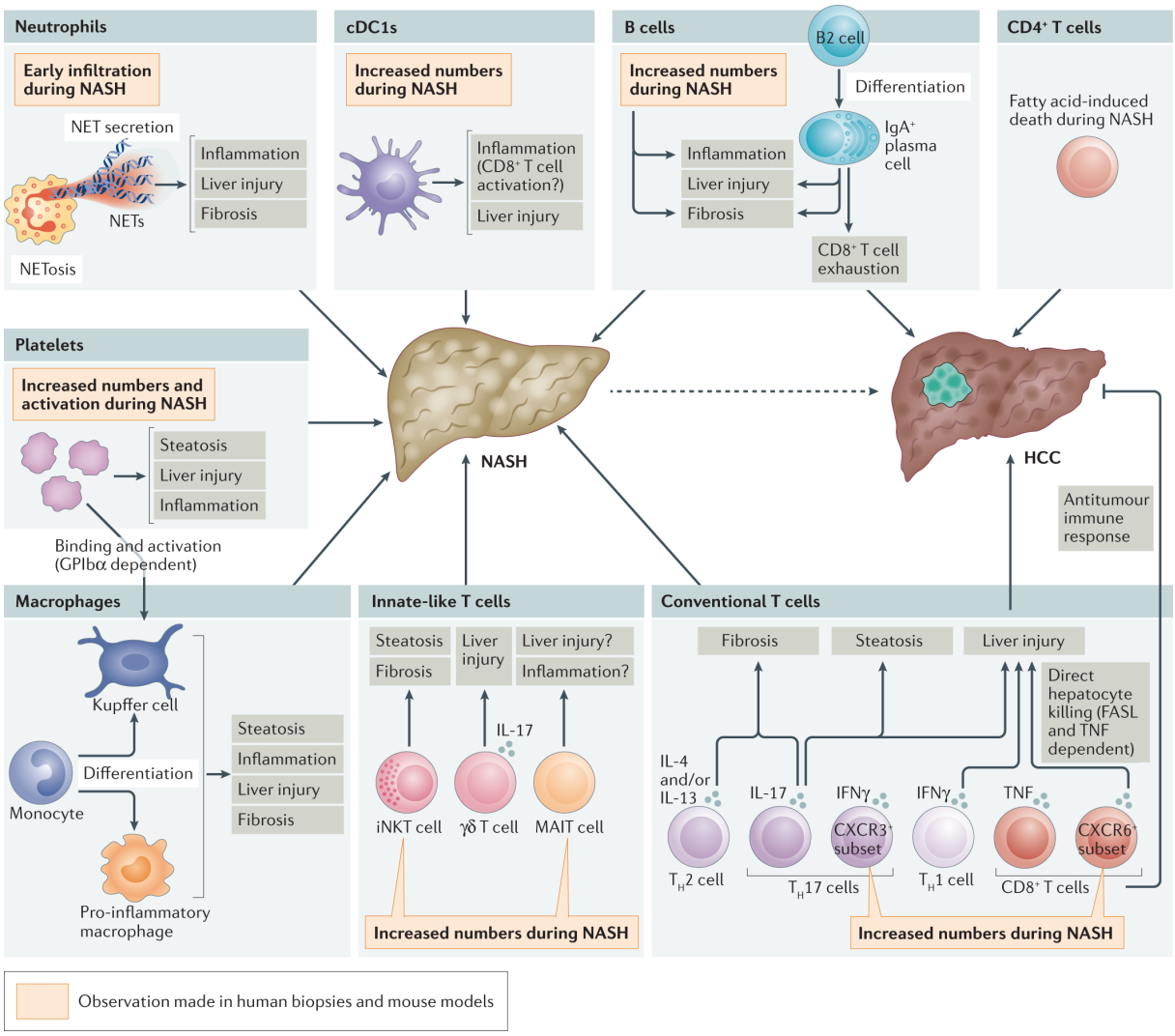


Figure 1.9. Role of hematopoietic cells in the development of NAFLD-induced HCC.

Image taken from Huby, T. & Gautier, E. L. [101]. Reprinted with permission from Springer Nature through s100.copyright.com.

2

Aims of the thesis

2.1 Aims project I

The project I of this dissertation broadly aims to reassess the fundamental properties of hematopoietic stem cells (HSCs) using single cell functional approaches. The vast majority of studies have focused their research on specific facets of HSC biology, such as self-renewal or multipotency. For instance, heterogeneity in the capacity to sustain the hematopoietic system, akin self-renewal potential, has been reported in HSCs. From these studies, well-accepted definitions such as long-term or short-term HSCs were established, which determine the time span during which HSCs can sustain the production of blood cells. On the other hand, the multipotent nature of HSCs has been debated. Single cell transplantation and barcoding studies identified HSCs with a biased production of either the myeloid or lymphoid lineage, whereas HSCs rarely generated multilineage balanced output. Nonetheless, how all these layers contributing to HSC heterogeneity are linked to each other has not been explored yet.

Self-renewal is a unique property of stem cells, which theoretically enables HSC perpetuation with the aim of sustaining hematopoiesis for the entire life of an organism. However, there is recent evidence suggesting that HSC self-renewal is not infinite. Instead, HSCs lose functional potency as they divide leading to a functional decrease in potency during aging.

Another line of investigation in this project focusses on understanding which factors influence HSC heterogeneity. Although it is generally believed that intrinsic features of HSCs are to some extent stable and inheritable by their progeny, little is known about whether extrinsic mechanism may play a role in determining HSC functional outcomes.

To gain greater understanding of HSC biology, the aims of project I are as follows:

- Characterize the functional outcomes of individual HSC over time through single cell transplantation assays.
- Identify biological parameters that predict HSC fate.
- Investigate the impact of HSC self-renewal divisions on their functional potency using serial single cell transplantations.
- Utilize mathematical modelling on the single cell transplantation data to dissect the mechanistic processes governing HSC functional outcomes.
- Explore the influence of extrinsic cues on modulating the functional output of individual HSCs.

2.2 Aims project II

Hepatocellular carcinoma (HCC) induced by non-alcoholic fatty liver disease (NAFLD) is emerging as a major cancer entity in Western countries, primarily attributed to sedentary lifestyles and excessive caloric intake. Prolonged exposure to these factors can lead to chronic liver inflammation and eventual progression to liver cancer. While NAFLD affects a significant portion of the global population, only a minority of individuals progress to advanced stages of the disease or develop HCC. Consequently, there is a critical need for diagnostic tools capable of stratifying patients at high risk for HCC progression.

Several clinical reports have shown that individuals with clonal hematopoiesis of indeterminate potential (CHIP) exhibit an increased risk of all-cause mortality. Furthermore, CHIP can play a causal role in the development of hematologic and non-hematologic diseases, such as cardiovascular diseases and solid cancers. However, there is limited understanding of the mechanistic processes via which clonal hematopoiesis contributes to the evolution of these diseases.

Unpublished clinical data from Dr. Robert Vanner (UHN, Toronto) indicate a frequent occurrence of CHIP-related mutations, particularly *TET2* CHIP mutations, in peripheral blood cells of HCC patients. Building on this observation, this part of the dissertation aims to

investigate *Tet2* CHIP as a potential biomarker for NAFLD-HCC development. The specific objectives of this study are as follows:

- Generate a mouse model of NAFLD-HCC induced by a high caloric Western diet, together with or without *Tet2* clonal hematopoiesis.
- Characterize the potential of *Tet2* clonal hematopoiesis to enhance or accelerate NAFLD-HCC development by assessing the synergy between the diet- and Tet2 CHIP-induced phenotype.
    - Evaluate NAFLD development through body composition measurements, and histopathological, serological, and molecular parameters.
    - Assess the incidence of transition from NAFLD to HCC.
- Investigate the mechanisms via which *Tet2* CHIP contributes to the evolution of NAFLD-HCC.
    - Evaluate systemic hematopoietic changes resulting from the administration of the diet and *Tet2* CHIP.
    - Assess immune cell recruitment and immune composition of NAFLD livers.
    - Explore potential synergistic molecular programs in liver-infiltrating hematopoietic cells related to disease progression.
    - Interrogate whether *Tet2* CHIP accelerates disease progression using the same mechanistic basis as in the WT setting.
- Explore the metabolic reprogramming in hematopoietic cells induced by the Western diet.

3

Results project I

3.1. Serial single cell transplantations to assess HSC functional heterogeneity

In order to interrogate the functional behavior of individual HSCs, I used single cell transplantations (**Figure 3.1**), which is considered the gold standard method to assess the HSC functional heterogeneity. Primary transplantations consisted of the isolation of a highly pure population of LT-HSCs by flow cytometry, defined as Lin^- Sca^+ $cKit^+$ (LSK), $CD48^-$, $CD150^+$, $CD34^-$, $EPCR^{high}$, isolated from UBC-GFP or Kusabira orange (KuO) transgenic mice. Transplantations of either only 1 GFP^+ LT-HSC, or co-transplantations of 1 GFP^+ LT-HSC and 1 KuO^+ LT-HSC were performed. Co-transplantations were implemented as a strategy to increase the proportion of recipient mice with positive engraftment, as they would likely double the number of engrafting clones. Single LT-HSCs were transplanted along with $1.5x10^5$ supportive bone marrow cells into a total of 278 lethally irradiated mice. The reconstitution potential of each individual clone was assessed by measuring the chimerism (percentage of GFP^+/KuO^+ donor-derived cells) in peripheral blood every 4 weeks post-transplantation. 36.44% of the clones showed positive chimerism (>0.1%) at any timepoint. Additionally, bone marrow chimerism was measured at 24 weeks post-transplantation. Periodic chimerism assessments allowed for the comprehensive characterization of multiple single HSC-derived hematopoietic systems.

Traditionally, self-renewal has been considered a unique property of stem cells that enables them to generate identical daughter cells with an equal potential to repopulate a whole system. Recent studies have questioned this concept, showing that HSC potency is not unlimited, and declines over self-renewal divisions. To further interrogate how self-renewal

divisions impact on HSC functionality, I performed serial single cell transplantations (**Figure 3.1**). Experimentally, I transplanted single FACS-sorted HSCs derived from primary recipients into lethally irradiated secondary recipient mice. Peripheral blood chimerism was also evaluated over time post-transplantation and bone marrow chimerism at the experimental endpoint, 24 weeks post-transplantation; as done for the primary transplants. Using this approach, I was able to perform a paired analysis of the transplantation outcomes of parent and daughter HSCs.

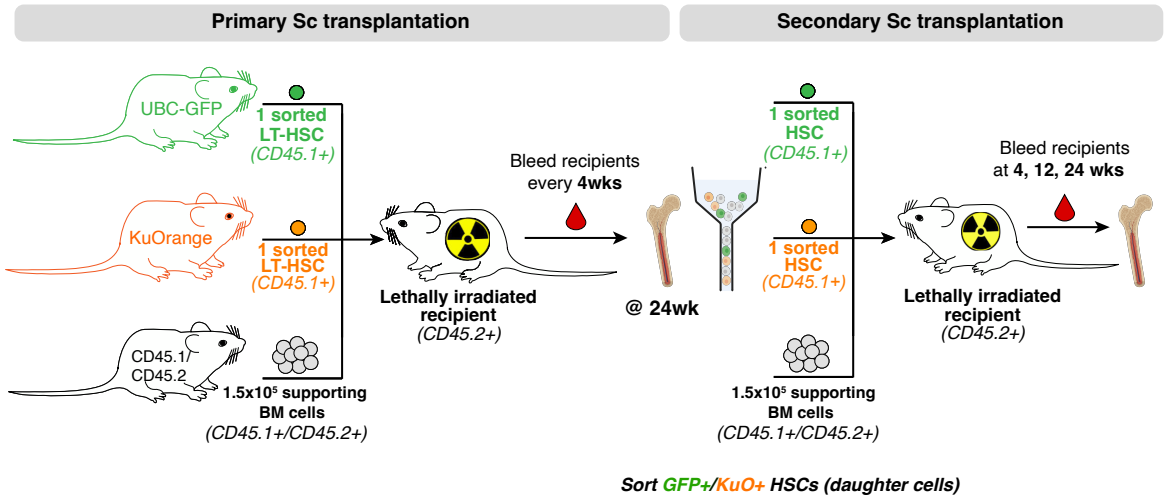


Figure 3.1. Experimental design for serial single cell transplantations to interrogate fundamental properties of HSCs. In primary single cell (sc) transplantations, 278 single LT-HSCs derived from 5 different UBC-GFP or KuO donor mice were transplanted together with 1.5x10^5 bone marrow cells into individual lethally irradiated recipient mice. LT-HSCs were defined by the marker combination Lin$^-$Sca$^+$ cKit$^+$ (LSK), CD48$^-$, CD150$^+$, CD34$^-$, EPCR^{high}. In secondary single cell transplantations, 525 single HSCs (Lin$^-$ Sca$^+$ cKit$^+$ (LSK), CD48$^-$, CD150$^+$) derived from 6 primary recipients were transplanted into individual recipient mice together with 1.5x10^5 bone marrow cells. Experimental details are summarized in the methods section 7.3.2.

3.2. Reconstitution outcomes from primary single cell transplantations confirmed reported HSC lineage biases

Single HSC transplantations into primary recipients revealed 3 broad different types of reconstitution outcomes. In line with previous studies, I identified HSCs with a balanced multilineage reconstitution, and others biased towards the lymphoid or the myeloid lineages (**Figure 3.2**). Notably, this categorization was made based on the clonal output detected at 24 weeks post-transplantation in the peripheral blood, as in previous single cell transplantation studies[33,34]. Interestingly, myeloid bias correlated with a higher degree of HSC self-renewal, as evidenced by a higher HSC chimerism in these clones. Balanced mice had a significantly lower

HSC chimerism, whereas in lymphoid-biased systems, there were no remaining donor-derived HSCs.

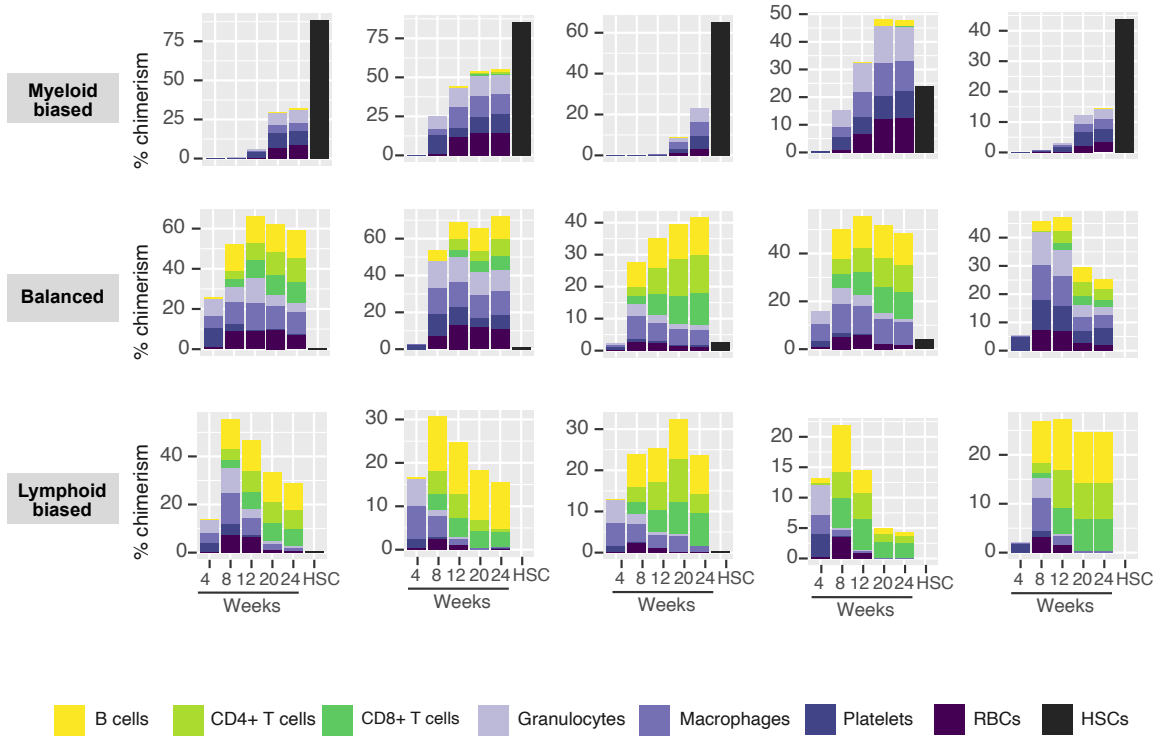


Figure 3.2. Chimerism analysis of single cell transplantations based on their final lineage output. Clones are classified based on their capacity to reconstitute the lymphoid, myeloid or both lineages. Each graph is a clonally-derived hematopoietic system from individual representative mice, showing the percentage of chimerism in peripheral blood at 4-, 8-, 12-, 20- and 24-weeks post-transplantation, as well as the HSC chimerism measured in the bone marrow at the endpoint. For each timepoint, column height shows overall chimerism, and within stacked plot illustrates the relative donor contribution to each cell type.

3.3. Kinetics of reconstitution as a novel parameter to predict HSC fate

Previous single cell studies have deconvoluted HSC functional heterogeneity solely based on the final lineage output 24 weeks after transplantation, without considering how the clone repopulates the blood system over time. In contrast, I examined the overall stem cell behavior across several timepoints. Chimerism values in different peripheral blood populations, acquired at variable timepoints, together with information regarding chimerism in bone marrow were used to construct an unbiased clustering heatmap (**Figure 3.3**). This type of data representation revealed a novel parameter capable of segregating stem cell functional behavior - the reconstitution kinetics. Broadly, two clusters of HSC clones with slow and fast

reconstitution kinetics were identified. Fast-reconstituting clones generated all myeloid populations already at 4 weeks post-transplantation, swiftly followed by lymphoid generation. In contrast, slow-reconstituting clones had only initiated platelet production at the 4-week time point, and reconstituted all other cell types with a delay. I also observed a consistent order in the production of each cell type, starting with platelets, followed by RBCs, granulocytes, and macrophages, B cells, and finally $CD4^+$ and $CD8^+$ T cells.

Interestingly, reconstitution kinetics correlated with the classical categorization of HSC clones based on endpoint lineage biases. Fast clones were subdivided into two clusters: one exhibiting a final lymphoid bias, and a second with multilineage balanced output. However, it is worth noting that lymphoid-biased clones were not restricted to the lymphoid compartment, as they generated all the myeloid populations early on in the reconstitution process. Therefore, their fast kinetics and consequent fast exhaustion process made them look lymphoid-biased at the endpoint. The other cluster of fast clones had a balanced final output, indicating that the myeloid compartment was not exhausted yet, as in the case of lymphoid-biased clones. It could be therefore inferred that lymphoid-biased HSCs are the fastest reconstituting clones, consequently exhausting, while the balanced clones have an intermediate pace and manage to sustain myelopoiesis until the experimental endpoint. In the opposite scenario, slow clones initiated the reconstitution process with platelets, RBCs, granulocytes and macrophages, but did not contribute to lymphopoiesis over the analysis period.

Moreover, the kinetics of reconstitution appeared to be a key determinant of HSC/progenitor content in the bone marrow at the endpoint. While very fast clones with a final lymphoid output showed no donor-derived HSCs in the bone marrow, clones with intermediate kinetics exhibited low HSC chimerism, and slow clones presented the highest HSC chimerism. This observation aligns with the fact that the faster the blood reconstitution, the faster the exhaustion at the stem cell level and downstream peripheral blood populations.

Taken together, clonal analysis over time demonstrated that dynamics of reconstitution is an ideal parameter to predict the functional potency of HSCs and determine the type of lineage output detected at the endpoint analysis. Hence, instead of the classical

model of HSC heterogeneity based on lineage biases, I propose a model supporting a linear hierarchy of functional potency in the HSC compartment transitioning from fast to slow reconstituting clones (**Figure 3.4**).

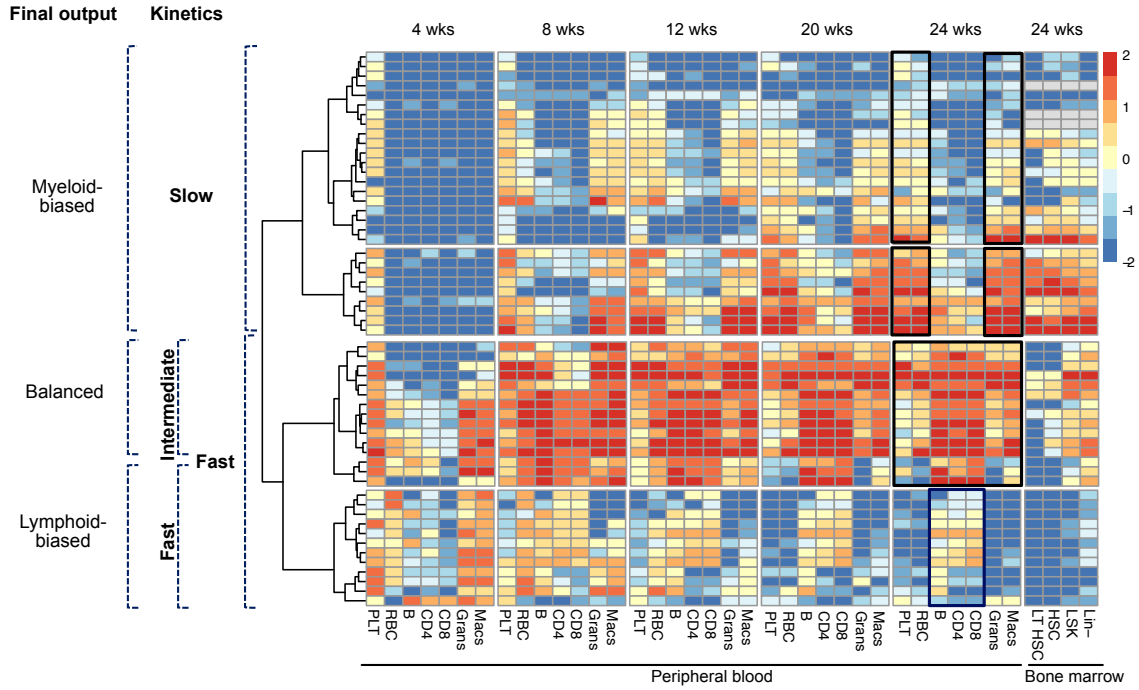


Figure 3.3. Single cell reconstitution outcomes. Heatmap illustrating the percentage of chimerism in peripheral blood at different timepoints (4-, 8-, 12-, 20-, 24-weeks) post-transplantation and in the bone marrow at the endpoint (24 weeks). Each row represents a single HSC transplantation that had positive chimerism at any timepoint. An unbiased clustering segregates the clones based on their reconstitution kinetics (slow, intermediate and fast). Further sub-clustering divides each clone based on their final lineage output (myeloid, lymphoid or balanced). Black boxes highlight the lineages generated at the endpoint. PLT: platelets, RBC: red blood cells, B: B cells, CD4: $CD4^+$ T cells, CD8: $CD8^+$ T cells, Grans: granulocytes, Macs: macrophages.
(n=54 clones; agglomerative clustering, named AGNES (AGglomerative NESting) was used).

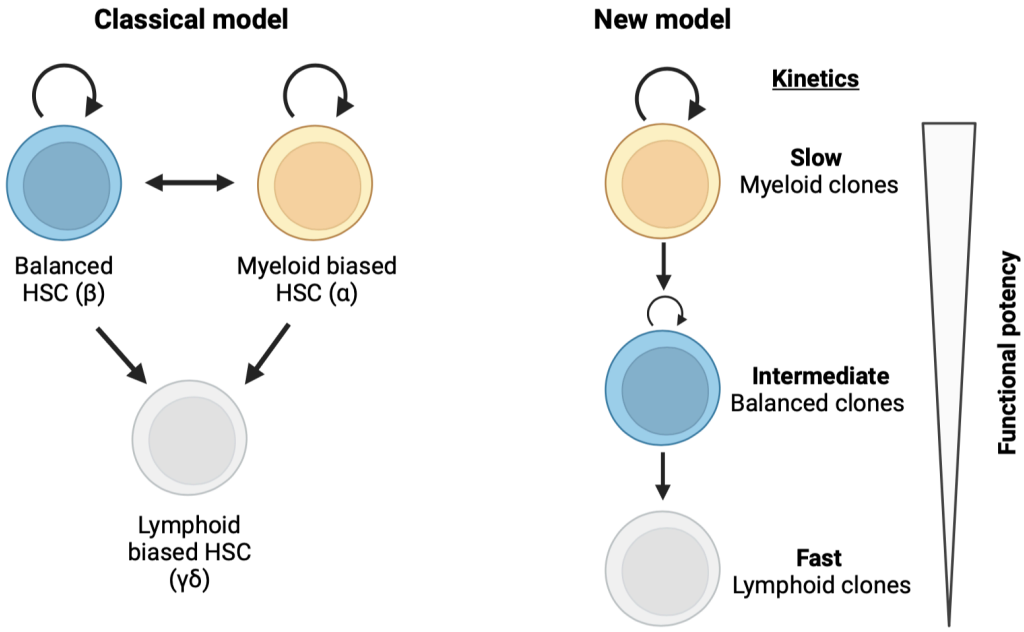


Figure 3.4. Comparison between classical and new model describing the functional heterogeneity within the HSC pool. Classical model categorizes HSCs based on their lineage biases (balanced, myeloid, lymphoid)[34], while the new model suggests a linear hierarchy in the HSC compartment transitioning from slow- to fast-reconstituting clones, introducing kinetics as a better predictive factor for HSC functional potency and lineage bias.
Image created using Biorender.

3.4. Daughter HSCs exhibited a significant decline in reconstitution potential compared to the parent HSC

Secondary single cell transplantations were performed to investigate whether the functional potency and lineage output was maintained in the HSC progeny. While previous barcoding experiments have been able to trace lineage relationships throughout serial transplantations[25], they exclusively addressed the combined functional output of multiple daughter stem cells derived from an individual clone. The same limitation applies to single cell transplantations followed by bulk secondary transplantations. Instead, I aimed to formally interrogate the degree to which individual daughter HSCs retain the lineage output and functional potency of their parent. Experimentally, I isolated and transplanted 525 individual donor-derived HSCs from a total of six primary recipients with sufficient HSC reconstitution to allow serial transplantations. These primary recipients exhibited either balanced (B1, B2) or myeloid-biased reconstitution (M1, M2, M3, M4), therefore intermediate or slow reconstitution kinetics. 141, 60, 60, 132, 68, 64 single HSCs were transplanted from B1, B2, M1, M2, M3, M4 primary recipients into secondary recipient mice; respectively.

Generally, the percentage of daughter HSCs with positive engraftment (9.89%) was significantly reduced compared to the primary transplantation (36.28%), with a 3.6-fold reduction (**Figure 3.5A**). Moreover, the percentage of clones with long-term engraftment capacity was even more impacted in daughter stem cells. In this case, 24.77% of primary clones exhibited blood chimerism above 0.1% at 24 weeks post-transplant, whereas only 2.6% of secondary clones sustained long-term hematopoiesis, indicating a 9.5-fold reduction.

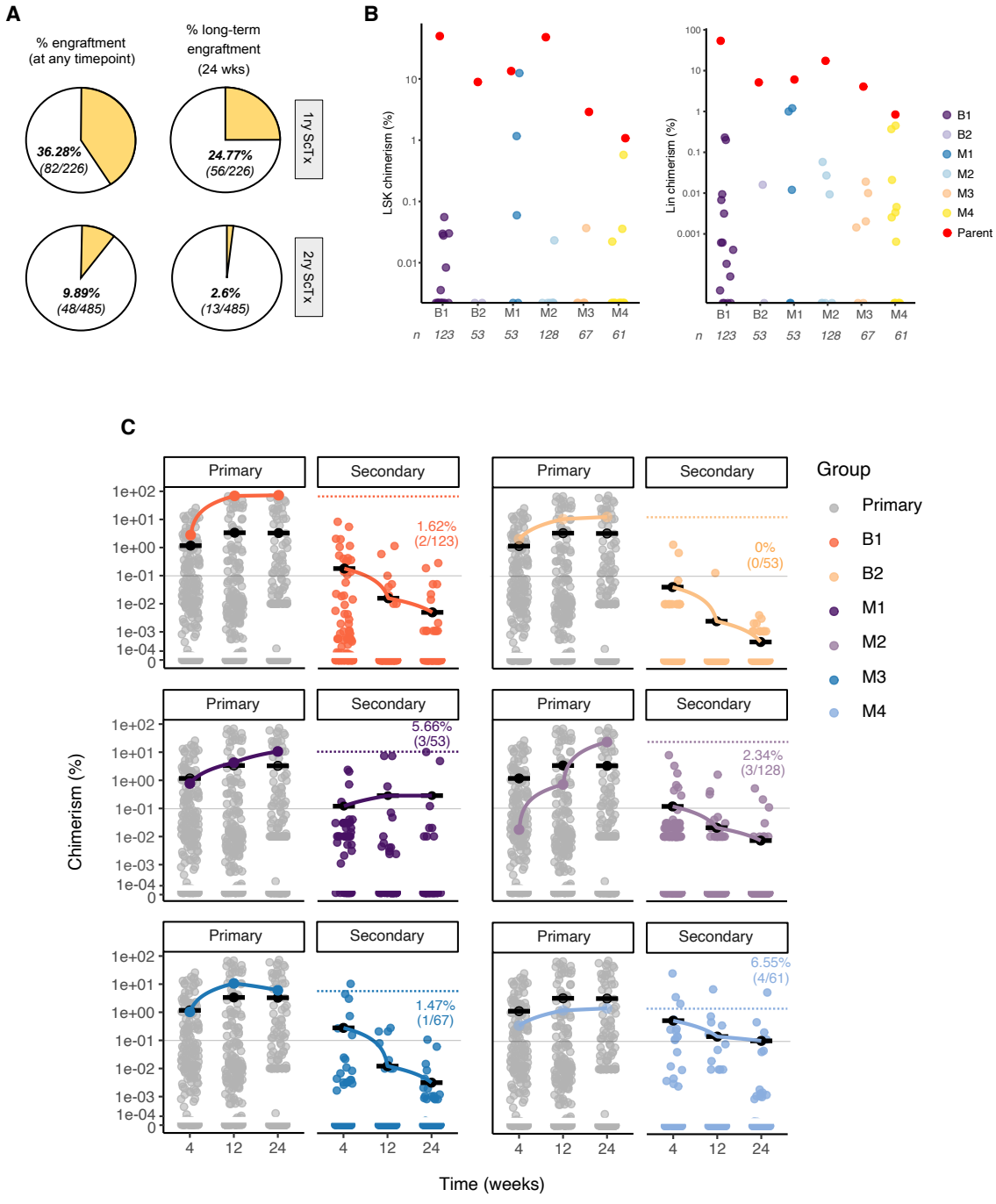


Figure 3.5. Paired analysis of transplantation outcomes between parent and daughter HSCs. A) Left pie charts: percentage of clones with successful engraftment (>0.1% chimerism in peripheral blood) at any timepoint post-transplantation comparing primary and secondary transplants. Right pie charts: percentage of clones with positive long-term chimerism (at 24 weeks post-transplantation) comparing primary and secondary transplants. Number of positive clones out of the total transplanted is shown in brackets. **B)** LSK and Lineage negative (Lin-) chimerism in bone marrow of daughter HSCs compared to their parent (highlighted in red). B1-2 correspond to clones with balanced reconstitution in the primary transplantation, while M1-4 displayed a myeloid bias. **C)** Overall chimerism in peripheral blood at 4-, 12- and 24-weeks post-transplantation comparing primary and secondary single cell transplantations. Within each primary plot, the chimerism of the parent HSC is highlighted in a color. Dotted lines indicate the maximum chimerism reached by the parent HSC in the primary transplantation.

To evaluate how the primary heterogeneity of HSCs impacts on the functional potency of their progeny, I conducted paired analyses of each parent and their corresponding daughter clones. As shown in **Figure 3.5B-C**, all six paired analyses demonstrated a significant functional reduction in the daughter stem cells compared to the parent donor, especially in terms of long-term repopulation capacity. Despite this, some variation was still noticeable among the donors. While the secondary recipients of balanced primary HSCs (B1, B2) never reached the chimerism of the parent, the myeloid-biased and slowest-reconstituting clones occasionally did. This is in line with the concept that faster reconstitution of the hematopoietic system tends to lead to faster exhaustion of the stem cell pool.

Taken together, these results suggest that self-renewal divisions compromise stem cell functionality, and that the kinetics of reconstitution determine the extent to which HSC preserve their functional potential.

Previous studies have shown that daughter HSCs often preserve the differentiation output of the parent[33,34]. Myeloid-biased (or α) and balanced (β) clones, characterized by extensive self-renewal capacity, were capable of sustaining their lineage, and in some instances, transitioning to a lymphoid-biased state (γδ) or exchanging phenotypes. Since these studies typically involved the transplantation of daughter HSCs in bulk (often millions of daughter HSCs), I hypothesized that the collective output might contribute to the preservation of lineage outputs. In contrast to this work, I never observed HSCs switching from a balanced to a myeloid-biased output and vice versa in secondary recipients (**Figure 3.6A**). Instead, there was an acceleration of reconstitution in all analyzed clones, correlating with a higher incidence of exhaustion patterns. This was evidenced by an early production of blood cells, followed by

the decline of the myeloid lineage, and often, the lymphoid lineage as well. In the case of balanced parents (B1, B2), all daughter HSCs experienced complete exhaustion or only sustained lymphopoiesis by the experimental endpoint at 24 weeks post-transplantation (**Figure 3.6B**). Therefore, balanced clones never remain balanced nor transform into a myeloid-biased clone. On the other hand, myeloid-biased (=slowest) parents could either exhaust completely, exhaust only the myeloid lineage, or albeit rarely, preserve their slow kinetics and exhibit a myeloid-biased phenotype at the endpoint (**Figure 3.6C**). These latter clones also showed significant HSC chimerism, denoting a high preservation of functional potency compared to the parent. These findings reinforce the idea that reconstitution kinetics predicts overall functional potency, as the faster reconstitution in the primary transplantation, the higher degree of exhaustion is observed when transplanting the HSC progeny in secondary transplantations.

In summary, these data demonstrate that over self-renewal divisions, HSCs acquire faster reconstitution kinetics upon transplantation, which correlates with a loss of functional potential, akin to "exhaustion" (**Figure 3.7**). Consistent with the loss of functional potency, the majority of the clones thus transform into classical "lymphoid-biased" outputs, showing a reduced long-term sustainability of the myeloid lineage.

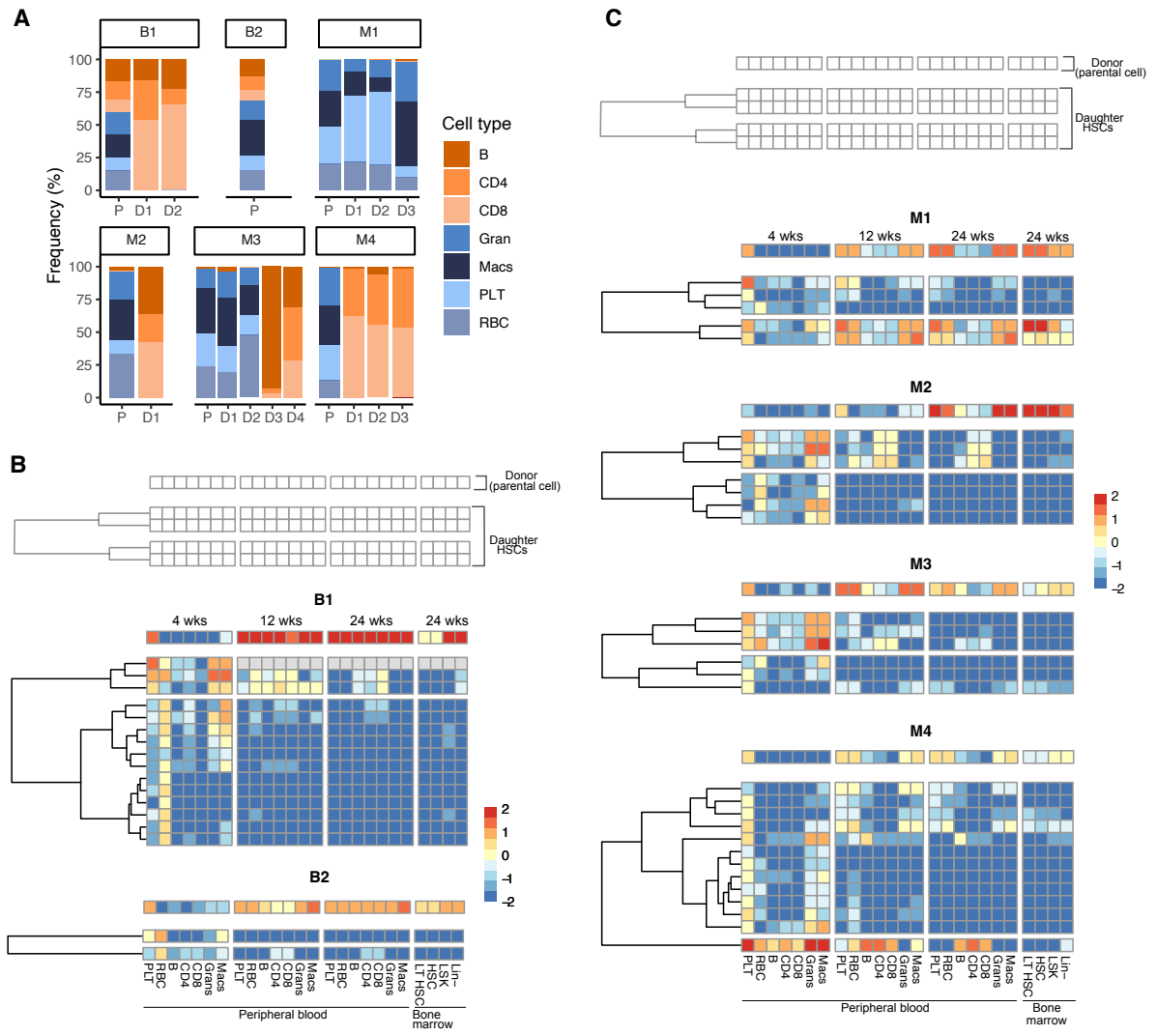


Figure 3.6. Daughter HSCs acquire faster kinetics compared to the parent, correlating with changes in their lineage bias. A) Contribution to peripheral blood cell types in the parent (P) and corresponding daughter HSCs (D1, D2, etc.), measured at 24 weeks post-transplantation. **B)** Heatmap illustrating the percentage of chimerism in peripheral blood at different timepoints (4-, 12-, 24-weeks) post-transplantation and in the bone marrow at the endpoint in parent and corresponding daughter HSCs from primary balanced clones (B1, B2). **C)** Data derived from primary myeloid-biased clones (M1, M2, M3, M4). Upper row shows the parent reconstitution, while the rest represents single daughter HSC transplantations. PLT: platelets, RBC: red blood cells, B: B cells, CD4: CD4+ T cells, CD8: CD8+ T cells, Grans: Granulocytes, Macs: Macrophages.

(n=48 clones; agglomerative clustering, named AGNES (AGglomerative NESting) was used in B and C).

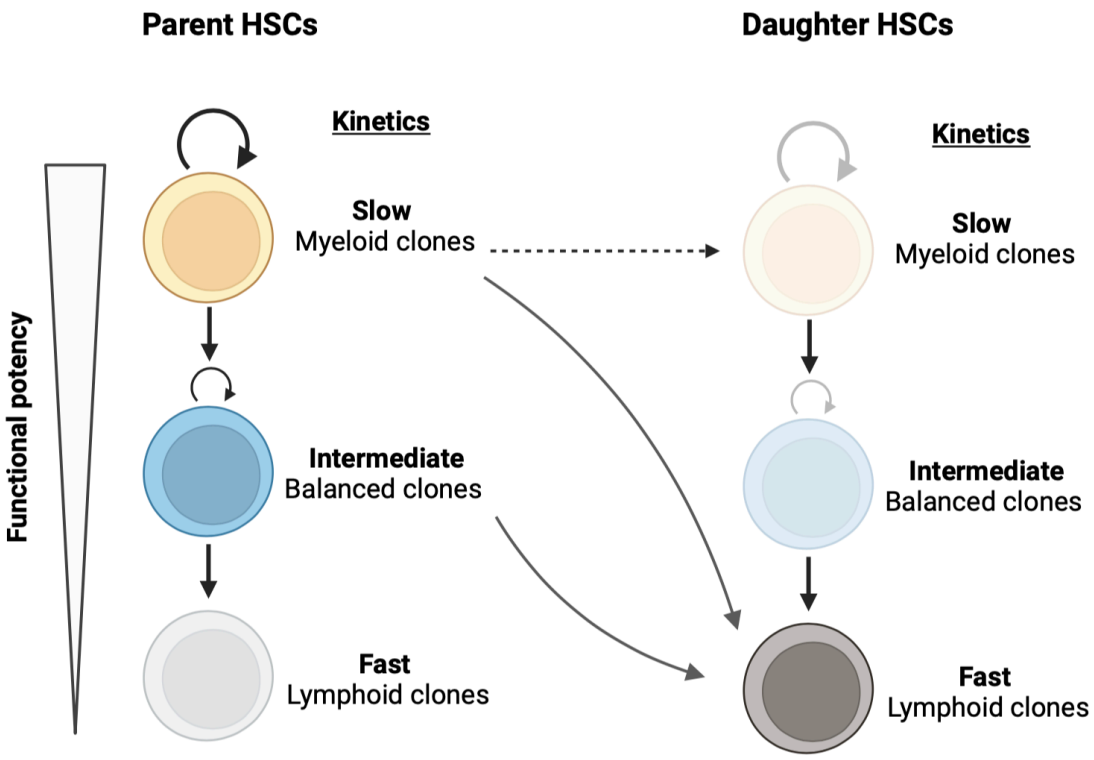


Figure 3.7. Daughter HSCs displayed faster reconstitution kinetics and reduced functional potency than their parent HSC. Comparative model illustrating the transition of daughter from slow reconstituting clones with high functional potency to fast exhausted clones.
Image created using Biorender.

3.5. Mathematical modelling of single cell transplantation outcomes

Mathematical modelling of primary transplantation outcomes was conducted by Tamar Nizharadze (Division of Theoretical Systems Biology, DKFZ), using absolute numbers of each hematopoietic compartment, collected over various timepoints post-transplantation. The model contained multiple layers of data: 1) GFP^+ clonal reconstitution, 2) KuO^+ clonal reconstitution and 3) supportive bone marrow reconstitution (**Figure 3.8A**). Depending on whether the transplantation consisted of 1 GFP^+ HSC or co-transplantations of 1 GFP^+ and 1 KuO^+ HSC, the model was built with 2 or 3 layers of information, respectively. Consideration of the supportive bone marrow layer in addition to the single clonal reconstitutions was essential for the model, as no model fitting was possible when only considering a single HSC's output. This indicates that the supportive bone marrow also contributes to the HSC reconstitution outcome.

The 3-layer model structure was supported by our data. Considerably low coefficients of variation were observed in blood populations, suggesting that the absolute production of mature cells remained relatively constant between single cell transplantations (**Figure 3.8B**). This observation implies that absolute size limits exist for each mature blood compartment, which are particularly stringent for platelets and RBCs, followed by granulocytes, macrophages and lymphocytes. In contrast, HSCs exhibited a significantly high coefficient of variation, suggesting a higher degree of freedom for HSC expansion. Further analysis demonstrated that mature compartments were reconstituted by both labeled (GFP^+ or KuO^+) and unlabeled (supportive bone marrow) cells, as shown by the negative correlation between the two experimental layers (**Figure 3.8C**). The maximum negative correlation was observed at the last timepoint post-engraftment, indicating that the compartments have reached their maximum capacity by the experimental endpoint (**Figure 3.8D**). The fact that all clonally-derived hematopoietic systems achieved homeostasis at the mature cell level suggests a high degree of regulation, potentially via feedback mechanisms to upstream cell compartments of the hierarchy.

Taken together, modelling of single cell transplantation outcomes demonstrated compartment size regulation in blood cell populations. This regulation may involve feedback upstream in the hierarchy, modulating the interplay between the donor and neighboring HSCs to replenish the hematopoietic hierarchy.

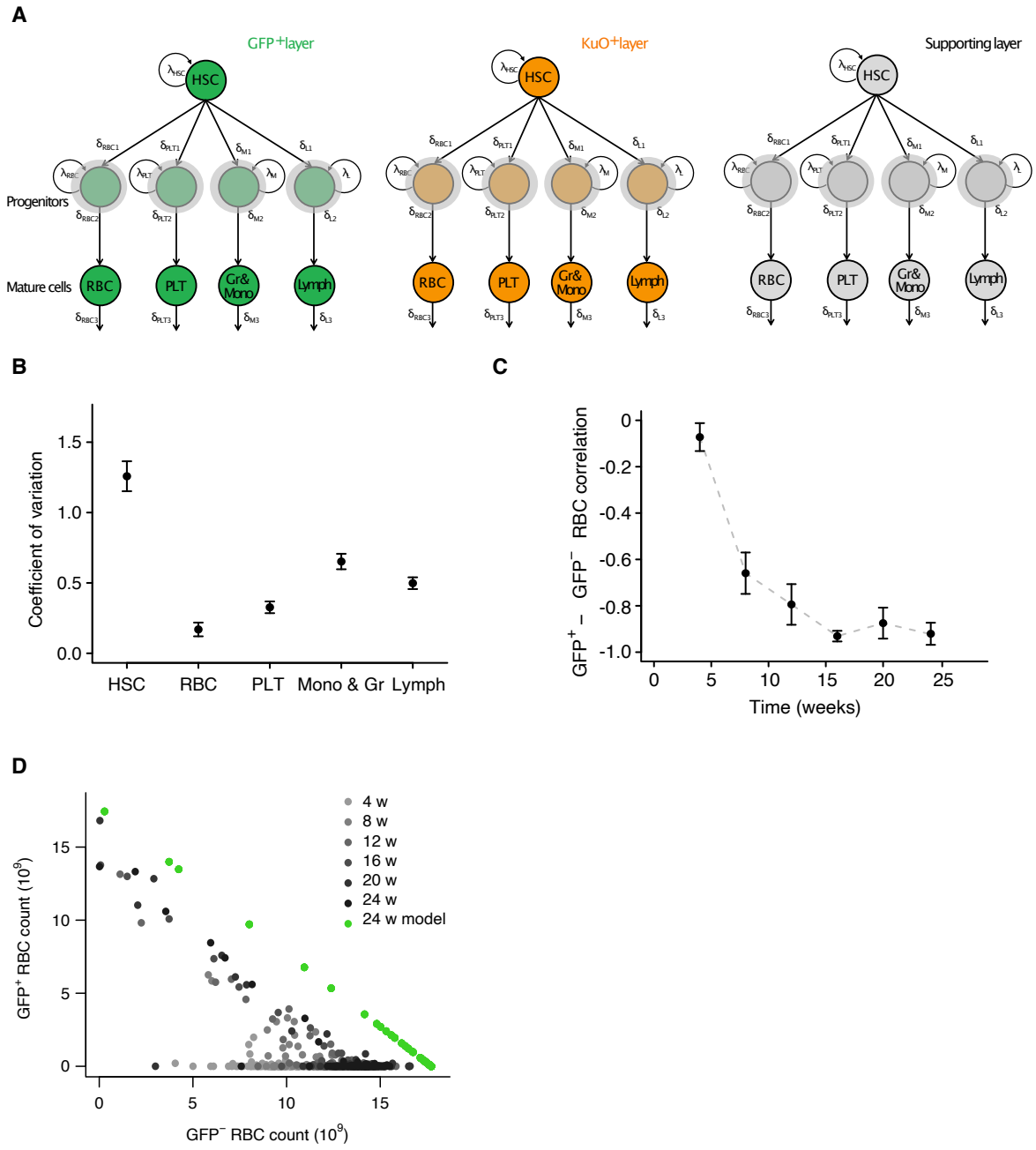


Figure 3.8. Mathematical modelling of single cell transplantation outcomes. A) Experimental scheme of mathematical model, including three layers of experimental data: reconstitution from GFP⁺ single HSC, reconstitution from KuO⁺ single HSC (in co-transplantation cases), and reconstitution from supportive bone marrow cells. λ indicates proliferation/self-renewal rates, while δ indicates differentiation rates. **B)** Coefficient of variation observed in different hematopoietic populations after single cell transplantations. **C)** Correlation coefficient between the label (GFP⁺) and unlabeled (supportive bone marrow) layers over time for the RBC compartment. **D)** Absolute RBC counts from the unlabeled or labeled layers at different weeks (w) post-transplantation, as well as predicted by the mathematical model. RBC= red blood cell, PLT= platelet, Gr= granulocyte, Mono= monocyte, Lymph= lymphocytes

Figures were made by Tamar Nizharadze.

3.6. Lineage biases can be compromised by modulating the neighboring HSC activity

The fact that supportive bone marrow cells play an essential role in the reconstitution outcome has significant implications for understanding HSC behaviors, as that would suggest that the functional output of individual stem cells would be, at least partially, determined by the activity of the surrounding HSCs. Building on my previous observation, which highlighted reconstitution kinetics as the most accurate surrogate of HSC functional outcomes, I hypothesized that slow-engrafting HSCs might seem "myeloid-biased", since supportive bone marrow fast clones may have filled the mature blood cell lineages to the limit of their compartment. Myeloid lineages turn over more rapidly than lymphoid, hence slow-engrafting clones first contribute to myeloid output, and appear biased towards this lineage. This hypothesis is illustrated in **Figure 3.9**, where the combined differentiation output from fast- and slow-engrafting HSCs fills each blood cell compartment to its maximum size. Thereby, biases arise as a consequence of the type of kinetics and the "competition" among all transplanted HSCs.

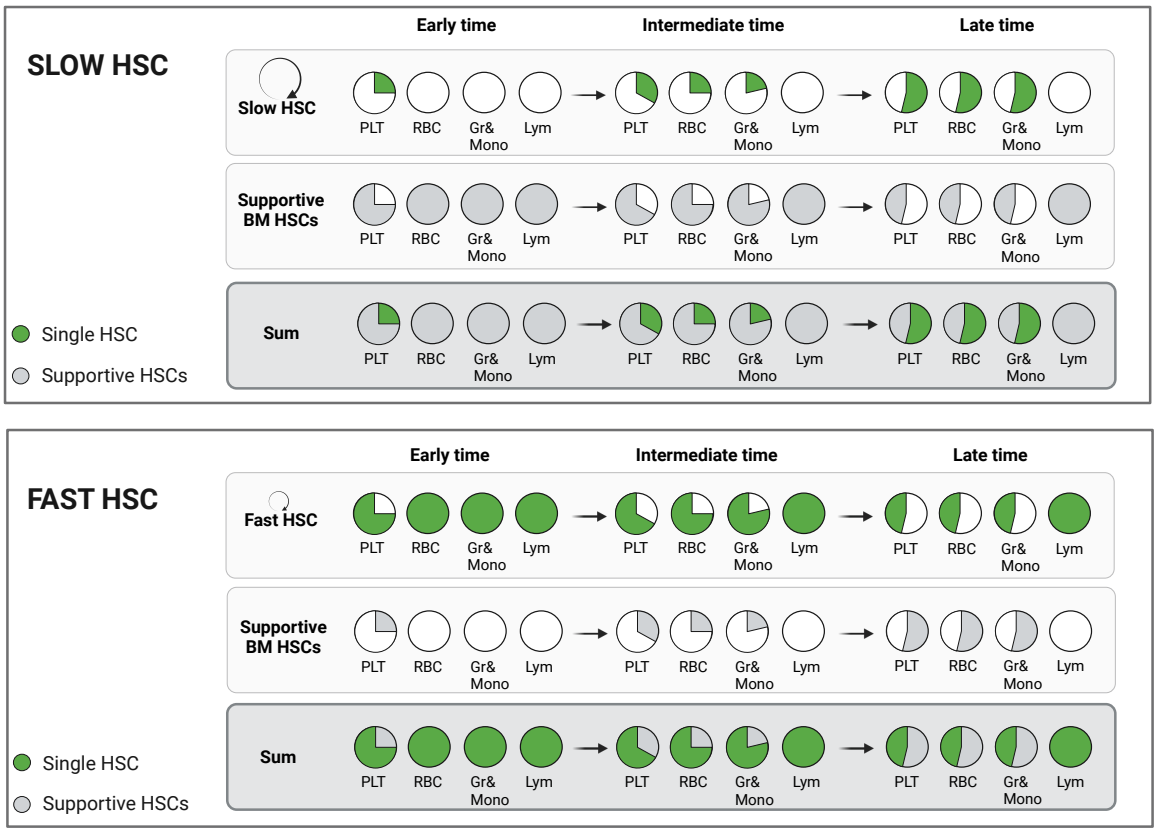


Figure 3.9. Single HSC functional outcome is determined by the activity of the neighboring HSCs. Fast HSCs repopulate all mature populations early on until their absolute capacity. Slow-engrafting clones initiate the reconstitution with a delay, when fast clones have exhausted. Since the myeloid lineage has a faster turnover than the lymphoid, this is the first lineage to be generated, making slow clones seem myeloid-biased.
Image created using Biorender.

In order to formally interrogate this hypothesis, I utilized a *Rag2*$^{-/-}$ (= Rag2 KO) mouse model, which lacks mature lymphoid progeny, as supportive bone marrow and recipient mice for single cell transplantation assays. Using this model, I eliminated the potential competition to fill the lymphoid lineage, since only the GFP^{+} or KuO^{+} HSC clones would be lymphoid-sufficient. Specifically, I transplanted 134 single GFP^{+} or KuO^{+} LT-HSCs together with 1.5x10^{5} *Rag2*$^{-/-}$ derived supporting bone marrow cells into *Rag2*$^{-/-}$ recipient mice (**Figure 3.10**). Using this experimental approach, I could assess whether reconstitution properties such as the engraftment kinetics or the lineage output were influenced by alterations in the neighboring HSC activity.

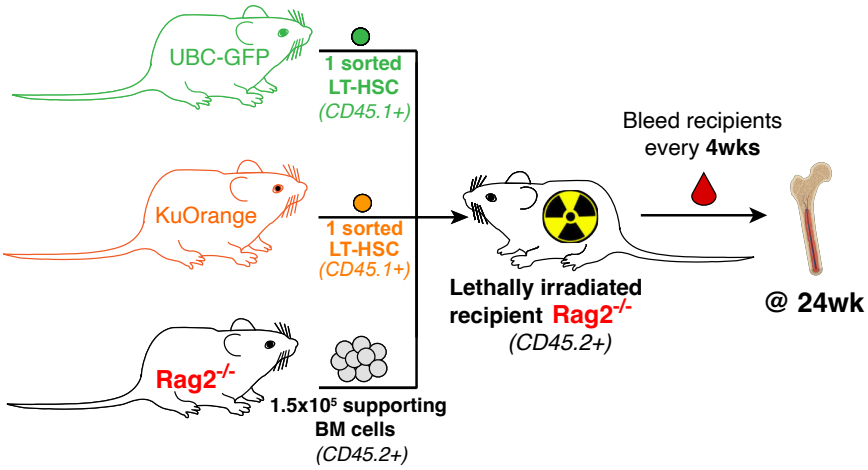


Figure 3.10. Experimental scheme for single cell transplants using *Rag2*$^{-/-}$ supportive BM and recipients. 134 single LT-HSCs derived from 6 different UBC-GFP or KuO donor mice were transplanted together with 1.5x10^{5} bone marrow cells into individual lethally irradiated recipient mice. LT-HSCs were defined by the marker combination Lin^{-} Sca^{+} cKit^{+} (LSK), CD48^{-}, CD150^{+}, CD34^{-}, EPCR^{high}. Experimental details are summarized in the methods section 7.3.2.

Consistent with previous experiments using WT mice (**Figure 3.3**), I was able to identify fast and slow reconstituting clones, suggesting that repopulation dynamics are mostly an intrinsic feature of HSCs (**Figure 3.11**). However, I no longer observed canonical "myeloid-biased" outcomes, as all clones were able to contribute to some extent to the production of the

lymphoid lineage. As shown in **Figure 3.12A**, HSCs mostly generated lymphocytes when transplanted with lymphoid-deficient supportive bone marrow. In specific instances, such as in *Rag2*$^{-/-}$ recipient mouse #1, #2 and #3, there was a predominant production of myeloid cells. It is worth noting that these particular mice exhibited positive engraftment from both the GFP^{+} and KuO^{+} clones, and one of them consistently generated the lymphoid arm. This would therefore explain why the other clone appeared primarily myeloid, as competition exists in this case. This observation reinforced the idea of competition between bone marrow HSCs to fill each mature cell compartment to its absolute size.

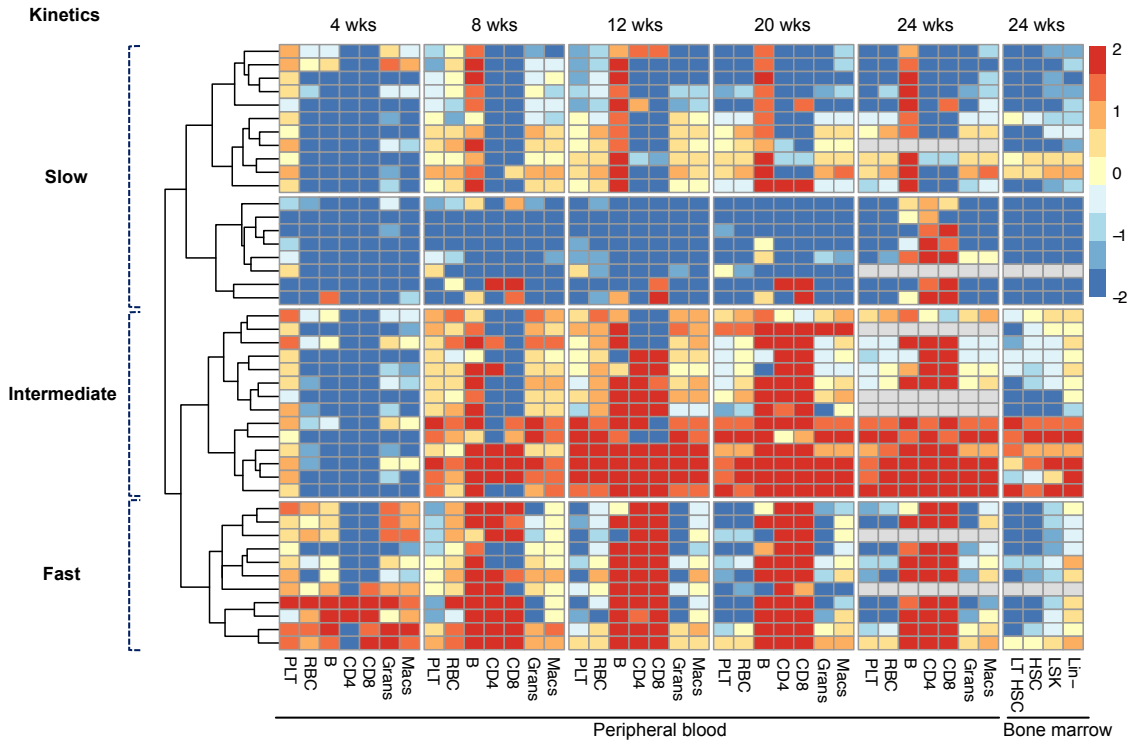


Figure 3.11. Slow and fast reconstituting kinetics were still present when transplanting single HSCs with lymphoid-deficient supportive bone marrow cells. Heatmap illustrating the percentage of chimerism in peripheral blood at different timepoints (4-, 8-, 12-, 20-, 24-weeks) post transplantation and in the bone marrow at the endpoint (24 weeks). Each row represents a single HSC transplantation that had positive chimerism at any timepoint. 90 mice were not included in the anlysis as they remained GFP/KuO negative. An unbiased clustering segregates the clones based of their reconstitution kinetics (slow, intermediate and fast). PLT: platelets, RBC: red blood cells, B: B cells, CD4: CD4^{+} T cells, CD8: CD8^{+} T cells, Grans: Granulocytes, Macs: Macrophages.
(n=44 clones; Agglomerative clustering, named AGNES (AGglomerative NESting) was used).

Single clones with varying reconstitution kinetics (slow vs fast) were assessed for their contribution to the lymphoid and myeloid lineages (**Figure 3.12B**). In regular single cell transplantations using wild type C57BL/6 mice (B6), fast-reconstituting clones sustained

lymphoid production until the endpoint, whereas slow clones had none or limited lymphoid production, therefore appearing myeloid-biased. This phenomenon was clearly impacted by modulating clonal competition, as when using *Rag2*$^{-/-}$ mice both slow and fast clones significantly contributed to lymphopoiesis and decreased their differentiation bias from the myeloid lineage (**Figure 3.13**). Collectively, these findings suggest that the lineage output of individual HSCs is determined to a high extent by the activity of the surrounding HSCs.

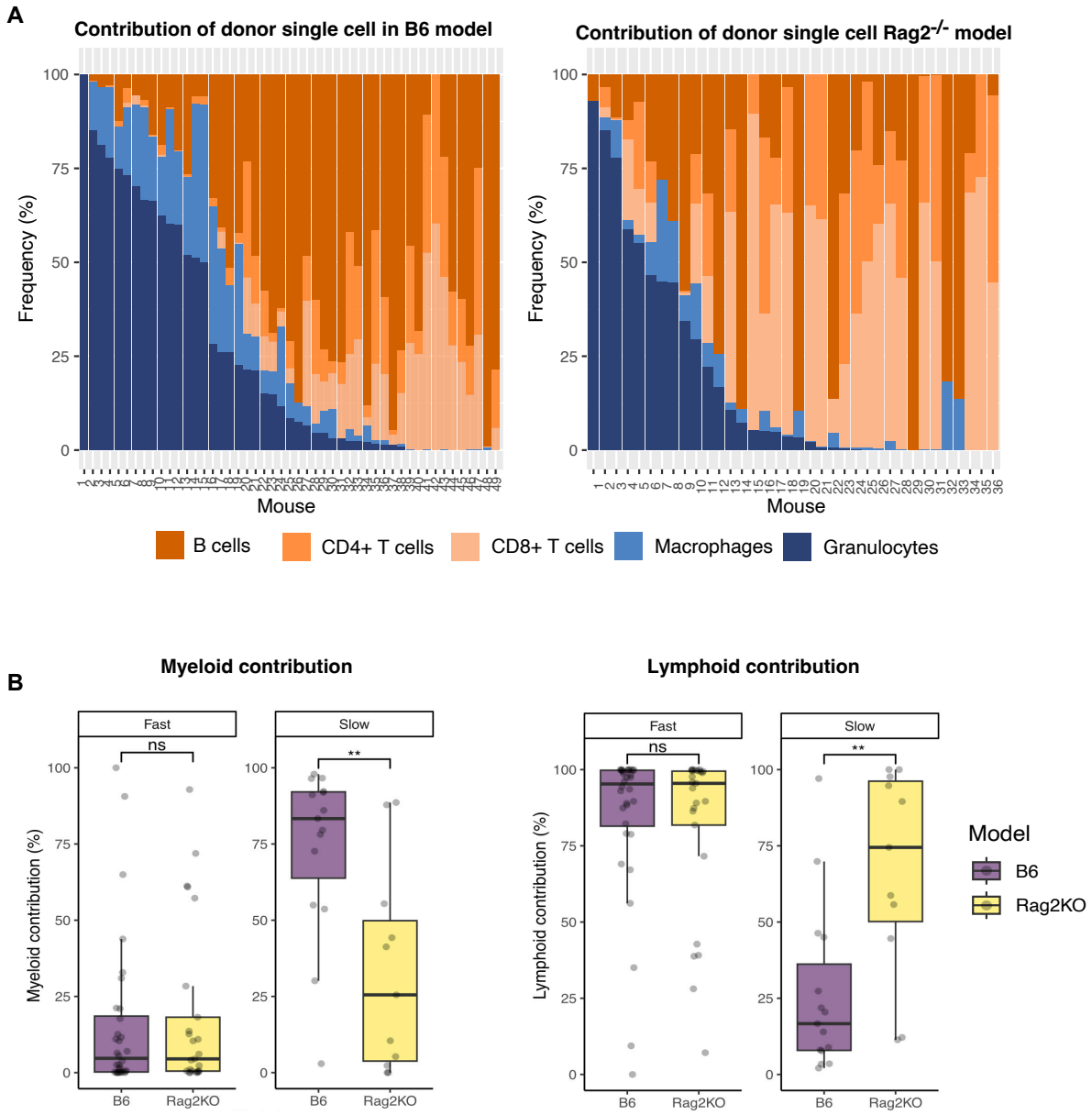


Figure 3.12. HSC lineage biases are modulated by the presence of *Rag2*$^{-/-}$ HSCs with impaired lymphoid differentiation. A) Percentage of B cells, CD4^{+} T, CD8^{+} T, granulocytes and macrophages derived from a single GFP^{+} or KuO^{+} transplanted HSC at 24 weeks post-transplantation when using *Rag2*$^{-/-}$ supportive bone marrow and recipients (right) or using B6 strain as recipients and supportive bone marrow (left). **B)** Myeloid and lymphoid contributions of single HSCs with either fast or slow reconstitution, when supportive bone marrow cells and

recipient mice are wild type B6 or *Rag2*$^{-/-}$.

(n=36-49 mice per group. Data in B were analyzed using an unpaired two-samples Wilcoxon test. Significant differences between specific groups are denoted by asterisk (* p<0.05, **p<0.01, ***p<0.001). ns indicates non-significance).

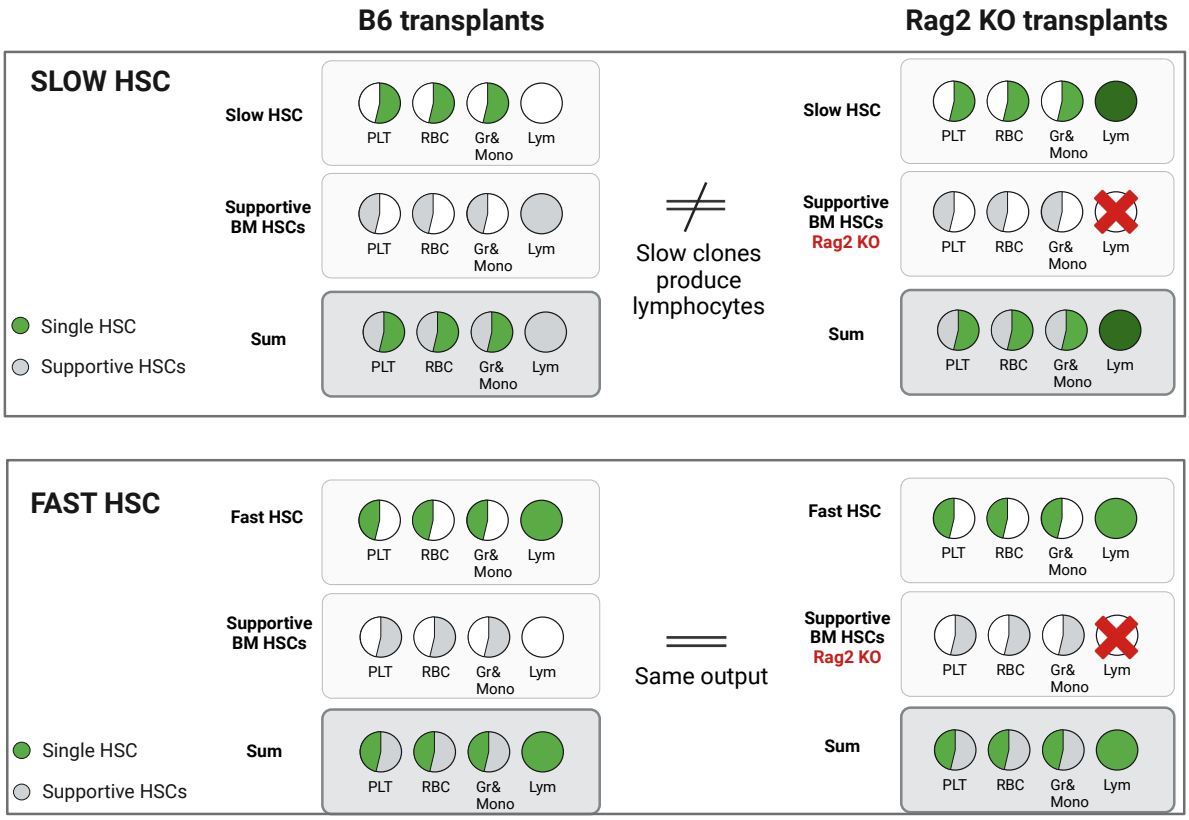


Figure 3.13. HSC outcomes with WT or *Rag2*$^{-/-}$ supportive BM environment. Slow clones showed limited contribution to lymphopoiesis in transplantations into B6 mice. In contrast, transplantations with lymphoid-deficient (*Rag2*$^{-/-}$) supportive HSCs pushed slow clones to generate the lymphoid compartment to reach homeostasis in the hematopoietic system. On the other hand, fast clones, which produced lymphocytes in standard transplantations into B6 mice, remain the same in the *Rag2*$^{-/-}$ experimental model.

Image created using Biorender.

4

Discussion project I

4.1. Deconvoluting the heterogeneity within the HSC compartment

Numerous studies in recent years have unveiled significant functional and molecular diversity within the HSC pool[10]. This diversity extends to their capacity for self-renewal and differentiation into various hematopoietic lineages, which are the defining characteristics of stem cells within the hematopoietic hierarchy. In terms of self-renewal potential, HSCs have been shown to be variable in the extent to which they can sustain the production of mature blood cells after transplantation[3]. Long-term and short-term HSCs, as well as multipotent progenitors (MPPs) have been described, and isolated using a combination of cell surface markers that enriched for these specific populations. Further investigations at the single-cell level, including single cell transplantations and barcoding experiments, have revealed even greater functional diversity within the long-term HSC population[25,31,33,34].

The multipotent capacity of HSCs is also highly diverse, with evidence of biases towards specific lineages within the hematopoietic system. The group of Hiromitsu Nakauchi identified HSCs with long, intermediate or short reconstitution potential, as well as a subset of cells exclusively differentiating into the myeloid lineage, termed myeloid-restricted progenitors[33,102]. Initial studies from Connie Eaves laboratory categorized HSCs as myeloid-biased (α), balanced (β), and lymphoid-biased (γδ)[34,103]. More recent research has identified platelet-biased clones, which are particularly present in HSCs expressing high levels of the Von Willebrand factor (Vwf)[36,39]. Notably, lymphoid-biased HSCs exhibited limited self-renewal potential across all different studies, denoting a less potent population compared to balanced and myeloid-biased stem cells. Another remark related to lymphoid-biased clones is

that despite having a final production of lymphoid cells, they also generate myeloid cells early in the reconstitution process but are unable to sustain this production until the endpoint. Balanced and myeloid-biased HSCs have shown substantial self-renewal potential. A seeming contradiction in these studies is the detection of myeloid-restricted HSCs showing the highest self-renewal and even being able to convert to a multilineage balanced output in secondary transplantations. This challenges the classical notion of multipotency as an essential property of HSCs. Therefore, the link between lineage biases and self-renewal, as well as overall functional potency, remains unclear.

4.2. Reconstitution kinetics explains reported lineage biases and predicts stem cell functional potency

In this project, I undertook a broader and more comprehensive approach to study the functional potency and behavior of individual HSCs. Unlike previous studies that focused solely on the final timepoints post-transplantation, I assessed HSC functionality at multiple timepoints to capture the dynamic nature of clonal behavior. The rationale behind this approach was to avoid missing relevant information regarding clonal dynamics that would be overlooked when looking at only one timepoint. Additionally, the study aimed to identify parameters differentiating HSC functional heterogeneity, as opposed to relying on classical definitions based on arbitrarily-defined cutoffs or categories, such as myeloid-biased, balanced, or lymphoid-biased HSCs. Indeed, it is evident in these studies that the clones falling into the same category are significantly different to each other. Therefore, I aimed to uncover additional layers of heterogeneity that had been previously ignored in studies assessing HSC functional heterogeneity.

An unbiased and time-wise analysis of HSC clonal reconstitution revealed a novel parameter, the reconstitution kinetics, as the most significant parameter describing stem cell functional diversity. Large-scale single cell transplantations with detailed reconstitution analysis across various timepoints post-transplantation uncovered differences with regards to the time at which HSCs begin their differentiation process, their duration of blood production, and time to exhaustion. Consistent with previous literature, I also identified at the endpoint analysis HSCs with multilineage balanced output, and others with exclusive generation of

lymphoid or myeloid cells, correlating with the described biased HSCs. Nevertheless, as hypothesized in this thesis, lineage biases result from snapshots of the clone at a single timepoint. In my data set, kinetics of reconstitution showed significant correlation with stemness properties, such as self-renewal potential, as well as with detectable lineage biases at the final analysis. Clones with fast reconstitution exhibited signs of exhaustion, showing none or limited self-renewal, and were unable to sustain myelopoiesis over the whole timeframe of analysis, thereby appearing as lymphoid-biased. HSC clones with an intermediate pace of reconstitution retained some self-renewal potential and generated both lineages until the endpoint. In contrast, the slowest clones exhibited the highest self-renewal and only showed myeloid production due to their slow nature. The interpretation from this data suggested that the final lineage output (myeloid, lymphoid or balanced) is caused by the type of reconstitution kinetics of the clone. Of note, depending on the timepoint, the HSC clone might exhibit a different differentiation profile to the classical categorization (**Figure 4.1**). Taken together, I propose kinetics of reconstitution as a novel feature of HSCs capable of predicting their functional potential and explaining observed lineage biases.

This interpretation is supported by existing literature on single cell transplantations studies, which demonstrate differences in the time at which HSCs start to differentiate[33,34,36,104]. Moreover, barcoding studies have also identified HSCs with a so called "low output" or "high output"[105]. Although these definitions do not rely on kinetics data, it could be hypothesized that slow clones correlate with "low output" clones, displaying high HSC chimerism and low differentiation rate, while fast clones correlate with "high output" HSCs with limited self-renewal potential.

Differential reconstitution kinetics have also been reported in human studies tracking the activity of genetically-engineered hematopoietic cells in gene therapy (GT)-treated patients after hematopoietic stem cell transplantation (HSCT)[106]. These studies identified subpopulations involved in the initial engraftment, early phase of reconstitution or long-term steady-state hematopoiesis, therefore denoting HSC with different activity kinetics. Interestingly, the dynamics of reconstitution also determined the overall potential or self-renewal of the HSC clones, with faster clones exhausting first. This aligns with the data in this thesis linking higher rates of blood reconstitution to faster loss of functional potential.

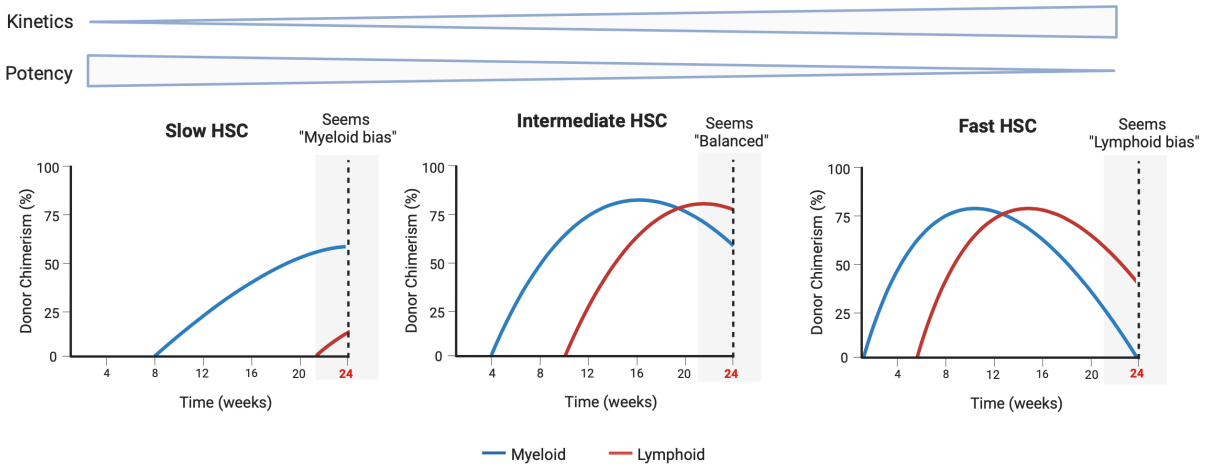


Figure 4.1. Reconstitution kinetics correlates with final lineage outputs. Schematic illustrating how the chimerism of myeloid (blue) and lymphoid (red) populations varies over timepoints of analysis. Analyses at 24 weeks post-transplantation in previous studies suggest that HSC can be myeloid-biased, balanced, or lymphoid-biased. Instead, our kinetics-based analysis demonstrates different paces of hematopoietic reconstitution, determining the type of lineage output.
Image created using Biorender.

4.3. HSC heterogeneity is best explained by a continuum rather than discrete categories

In an attempt to deconvolute the heterogeneity of the HSC pool, broad categories have been described, such as the dichotomy of short-term and long-term HSCs, or the HSC categories based on lineage biases. In this thesis, I also report HSCs with slow, intermediate or fast reconstitution kinetics. However, it is worth noting that within any of these groups, there is still high functional diversity. In fact, no clone was identical to another in terms of reconstitution kinetics. Therefore, instead of describing the heterogeneity with discrete groups, the HSC compartment is best represented by a continuum transitioning from slow to fast reconstitution. While utilizing individual groups is useful for broadly examining statistical differences between fast and slow clones, there is a need to develop quantitative metrics describing the kinetics of the clones. This approach would involve ordering the clones within the continuum landscape of the HSC compartment, rather than assigning them to specific categories (**Figure 4.2**).

Despite not presented in this thesis, I have recently collaborated with Florian Grünschläger (Division of Stem Cells at the Interface of Hematopoiesis, Immunity and Cancer, HI-STEM), to model the data shown in this thesis and extract parameters that describe reconstitution kinetics. This work is beyond the scope of my thesis; however, it will enable us to quantify the time an HSC requires to initiate the reconstitution of peripheral blood cells, the duration of sustained blood production and the time until clonal exhaustion. By establishing correlations between the kinetics parameters and lineage biases and stemness properties, I will be able to quantitatively predict functional outcomes based on kinetics.

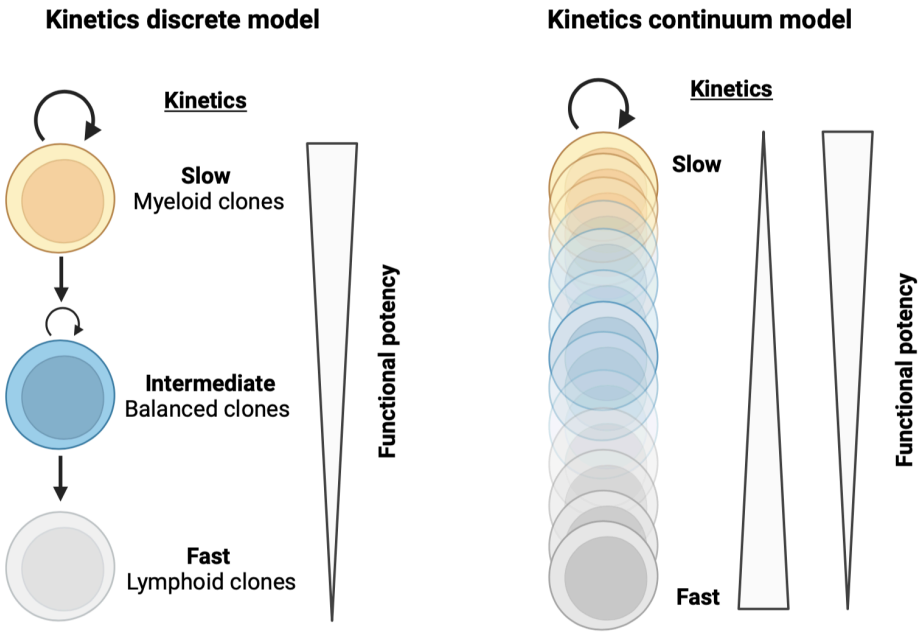


Figure 4.2. Discrete or continuum transitions from slow- to fast-reconstituting clones. My data is best described by a continuum of HSC clones transitioning from slow to fast reconstitution, correlating with loss of functional potency, instead of through discrete stages.
Image created using Biorender.

4.4 Self-renewal compromises the functional potency of HSCs

Self-renewal is a fundamental feature of HSCs, theoretically enabling them to replicate and generate daughter cells with identical self-renewal and multipotent capacity. However, current research challenges the traditional notion of HSCs possessing unlimited potential to replicate and sustain the hematopoietic system. In this project, I aimed to address this question using a paired single cell transplantation approach, in which parent and progeny were

interrogated individually in a transplantation setting. This approach significantly differs from previous research in the field. Previous single cell transplantation studies tested self-renewal potential through secondary bulk transplantations, involving millions of cells, rather than transplanting single cells into secondary recipients[33,34]. This difference is crucial, as bulk secondary transplantations only address the combined output of multiple daughter HSCs derived from a single clone. On the contrary, I was able to interrogate the potency of single daughter HSCs and compare them to the parent HSC. The same experimental limitation applies to previous barcoding experiments, in which secondary transplantations tracked all HSC progeny derived from the original clone[105].

The difference in my experimental design likely explains the contrasting findings. While previous studies have claimed that HSCs often preserve their functional potency and lineage bias, my data demonstrates that individual daughter HSCs are unable to preserve the same functionality as the parent. This disparity is likely to be attributed to the dosage of cells transplanted into secondary recipients. While a single daughter HSC might not possess sufficient potency to recapitulate the outcome of the parent, the combination of several daughter HSCs might reach or even exceed the functional potency of the parent (**Figure 4.3**). This phenomenon is likely to be influenced by the number of divisions that HSCs undergo. In a bulk transplantation of a few million cells, only a certain proportion of HSCs will divide, retaining many HSCs fully functional. However, in a secondary single cell transplantation, the single cell must independently reconstitute the entire blood system, necessitating multiple cell divisions. In barcoding experiments, the pressure on HSCs to divide and repopulate the blood system is even less significant, as there are many HSCs as part of the graft already in the primary transplantation.

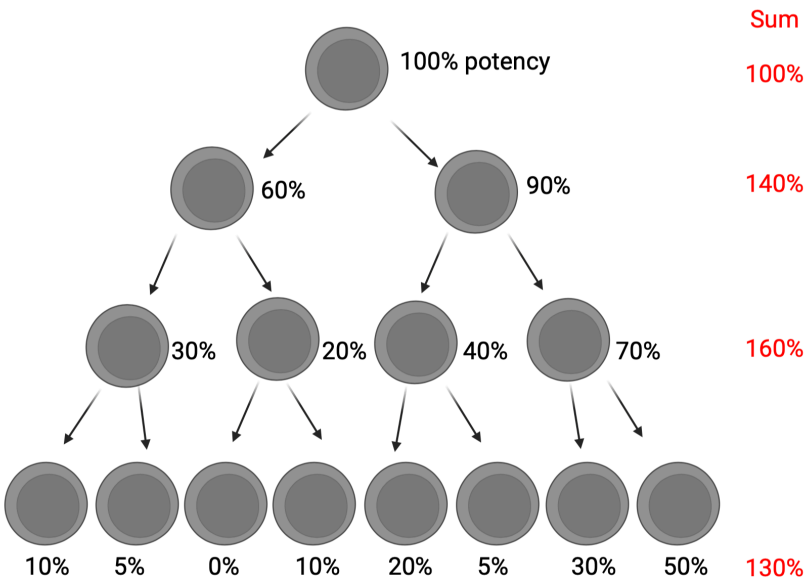


Figure 4.3. Schematic of the changes in potency with HSC division. Self-renewal divisions reduce the functional potency of individual daughter HSCs, however the combined functional potency (sum) of all daughter HSCs may exceed that of the parent.
Image created using Biorender.

Another variable which might have influenced the degree of HSC exhaustion in secondary transplantations is the type of conditioning in the recipient mice. While I used lethal irradiation conditioning, which depletes the whole bone marrow before transplantation, other studies have used sublethal irradiation in c-kit-deficient recipients as their conditioning regimen[34,103], which is known for being less stringent. When milder conditioning is used, resident cells from the host may persist and contribute to hematopoiesis, thereby reducing the demand on transplanted cells to divide and repopulate the blood system.

In addition to the sustained functional potency, daughter HSCs have been shown to exhibit similar patterns of reconstitution as their parent. For instance, myeloid-biased and balanced HSCs were able to maintain their phenotype in secondary transplantations. Notably, they could also interconvert phenotypes, and occasionally exhaust giving rise to lymphoid-biased HSCs. Conversely, I never saw transitions from balanced to myeloid-biased HSCs, or in other words, a backwards transition from fast to slow reconstitution kinetics. Instead, my data consistently showed unidirectional transitions. The variance in these findings is likely due to the high cell dosage in previously published secondary transplantation experiments.

The concept of HSCs losing functional potency upon self-renewal is in line with other studies from our laboratory and other groups, albeit employing different experimental approaches[107–109]. Our group has also shown that the loss of HSC functional potency is an irreversible process when HSCs are pushed to divide upon repetitive exposure to inflammatory agents[108]. This idea supports the unidirectionality in my data, transitioning only from slow (potent) to fast (exhausted) HSCs. Moreover, recent studies have proposed potential mechanisms underlying the loss of functionality in HSCs, such as dysfunctional mitochondrial inheritance to daughter cells or remodeling of the methylation landscape[109,110]. However, the precise mechanism triggering the decline in HSC functional capacity remains unclear and may result from a combination of different factors. Although this has not been addressed in this thesis, it is an interesting research question to investigate in the future.

4.5. Investigating the factors determining HSC functional outcomes

The existence of heterogeneous outcomes in clonal functional assays is widely accepted and confirmed in this thesis. However, the exact mechanisms governing this diversity remain unclear. Previous studies have focused on assessing transcriptomic and epigenetic programs that underlie the heterogeneity of the HSC pool. Conventional immunophenotypic markers used to isolate HSCs have shown a certain degree of correlation with HSC self-renewal and lineage biases. For instance, EPCR positivity and CD34 negativity are associated with the overall potency of stem cells[16]. CD150 expression or Hoechst dye flux, on the other hand, have been linked to myeloid-biased outcomes in transplantation settings[111,112]. Additionally, single cell transplantations of LT-HSCs expressing high levels of Vwf resulted in a higher proportion of platelet-biased HSCs than observed in other studies, thereby proposing Vwf as a marker enriching for HSCs with megakaryocyte priming[36,39].

More recent studies have conducted a more comprehensive analysis of the transcriptome, methylome, or chromatin accessibility in HSCs with defined functional outputs. Barcoding experiments from the group of Fernando Camargo demonstrated that TCF15 expression segregates HSCs with low or high differentiation output[105]. While gene

expression programs had been proposed for the megakaryocyte and myeloid branch, no detectable changes were proposed for the lymphoid bias.

Further studies have investigated the role of epigenetic lineage priming in HSCs using whole-genome bisulfite sequencing (WGBS) and Assay for Transposase-Accessible Chromatin using sequencing (ATAC-seq) assays[40,113]. These studies have revealed an even greater role of the epigenome compared to the transcriptome in regulating HSC lineage priming, identifying differences in accessibility of lineage specific upstream regulatory elements in HSCs with specific fate restriction[40,113]. Collectively, these studies have underscored the importance of examining the epigenome. While multipotent states are reported based on transcriptomic analysis, lineage constraints may be imprinted at the epigenome level.

Prior research has primarily focused on intrinsic programs of HSCs underlying the functional outcomes, however, there is limited knowledge regarding extrinsic influences on HSC functionality. In my thesis, I detected a degree of cooperation between the single transplanted HSC and the remaining HSCs derived from the supportive bone marrow in repopulating the hematopoietic compartment of recipient mice. My data suggest compartment size limitations in every mature blood cell population, which feedback to upstream populations of the hematopoietic hierarchy to regulate their activity (**Figure 4.4**). This implies a model in which HSC activity is regulated by the demand to produce peripheral blood cells. Consequently, when populations reach their maximum size, the activity of certain HSCs may be reduced, indicating that HSC functional outputs are, at least partially, determined by extrinsic mechanisms.

Experiments in this thesis involving the transplantation of single HSCs with lymphoid-deficient supportive cells (*Rag2*$^{-/-}$ model) demonstrated changes in the HSC lineage output. HSCs with slow reconstitution, which exhibited a myeloid bias when transplanted with WT supportive bone marrow, acquired multilineage capacity in the *Rag2*$^{-/-}$ setting. These experiments confirmed the influence of external cues on individual stem cell activity, representing a novel concept in our field. This is in line with recent studies confirming compensatory effects in cases of differentiation deficiencies in other HSCs[114].

Given that HSCs appear to cooperate in the bone marrow to replenish the hematopoietic system after transplantation, it could be hypothesized that the number of transplanted cells would thereby determine functional outcomes. Although not tested in this thesis, a future direction in this project would be to examine the type of reconstitution kinetics and lineage biases in single cell transplants compared to barcoding settings, where different cell dosages are transplanted. In line with this concept, a recent publication demonstrated that high number of transplanted HSCs correlated with an increased number of early differentiating clones[115], corresponding to the fast-engrafting clones in my data set.

Taken together, this thesis has revealed a cell-extrinsic role in modulating the function of individual HSCs. However, it does not exclude the possibility that intrinsic programs underlie stem cell heterogeneity. It is likely to be a combination of extrinsic- and intrinsic-mechanisms that best explains the final output of a single HSC. Notably, this thesis explores cell-extrinsic feedback mechanisms, but there are likely alternative extrinsic cues involved in the heterogeneity within the HSC compartment.

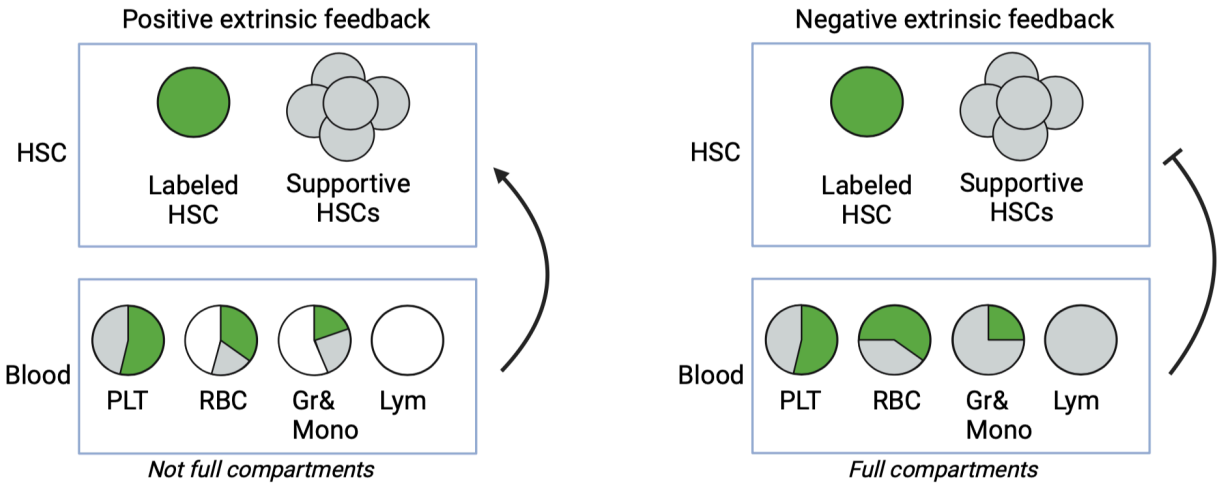


Figure 4.4. Cell-extrinsic mechanisms influencing HSC functional outcome. While unfilled peripheral blood compartments positively feedback upstream the hierarchy, full compartments will exhibit negative feedbacks on the HSCs.

Image created using Biorender.

5

Results project II

5.1. Establishing a model to study the impact of *Tet2* clonal hematopoiesis on the evolution of non-alcoholic fatty liver disease and liver cancer

In order to investigate whether *Tet2* clonal hematopoiesis modulates the development of HCC with NAFLD etiology, I employed an experimental approach consisting of two arms: induction of *Tet2* CHIP, and induction of liver damage (**Figure 5.1**). To generate a robust model of clonal hematopoiesis closely resembling the human scenario, I conducted bone marrow transplantations of whole bone marrow cells derived from a *Tet2*$^{fl/fl}$-SclCreERT2 mouse model into lethally irradiated recipient mice. The control group, without CHIP, received SclCreERT2 bone marrow cells. Once hematopoietic engraftment reached homeostasis three months post-transplantation, mice were treated for five consecutive days with tamoxifen. This treatment activated the Cre recombinase under the control of the Scl promoter, specifically in the hematopoietic stem and progenitor cell (HSPC) compartment, facilitating the knockout of the *Tet2* gene in the more primitive cells of the hematopoietic hierarchy. This aimed to mimic the acquisition of *Tet2* CHIP mutations in human HSCs.

Following the induction of *Tet2* deletion, both control and CHIP mice were further subdivided in two groups: one receiving a normal diet (ND), whereas the second group was exposed to a high caloric "Western diet" (WD) containing elevated levels of fat, cholesterol, and fructose. Disease monitoring was performed at 3-, 6-, 9- or 12-months after the initiation of the diet. With this experimental design, I aimed to explore how *Tet2* CHIP could modulate the evolution of NAFLD-HCC induced by the Western diet, thereby assessing whether the diet and *Tet2* CHIP synergize to promote cancer development.

Pilot experiments were also performed with a choline-deficient high-fat diet (CD-HFD). However, disease kinetics were significantly slower than the WD, resulting in no development of HCC by the 6-month timepoint (data not shown). Consequently, experiments involving this diet were not pursued beyond the pilot stage.

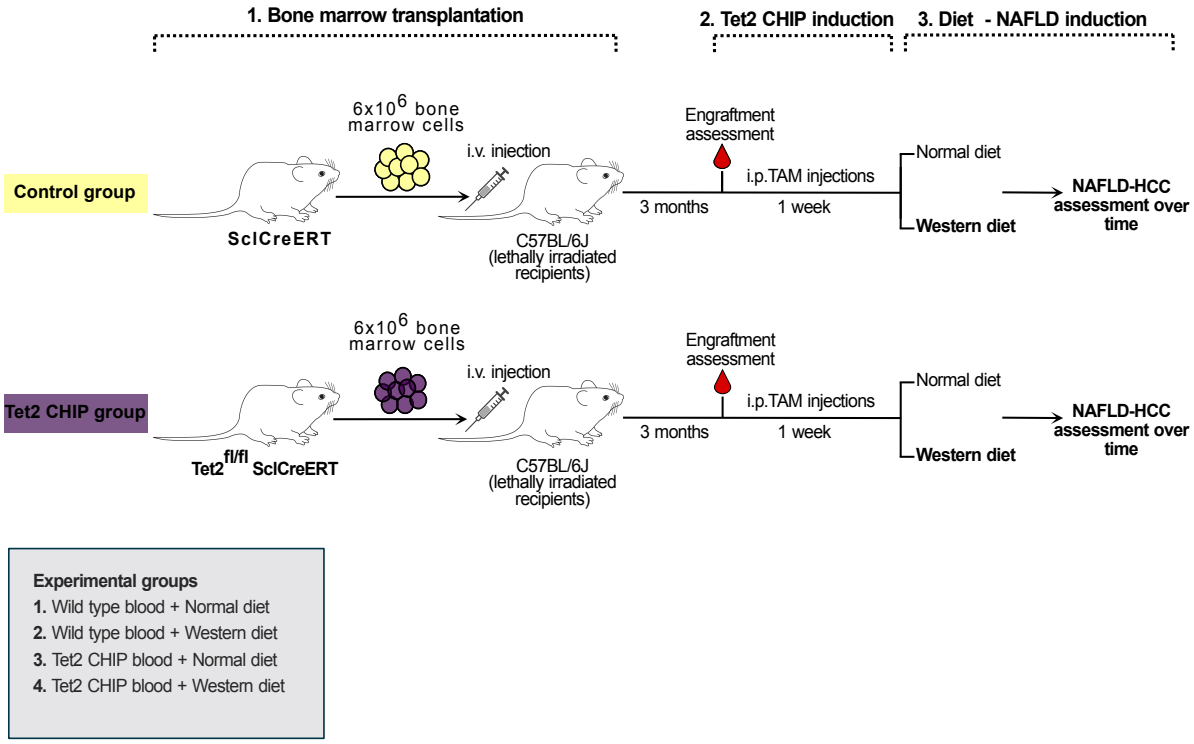


Figure 5.1. Experimental scheme for assessing the impact of *Tet2* CHIP on diet-induced hepatocellular carcinoma. *Tet2* clonal hematopoiesis was induced by performing a bone marrow transplantation of $Tet^{fl/fl}$ *SclCre* cells followed by exposure to tamoxifen during a week, able to trigger the knock out of the *Tet2* exon 3. Control group received bone marrow cells derived from the SclCre mouse line. After tamoxifen treatment, mice were either treated with a normal or high caloric "Western diet" over 3-, 6-, 9- or 12-months.

5.1.1 Validation of *Tet2* knock-out induction in the hematopoietic stem cell compartment

In order to assess the recombination efficiency of the *Tet2* allele in the HSC compartment, I FACS-sorted and cultured single LT-HSCs, expanded them in vitro for ten days, and genotyped each colony with specific *Tet2* primers able to distinguish between wild type, *Tet2*-floxed unrecombined, and *Tet2*-floxed recombined alleles (**Figure 5.2A**). I observed considerable variability in the recombination efficiency across different mice and cohorts, with an average of 25-30% variant allele frequency (VAF) (**Figure 5.2B**). Notably, the efficiency was comparable in normal and Western diet mice, suggesting that the WD does not select for *Tet2*-

$^{/-}$ clones. Surprisingly, the results revealed a notably higher prevalence of cells with heterozygous *Tet2* deletion, while clones with homozygous knock-out were rarely detected (**Figure 5.2C**).

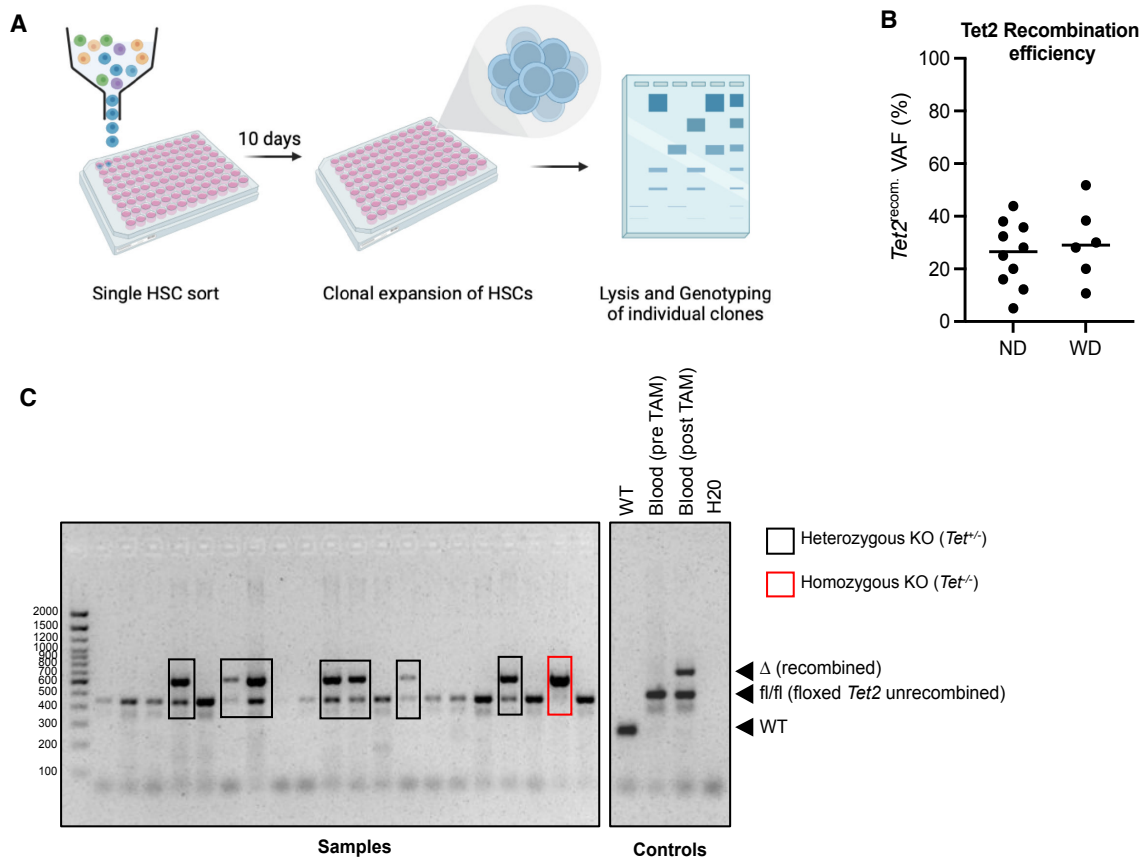


Figure 5.2. Induction of *Tet2* deletion in adult HSCs selects for heterozygosity. A) Experimental scheme for isolation and in vitro expansion of single HSCs, followed by colony lysis and genotyping PCR. **B)** Percentage of colonies with *Tet2* recombination, including heterozygous and homozygous colonies comparing mice on a normal or Western diet. **C)** Representative example of some genotyping PCRs. Controls include blood from a WT mouse (without the *Tet2*-floxed transgene), pre-tamoxifen and post-tamoxifen peripheral blood cells derived from a *Tet2*$^{fl/fl}$ SclCre transplanted mouse. Post-tamoxifen sample contains a mixture of both recombined and unrecombined cells, as recombination is never 100%. Black boxes highlight *Tet2*$^{+/-}$ heterozygous colonies, while red boxed *Tet2*$^{-/-}$ homozygous colonies.

Image A created using Biorender.

5.2. Exploring phenotypic synergy between *Tet2* CHIP and the Western diet

In order to understand whether *Tet2* CHIP contributes to the evolution of NAFLD-induced HCC, I performed a comprehensive assessment of the step-wise evolution of NAFLD, including the disease stage and HCC incidence over various timepoints.

5.2.1. Fatty liver disease development as a result of Western diet administration

Firstly, I assessed the initial development of fatty liver-related phenotypes in mice subjected to a WD. Monthly monitoring of body weight revealed a significant increase in mice fed with the Western diet compared to normal diet mice. As expected, this increase was present in both WT and *Tet2*$^{-/-}$ groups (**Figure 5.3A**). Likewise, the liver-to-body weight ratio was increased in WD mice, indicating pronounced hepatomegaly solely attributable to the administration of a high-caloric diet (**Figure 5.3B**). Moreover, cholesterol levels were significantly elevated in the serum of WD mice (**Figure 5.3C**), as anticipated due to the diet's high cholesterol content. Furthermore, I used EchoMRI for a body composition analysis, including whole body fat, lean, free water and total water masses. Western diet mice exhibited a significantly higher content of fat mass compared to mice on a normal diet (**Figure 5.3D**). As for previous parameters, this phenotype was consistent across all WD mice, regardless of their CHIP status.

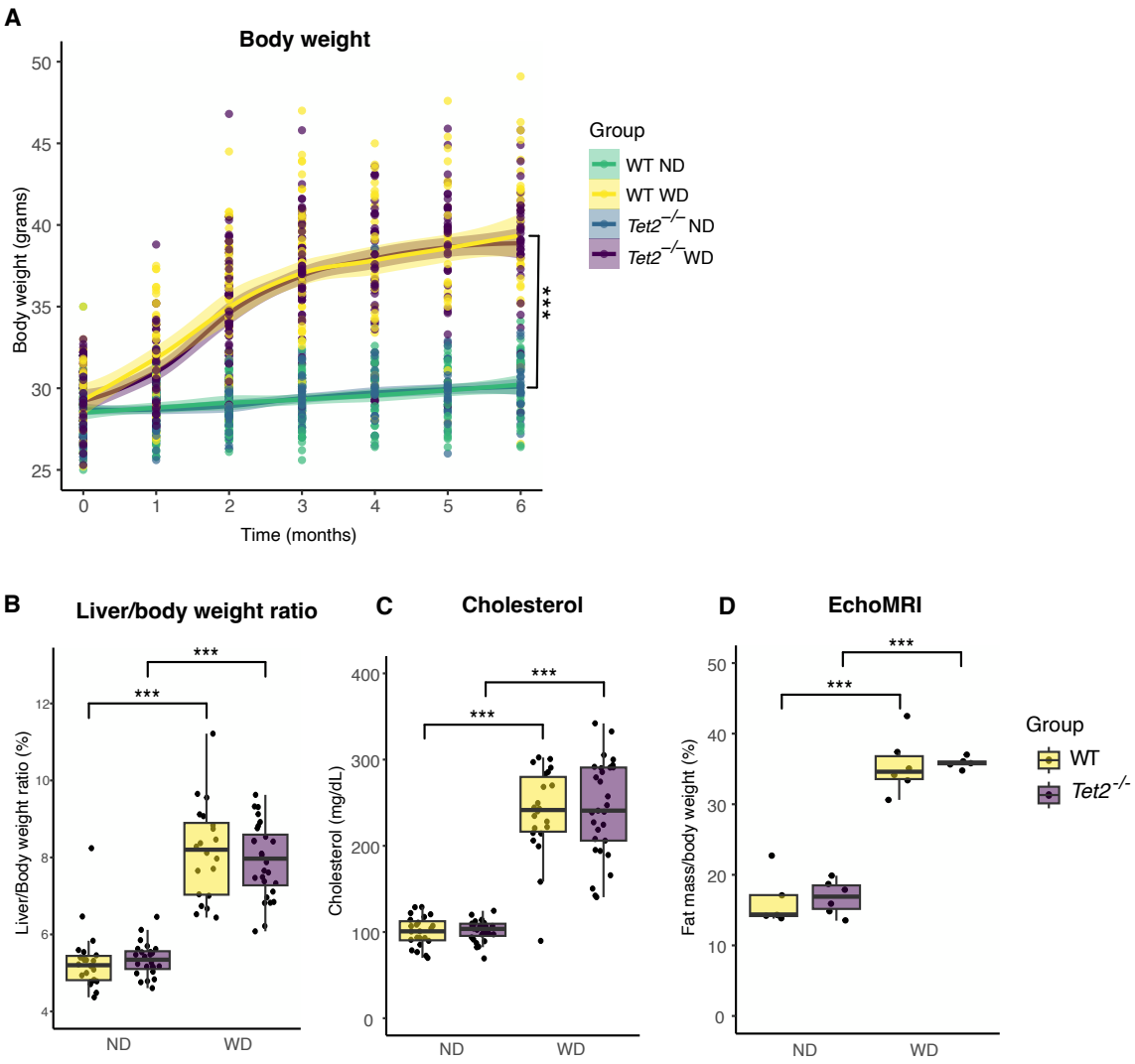


Figure 5.3. Development of obesity and hepatomegaly as a result of treating mice with a high caloric Western diet. A) Measurements of body weight at different timepoints from the start of the diets (normal or Western). Analysis at 6-months of **B)** Liver-to-body-weight ratio. **C)** Cholesterol levels analyzed in the serum of the mice. **D)** Fat mass to body weight ratio, assessed with by EchoMRI.

(n=62-73 mice per group in A, n= 5-29 mice per group in B, C, D. Data were analyzed using a two-way analysis of variance (ANOVA) followed by post-hoc multiple comparisons using the Tukey method. Significant differences between specific groups are denoted by asterisks (*p < 0.05, **p < 0.01, ***p < 0.001), only significant comparisons are indicated).

5.2.2. *Tet2* CHIP and the Western diet synergize in order to exacerbate the NAFLD phenotype

Histopathological analysis of liver sections is commonly used in clinical settings to score the severity of NAFLD and determine the disease stage. The widely used NAS score (NAFLD Assessment Score) is a common method that accounts for the degree of steatosis, lobular inflammation and hepatocyte ballooning - the latter indicating hepatocyte death due

to extensive liver damage. The criteria for this assessment are summarized in **Figure 5.4A.** The analysis of liver sections exposed to a Western diet revealed distinct histopathological alterations, as illustrated in **Figure 5.4B**. Steatosis was particularly increased in WD mice, indicating elevated liver fat accumulation—an early consequence of NAFLD pathology (**Figure 5.4D**). Moreover, both lobular inflammation and hepatocyte ballooning were increased in the WD groups (**Figure 5.4E, F**). Consequently, the overall NAS score was significantly elevated in mice fed with a Western diet compared to the normal diet groups (**Figure 5.4C**).

When comparing WT and *Tet2*$^{-/-}$ mice on a WD, I observed a synergistic increase in the NAS score as a result of combining the WD with *Tet2* CHIP. Analysis of individual NAS parameters revealed that this synergistic increase primarily stemmed from a higher scoring of lobular inflammation in *Tet2*$^{-/-}$ WD mice (**Figure 5.4E**), while hepatocyte ballooning (**Figure 5.4F**) and steatosis (**Figure 5.4D**) remained consistent across all WD-fed mice.

In summary, these findings suggest that, although all mice subjected to a WD developed NAFLD, *Tet2* clonal hematopoiesis synergized with the diet to exacerbate the liver phenotype.

Next, I measured the levels of serum alanine and aspartate aminotransferases (ALT, AST), which are known biomarkers of liver damage and hepatic injury in patients and mice[116]. This analysis demonstrated a significant increase in the levels of both enzymes in response to WD administration (**Figure 5.5**). Notably, the combination of *Tet2* CHIP and the diet showed significantly higher ALT and AST levels compared to mice with only WD. Interestingly, the levels of serum triglycerides were only significantly reduced in *Tet2*$^{-/-}$ mice upon WD, potentially due to a higher uptake into the liver to induce steatosis.

Altogether, clinically-used strategies to define NAFLD severity such as NAS score and serum biomarkers revealed a more severe stage of the liver disease in mice with *Tet2* clonal hematopoiesis, suggesting a synergistic interaction between the *Tet2*$^{-/-}$ hematopoietic cells and the WD.

A

Histological features	Score	Category definition
Steatosis	0	<5%
	1	5-33%
	2	34-66%
	3	>66%
	Plus	
Hepatocyte ballooning	0	None
	1	Few
	2	Many
	Plus	
Inflammation	1	1-2 foci per *20 field
	2	2-4foci per *20 field
	3	>4 foci per *20 field
NAS total 0-8		

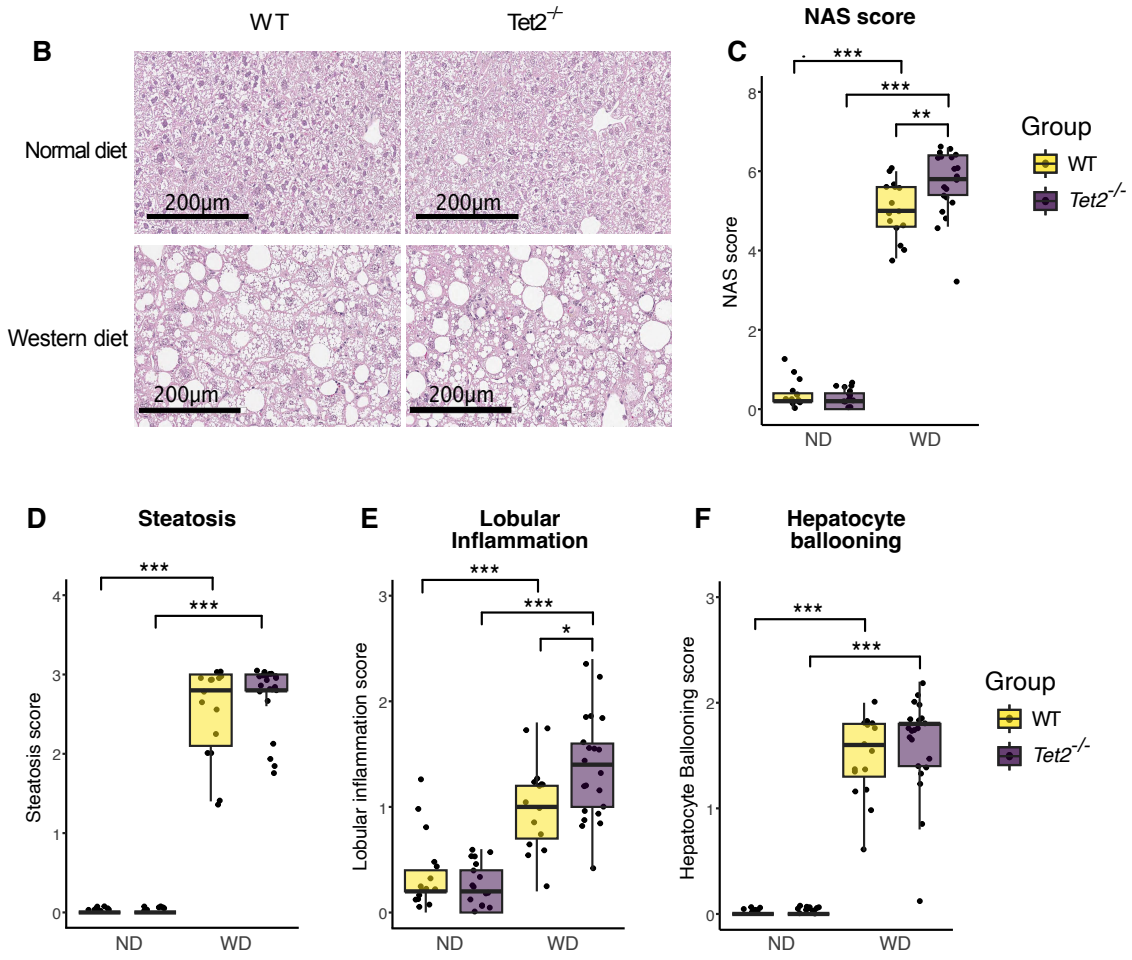


Figure 5.4. Histopathological analysis of liver sections to assess NAFLD stage. A) NAS scoring system, segregating the three parameters to be scored: steatosis, hepatocyte ballooning and inflammation. **B)** Representative example of hematoxylin and eosin (H&E) staining of liver sections from the four experimental groups. **C)** NAS score and **D)** steatosis, **E)** lobular inflammation and **F)** hepatocyte ballooning scores. Analysis corresponds to 6-months endpoint. (n=15-24 mice per group. Data were analyzed using a two-way analysis of variance (ANOVA) followed by post-hoc multiple comparisons using the Tukey method. Significant differences between specific groups are denoted by asterisks (*p < 0.05, **p < 0.01, ***p < 0.001), only significant comparisons are indicated).

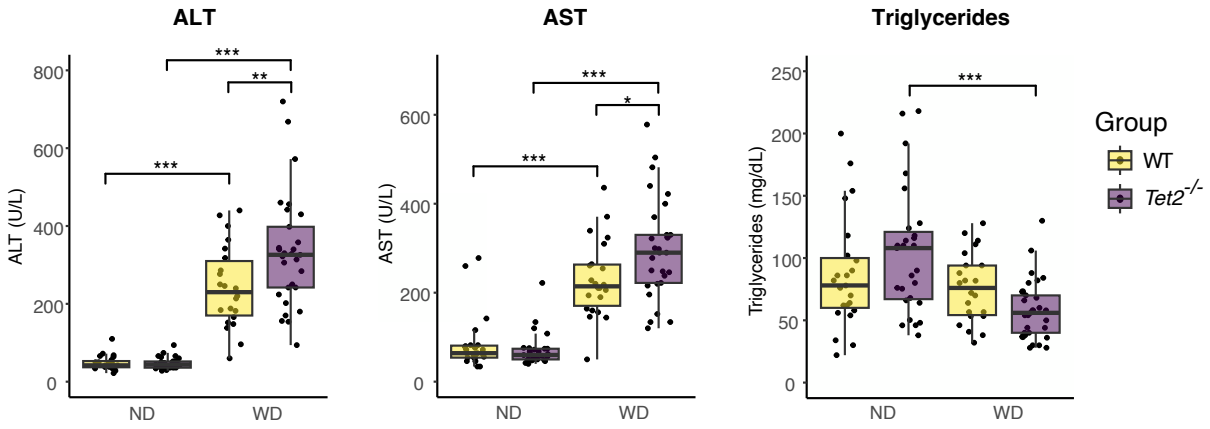


Figure 5.5. Serum levels of liver damage biomarkers. Alanine aminotransferase (ALT), aspartate aminotransferase (AST) and triglyceride levels were measured in the serum of the four experimental groups at 6-months after the start of the WD.

(n=22-29 mice per group. Data were analyzed using a two-way analysis of variance (ANOVA) followed by post-hoc multiple comparisons using the Tukey method. Significant differences between specific groups are denoted by asterisks (*p < 0.05, **p < 0.01, ***p < 0.001), only significant comparisons are indicated).

5.2.3. *Tet2* CHIP accelerates liver cancer development in WD-treated mice

Hepatocellular carcinoma (HCC) represents the final stage in the progression of NAFLD. Previous investigations have shown that regular C57BL/6 mice, subjected to prolonged exposure to high-caloric diets, develop HCC with an approximate penetrance of 25%[83]. However, the factors determining transformation within this 25% remain unclear. This resembles the human scenario, as the majority of patients with fatty liver disease never develop NASH nor HCC[117]. Here, my goal was to assess whether *Tet2* clonal hematopoiesis could accelerate or enhance the onset of HCC, thereby represent a potential risk factor for liver transformation.

HCC incidence was evaluated at 3-, 6-, 9- or 12-months from the start of the diet. A 3-month WD regimen proved insufficient for the occurrence of transformation (**Figure 5.6A-B**). However, by the 6-months timepoint, mice started to manifest liver cancer. At later timepoints spanning 9- to 12-months, the disease penetrance reached 100%. These kinetics data suggested that the optimal timeframe for detecting differences in terms of HCC development between Western diet mice with or without CHIP was at the 6-month timepoint.

Tet2 CHIP mice demonstrated a higher HCC incidence (60.61%) compared to the WT counterparts (38.46%) at the 6-month analysis. This suggests that *Tet2* CHIP can not only increase liver damage but also favor further transformation.

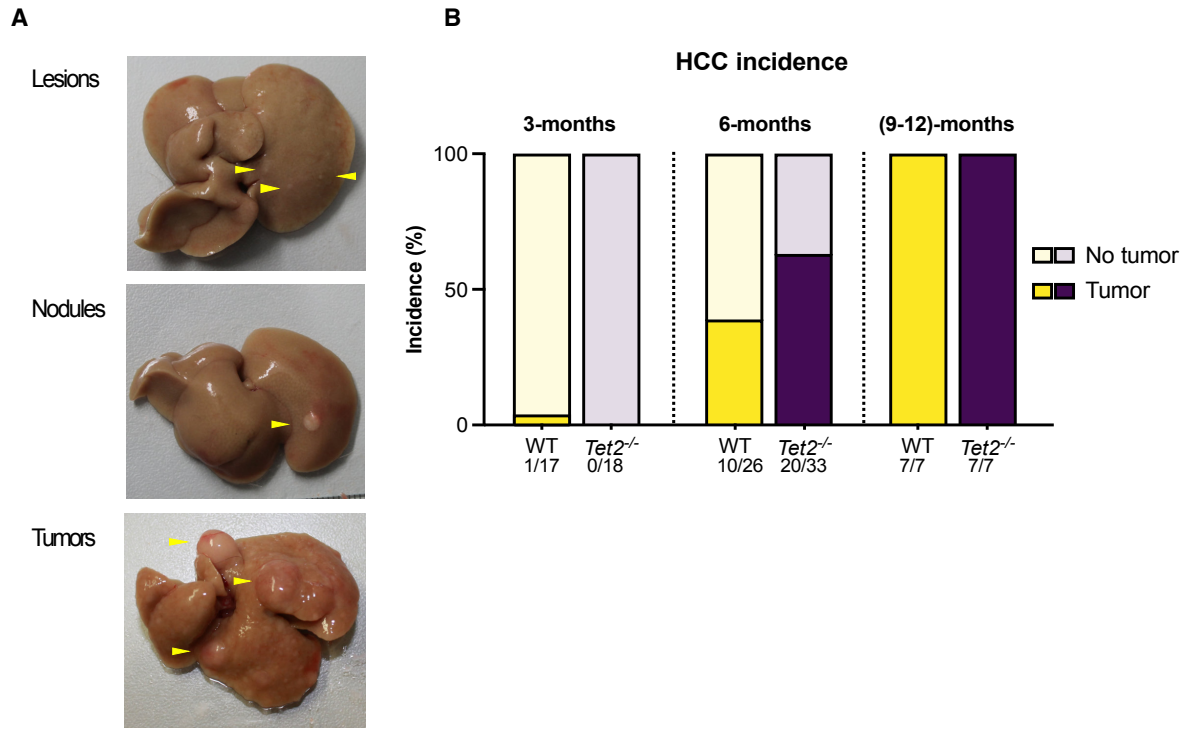


Figure 5.6. *Tet2* CHIP increased the incidence of hepatocellular carcinoma in WD-treated mice. A) Representative pictures of liver lesions, nodules and tumors observed at the 6-month diet timepoint. **B)** HCC incidence at 3-, 6-, and (9-12)-months of WD feeding, indicating below the number of HCC cases out the total analyzed mice.

5.2.4. Bulk RNA-seq of NAFLD-liver homogenates revealed molecular synergy with *Tet2* CHIP

The phenotype characterization of NAFLD was complemented by a molecular analysis of liver homogenates. Distinct molecular signatures identified in NASH livers from both human patients and mouse models hinted at their potential utility as valuable tools for investigating phenotypic changes in mice exposed to a WD, with or without *Tet2* CHIP. The experimental procedure, outlined in **Figure 5.7A**, involved isolating perfused livers, followed by tissue homogenization and RNA isolation. The isolated RNA served as input for subsequent RNA-seq library preparation. Principal component analysis (PCA) demonstrated

that the diet was able to segregate the principal component 1 (PC1), with 81.01% variance (**Figure 5.7B**). All normal diet samples clustered closely with minimal variance, whereas the *Tet2* status introduced a slight separation among samples from WD mice, particularly along PC1 and PC3. Still, the presence of *Tet2* CHIP did not emerge as a strong factor determining any of the principal components.

To delve deeper into the molecular landscape, I next ran a differential gene expression (DEG) analysis between the WT WD and *Tet2*$^{-/-}$ WD groups. This analysis aimed to explore the influence of *Tet2* CHIP in a model of diet-induced liver damage. Results unveiled various differentially expressed genes, with a focus on collagens and fibrillins—integral components of the extracellular matrix (ECM) associated with liver fibrosis and cirrhosis in NASH livers.

Interestingly, the expression of collagen genes (*Col5a1*, *Col5a2*, *Col5a3*, *Col3a1*, *Col6a2*) and the fibrillin gene (*Fbn1*) were significantly upregulated in *Tet2*$^{-/-}$ WD samples compared to their WT counterparts (**Figure 5.8A-B**). In fact, although the Western diet alone was able to increase the expression of ECM-related genes compared to normal diet livers, the presence of *Tet2* clonal hematopoiesis further enhanced the expression levels. Therefore, these molecular data underscored a molecular synergy between *Tet2* CHIP and the Western diet, worsening liver disease through increased fibrosis.

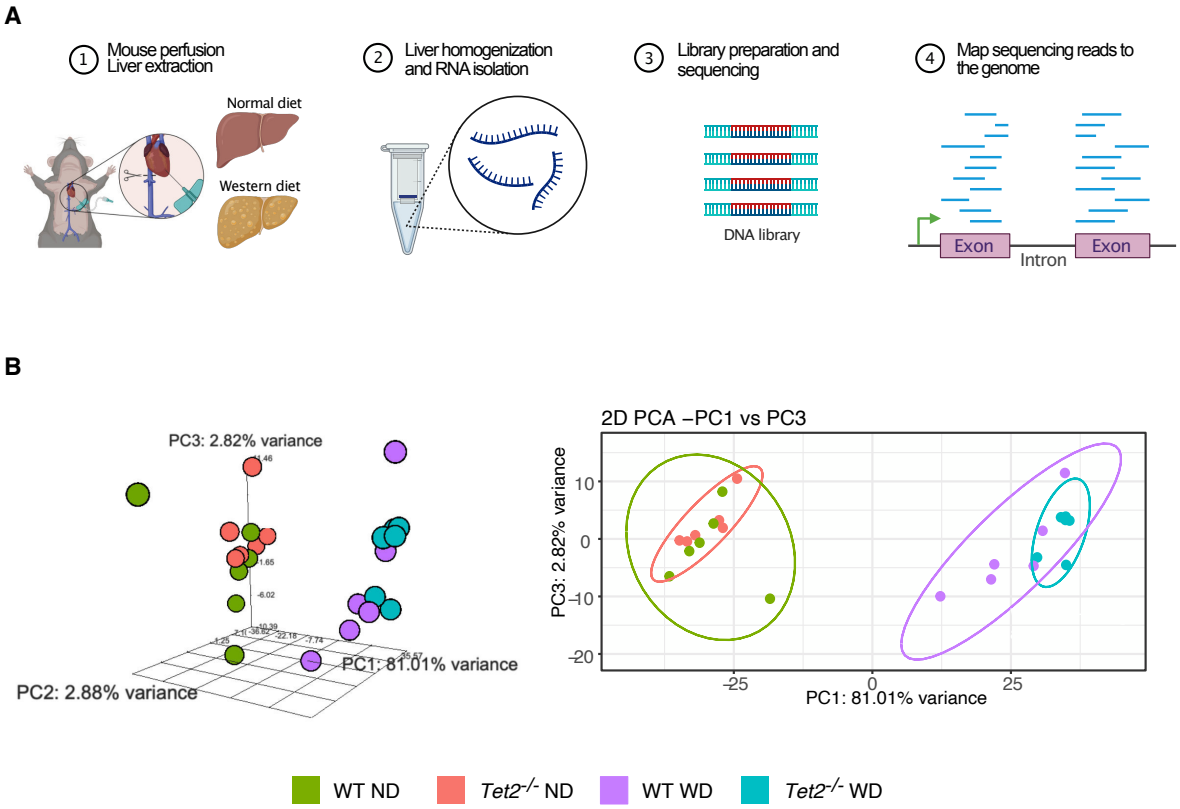


Figure 5.7. Bulk RNA sequencing of liver homogenates. A) Experimental scheme for bulk RNA-sequencing of liver homogenates. **B)** 3D (left) and 2D (right) principal component analyses (PCA) with all sequenced samples. Each dot represents a sequenced sample.

(n=6 samples per group)

Image A created using Biorender.

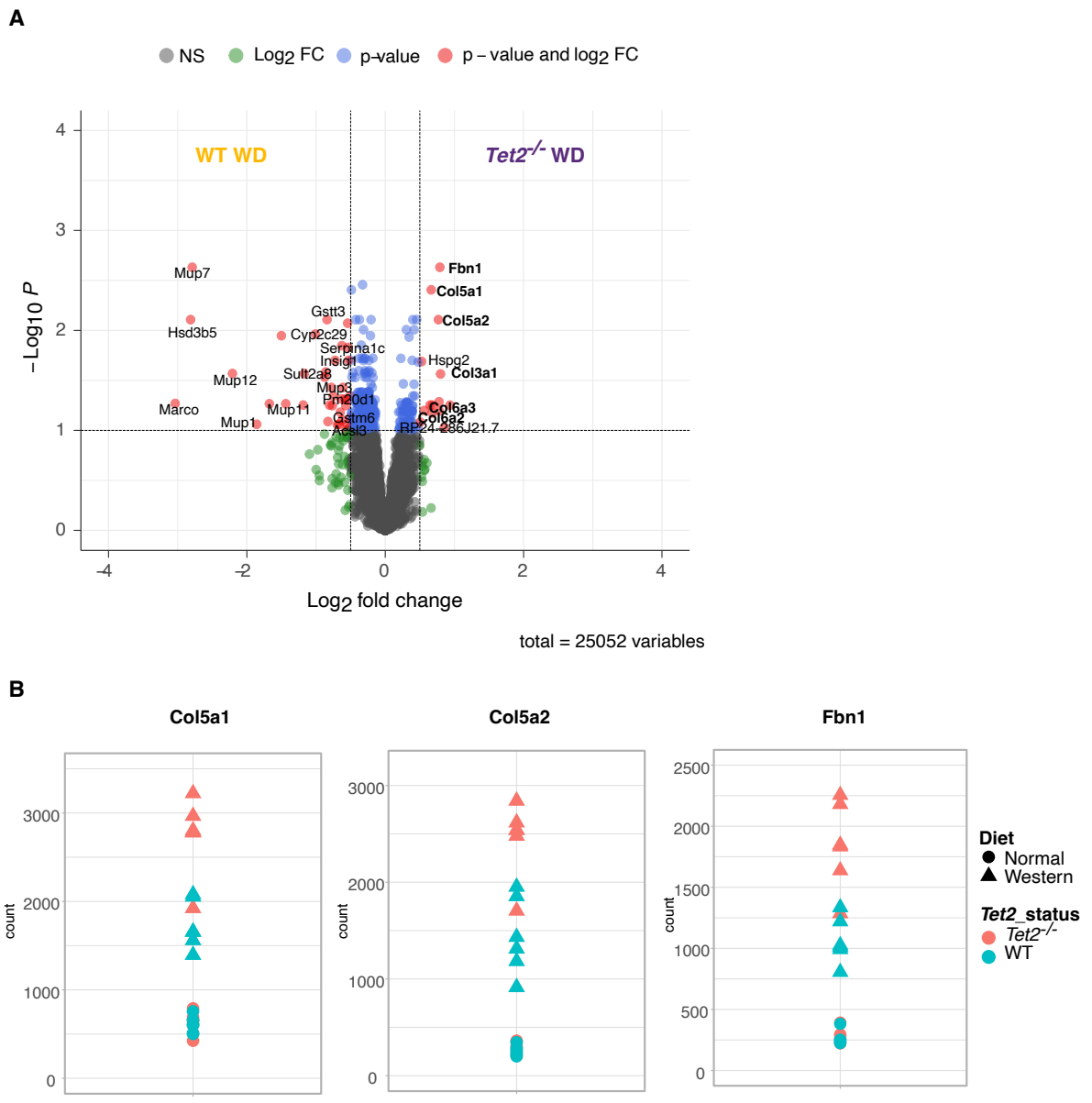


Figure 5.8. Increased expression of fibrosis-related genes in *Tet2* CHIP livers. A) Volcano plot illustrating differentially expressed genes comparing *Tet2*$^{-/-}$ WD and WT WD groups. Each dot represents a gene, with the x-axis indicating fold change and the y-axis denoting statistical significance (-log10 adjusted p-value). Genes exhibiting significant upregulation (right side) or downregulation (left side) are highlighted. Thresholds are Log2 fold change 1.5, and adjusted p-value 0.1. **B)** Normalized counts of *Col5a1*, *Col5a2* and *Fbn1* genes in all analyzed samples.
(n=6 samples per group).

Next, I performed gene set enrichment analysis (GSEA) in order to explore differentially regulated pathways. This analysis revealed a high number of upregulated or downregulated pathways in the *Tet2*$^{-/-}$ WD group compared to the WT WD. Notably, the most upregulated pathway was the hallmark associated with epithelial-mesenchymal transition (EMT), as illustrated in **Figure 5.9A**. This aligns with the findings from the DEG analysis,

where collagens and fibrillins were significantly upregulated, providing a plausible explanation for the observed enrichment of the EMT hallmark.

Moreover, I looked into inflammatory and metabolic pathways, as these are critical processes impacted in NAFLD pathology. In instances of NAFLD, inflammation is exacerbated, while metabolism is often repressed[83,118]. My data demonstrated that the presence of *Tet2* CHIP in WD-livers led to an elevated expression of inflammatory pathways, including IL2-STAT5 signaling, IL6-JAK2-STAT3 signaling, inflammatory response, TGFβ signaling, and TNFα signaling via NFKB, with the exception of the interferon alpha response, which exhibited higher expression in the WT setting (**Figure 5.9B**).

Regarding metabolic responses, all metabolic-related hallmarks—adipogenesis, bile acid metabolism, fatty acid metabolism, glycolysis, oxidative phosphorylation, and xenobiotic metabolism—were consistently downregulated in *Tet2*$^{-/-}$ livers compared to the WT, emphasizing a distinctive impact of *Tet2* CHIP on the metabolic landscape in the context of a Western diet (**Figure 5.9C**).

In summary, molecular analyses of liver homogenates revealed a substantial degree of molecular synergy between *Tet2* CHIP and the WD, leading to increased signatures related to fibrosis, inflammation and suppressed metabolism.

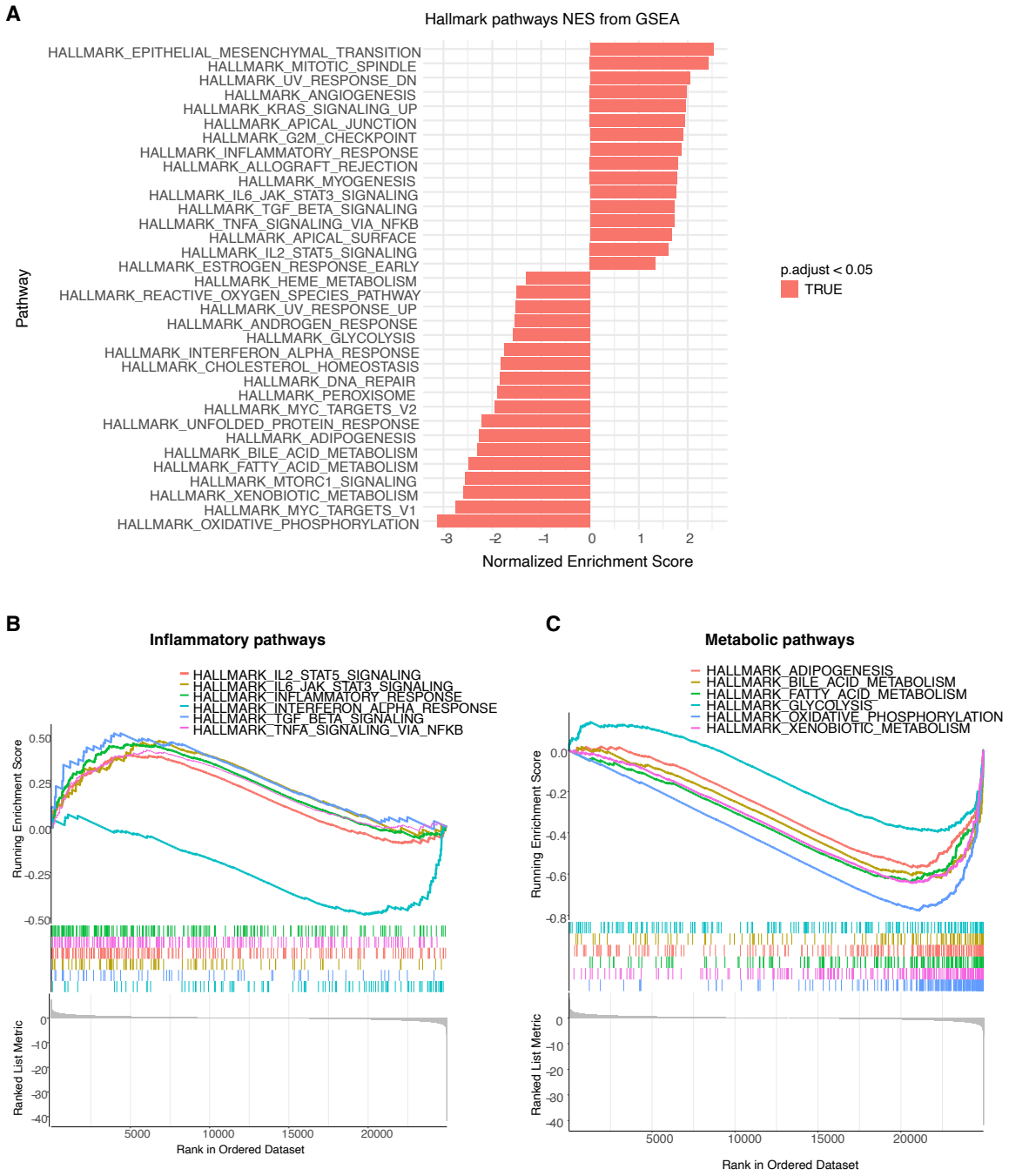


Figure 5.9. Inflammatory and metabolic pathways were differentially expressed in *Tet2* CHIP compared to their WT counterparts. A) GSEA comparing *Tet2*$^{-/-}$ WD to WT WD group, depicting up- and down-regulated pathways. GSEA of **B)** inflammatory and **C)** metabolic pathways comparing *Tet2*$^{-/-}$ WD to WT WD group. (n=6 samples per group).

5.3. Understanding the mechanisms via which *Tet2* CHIP exacerbates NAFLD and promotes HCC

Phenotypic characterization of Western diet mice combined with *Tet2* CHIP demonstrated a pronounced degree of synergy between the two variables, strongly predisposing towards the development of HCC. Based on these observations, my major goal has been to dissect the mechanistic basis behind this synergy. Specifically, I aimed to investigate whether the increased incidence/severity of NAFLD and HCC that occurs as a result of combining *Tet2*$^{-/-}$ CHIP with Western diet is caused by a synergistic acceleration or amplification of the previously characterized disease process, or whether this synergy instead results in the execution of a novel molecular mechanism. To interrogate this question, I performed a broad range of experimental assays characterizing the biology of *Tet2*$^{-/-}$ hematopoietic cells, and their potential impact on the liver disease. These analyses encompassed both functional and molecular investigations, spanning systemic and liver-specific evaluations. Moreover, to assess the effect of *Tet2* CHIP on disease kinetics, a series of experiments were performed at earlier timepoints.

5.3.1 Systemic analysis revealed distinct hematopoietic alterations due to the WD or *Tet2* CHIP

Published studies have shown that the induction of *Tet2* clonal hematopoiesis is able to alter healthy hematopoiesis, enhancing stem cell self-renewal while impairing differentiation to specific blood lineages, such as the erythroid lineage[119]. In this context, I first looked into the HSPC compartment. Two key observations emerged: Firstly, the Western diet increased the frequency of HSPCs in the bone marrow, while *Tet2* CHIP mice, under normal or Western diet feeding, exhibited a reduced frequency of HSPCs compared to WT groups (**Figure 5.10B**).

The erythroid lineage is defined in the hierarchical system by a step-wise differentiation process from MPP2 (multipotent progenitor with erythroid bias), to MEPs (committed progenitors to the erythroid and megakaryocyte lineages) to final differentiated RBCs (**Figure 5.10A**). Consistent with previous studies, my data revealed a significant erythroid differentiation impairment in *Tet2*$^{-/-}$ mice, evident in both normal and Western diet

groups. This was reflected by a decrease in MPP2 and MEP frequencies, the upstream progenitor populations for RBC production (**Figure 5.10C-D**). Systemic peripheral blood changes were also detected as a result of administering the Western diet, including an increase in peripheral WBCs (**Figure 5.10E**). Furthermore, WD also induced an increase in RBCs in WT mice, however, the increase was not significant in *Tet2*$^{-/-}$ mice (**Figure 5.10F**). This aligns with the erythroid impairment induced by *Tet2* clonal hematopoiesis.

Altogether, these results demonstrate that the Western diet and *Tet2* CHIP can impact different aspects of hematopoiesis, with no apparent synergistic effect.

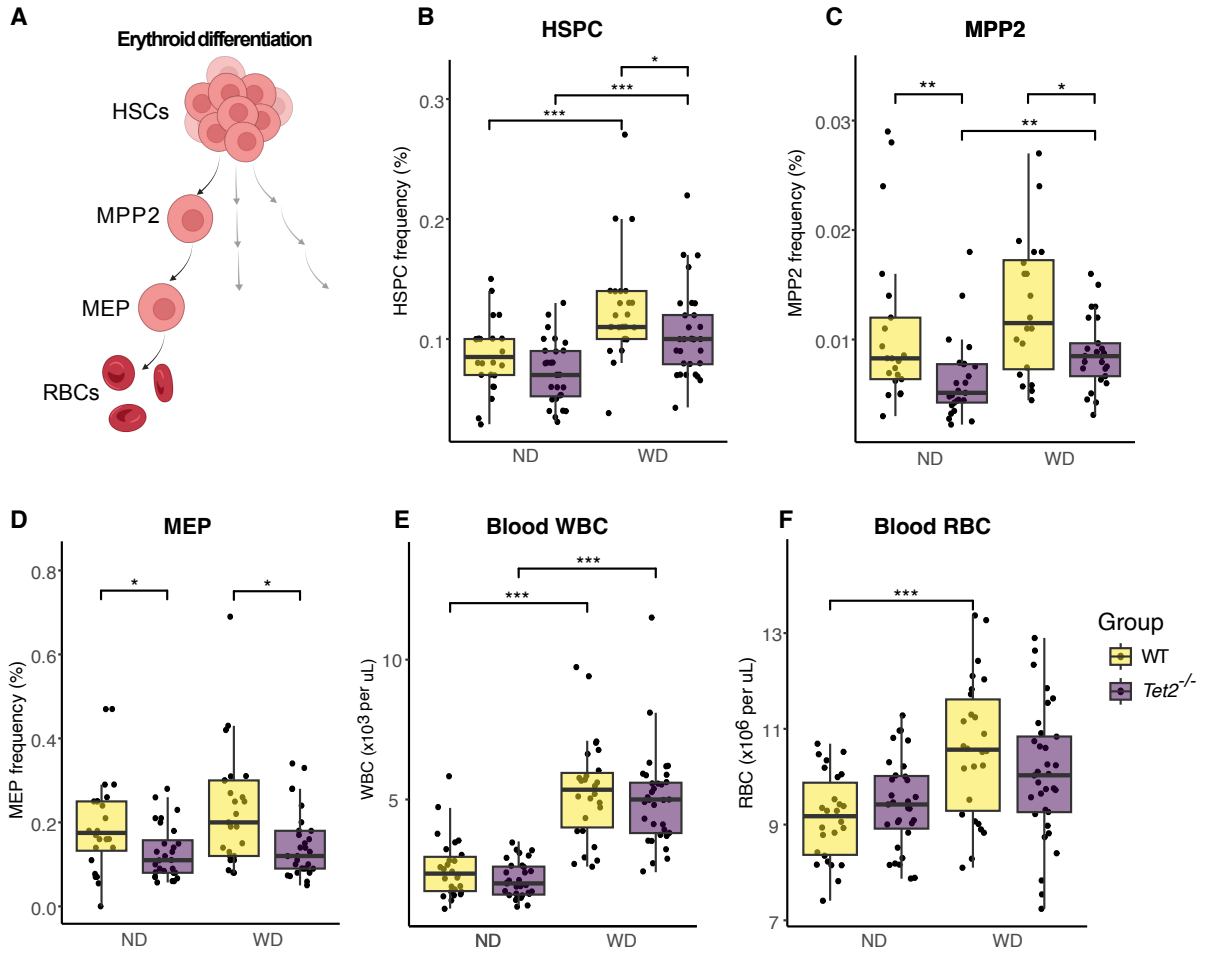


Figure 5.10. Erythroid differentiation was impacted in *Tet2* CHIP mice. A) Schematic of erythroid differentiation from HSCs. Frequency of **B)** HSPCs, **C)** MPP2s, **D)** MEPs in the bone marrow. Absolute **E)** WBC and **F)** RBC counts in peripheral blood. All measurements referred to the 6-month diet timepoint.

(n=20-33 mice per group; Data were analyzed using a two-way analysis of variance (ANOVA) followed by post-hoc multiple comparisons using the Tukey method. Significant differences between specific groups are denoted by asterisks (*p < 0.05, **p < 0.01, ***p < 0.001), only significant comparisons are indicated). Image A created using Biorender.

5.3.2 Local analysis of liver-infiltrating hematopoietic cells

With the understanding that *Tet2* CHIP amplifies liver damage and exacerbates HCC progression in synergy with the Western diet, my primary focus has been directed towards unraveling the functional and molecular basis of liver-infiltrating hematopoietic cells.

5.3.2.1 Similar degree of liver immune infiltration in WD mice with or without *Tet2* CHIP

Hematopoietic cell infiltration stands out as a prominent feature in NAFLD. In this context, I aimed to investigate whether *Tet2*-deleted hematopoietic cells had a preferential recruitment into the liver, potentially explaining the observed synergistic phenotype. In particular, I analyzed by flow cytometry absolute liver infiltration and relative composition of various immune cell types (**Figure 5.11A**). This analysis was done in collaboration with Chaofan Fan (Division of Chronic Inflammation and Cancer, DKFZ).

The liver is considered an important hematological organ, containing resident immune cells, with minimal influx from bone marrow-derived immune cells under homeostasis[120]. Flow cytometry analysis of liver-infiltrating immune cells revealed a significant increase in the frequency of donor CD45.1$^+$ cells, hence a decrease in the frequency of resident CD45.2$^+$ cells, as a result of administering a WD (**Figure 5.11B**). This implies that the diet alone is able to alter immune homeostasis in the liver, favoring the recruitment of bone marrow-derived cells that replace the long-term existing liver immune cells. Notably, this effect was observed in both WT and *Tet2*$^{-/-}$ groups exposed to the WD. Another observation from this analysis was that under normal diet conditions, the *Tet2*$^{-/-}$ group exhibited a higher frequency of CD45.2$^+$ resident cells, suggesting a greater occurrence of recruitment of bone marrow-derived or circulating cells in the WT scenario.

When examining the dynamics of CD45.1/2 in relation to ALT levels, a common indicator of liver damage, a significant correlation was found between ALT and an increased influx of immune cells into the liver. Notably, this correlation was evident only in *Tet2*$^{-/-}$ mice, with no correlation observed in the WT group (**Figure 5.11C)**.

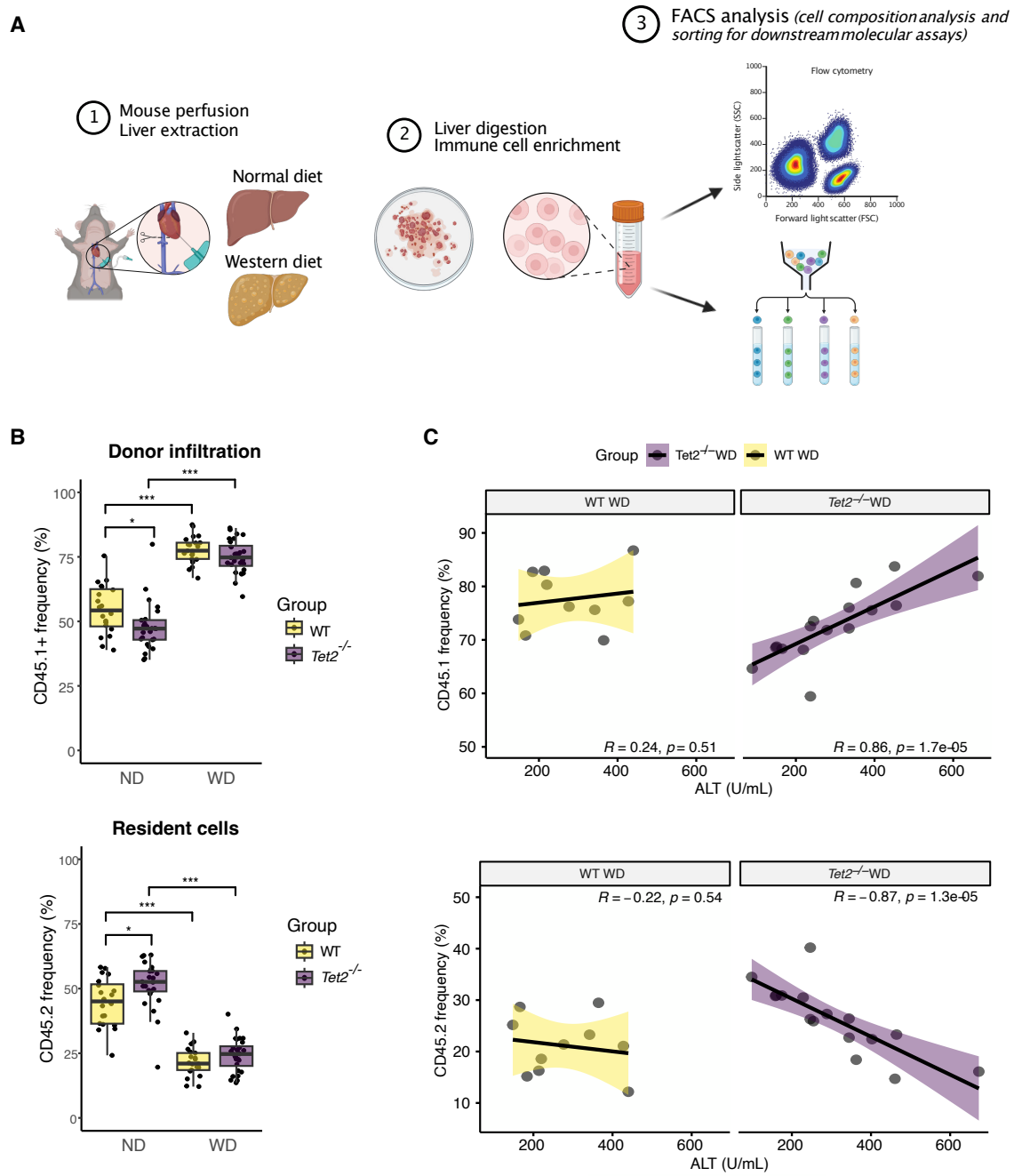


Figure 5.11. Influx of bone marrow-derived immune cells to the liver upon WD. A) Experimental scheme for analysis and isolation of CD45 hematopoietic cells from the liver. **B)** Frequency of liver CD45.1⁺ (donor) and CD45.2⁺ (recipient) cells. **C)** Correlation between serum ALT levels and the frequency of liver CD45.1⁺ and CD45.2⁺ cells in WD mice with or without *Tet2* CHIP.

(n=20-28 mice per group in B, n= 10-16 mice per group in C; Data were analyzed using a two-way analysis of variance (ANOVA) followed by post-hoc multiple comparisons using the Tukey method. Significant differences between specific groups are denoted by asterisks (*p < 0.05, **p < 0.01, ***p < 0.001), only significant comparisons are indicated). Image A created using Biorender.

Moreover, absolute quantification of infiltrated CD45.1⁺ cells demonstrated a pronounced infiltration induced by the WD (**Figure 5.12A**). However, no significant differences were noted between the WT and CHIP groups. Furthermore, I detected differences

in terms of cell type composition in the liver due to the WD, with elevated frequency of Kupffer cells, Ly6C^{hi} monocytes and CD8^{+} T cells (**Figure 5.12B**). Conversely, the *Tet2* status had a smaller impact on liver-immune cell composition than the diet. The most obvious observation came from the decrease in CD8^{+} T cell frequency in *Tet2*$^{-/-}$ mice compare to WT, as well as a mild increase in the frequency of Kupffer cells, suggesting that *Tet2* deletion induces a myeloid bias in hematopoietic cells.

Previous studies have shown that a subset of CD8^{+} T cells with high expression of PD1^{+} and CXCR6^{+} emerges in NASH livers, both in patients and mouse models[100]. In this line, I aimed to assess whether *Tet2* deletion could increase the frequency of this disease-related cell population. My data confirmed the increase in PD1^{+}CXCR6^{+}CD8^{+} T cells in livers exposed to a WD, however, regardless of the CHIP status (**Figure 5.12C-E**).

In summary, a comprehensive analysis of liver immune populations unveiled numerous changes resulting from WD feeding, and a mild myeloid bias induced by *Tet2* CHIP. Furthermore, CD45.1^{+} cell infiltration highly correlated with a biomarker of liver damage exclusively in the *Tet2* CHIP setting. However, it is important to note that causality cannot be addressed based on this observation.

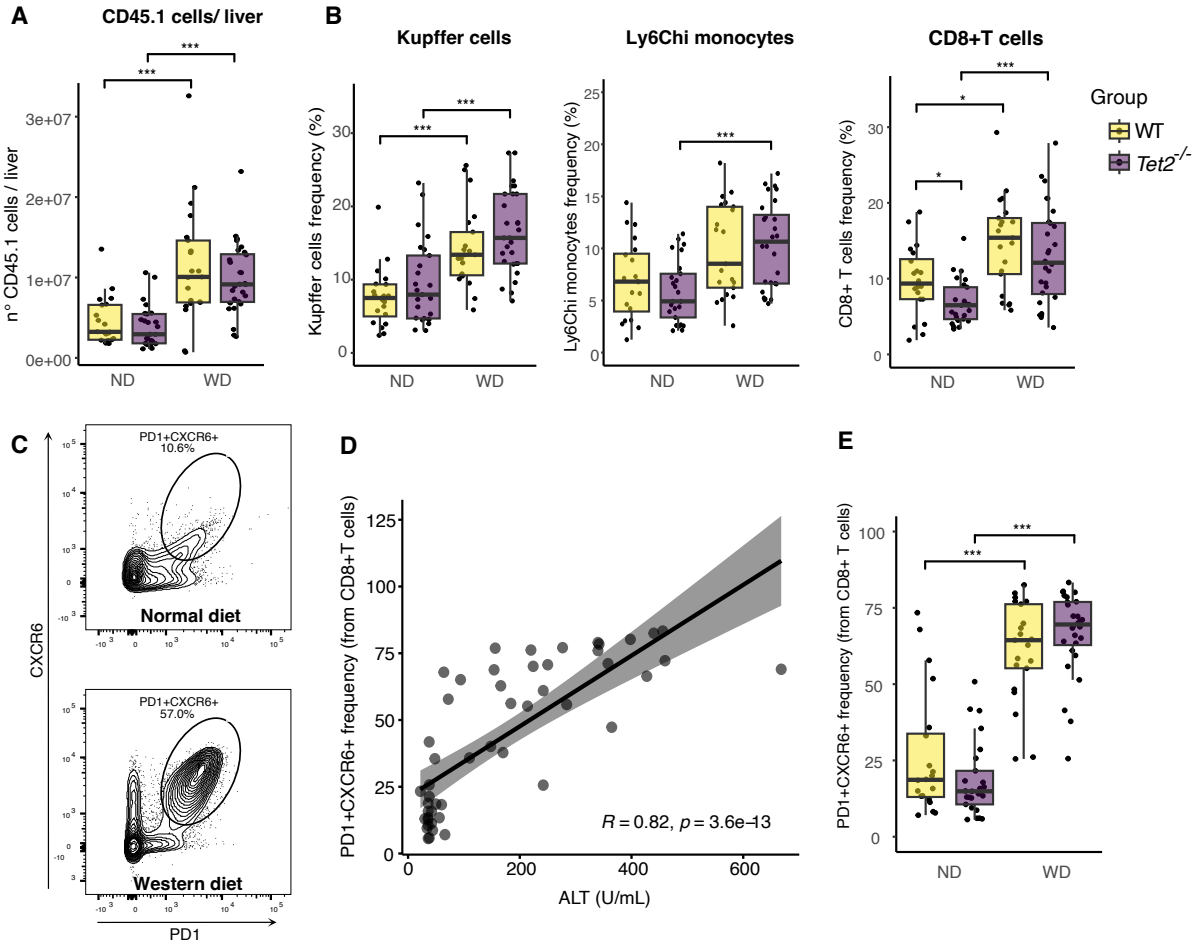


Figure 5.12. Similar immune cell composition in WD livers with or without CHIP. A) Absolute CD45.1^{+} cell count in livers, **B)** Frequency in percentage of Kupffer cells, Ly6C^{hi} monocytes and CD8^{+} T cells. **C)** Gating of PD1^{+}CXCR6^{+} cells within the CD8^{+} T population. **D)** Pearson correlation between ALT serum levels and the frequency of PD1^{+}CXCR6^{+} cells within the CD8^{+} T population. **E)** Frequency in percentage of PD1^{+}CXCR6^{+} cells within the CD8^{+} T population.

(n=20-28 mice per group; Data were analyzed using a two-way analysis of variance (ANOVA) followed by post-hoc multiple comparisons using the Tukey method. Significant differences between specific groups are denoted by asterisks (*p < 0.05, **p < 0.01, ***p < 0.001), only significant comparisons are indicated).

5.3.2.2 Molecular characterization of liver-infiltrating hematopoietic cells using bulk and single cell approaches

Although the degree of immune cell infiltration seemed consistent between WT and *Tet2*$^{-/-}$ WD-fed mice, there is the possibility that the molecular program differs between the groups. To explore the impact of the Western diet and *Tet2* deletion on gene expression, and evaluate potential synergies, I conducted a single cell RNA-sequencing (scRNA-seq) experiment of liver-infiltrating CD45.1^{+} cells at the 6-month timepoint from the start of the diet. This data was analyzed by Dr. Charles Dussiau, a postdoctoral fellow in our laboratory.

A total of 17 clusters were identified, representing distinct immune cell populations (**Figure 5.13A**). To assess differences in gene expression programs between WT and *Tet2*$^{-/-}$ WD groups, a Latent Embedding Multivariate Regression (LEMUR) analysis was used. The uniqueness of LEMUR lies in its framework, which disentangles the impacts of known covariates and their interactions, so it makes it an ideal tool to study the synergistic effect of combining WD and *Tet2* CHIP. As illustrated in **Figure 5.13B**, different genes were found up- or down-regulated in the *Tet2*$^{-/-}$ group compared to the WT in mice exposed to a WD. Of major importance are *Anxa2* and *Tox*, which were specifically upregulated in lymphocytes (**Figure 5.13C**). Previous studies have linked these genes to the prognosis of HCC. *Tox*, in particular, has been associated with the exhaustion of antitumor CD8^{+} T cells, therefore favoring tumor growth[121], and *Anxa2* has shown a strong correlation with a reduced overall survival (OS) rate in individuals diagnosed with HCC[122].

These findings suggest that *Tet2* deletion within the tumor immune microenvironment could play a causative role in the progression from NAFLD to HCC.

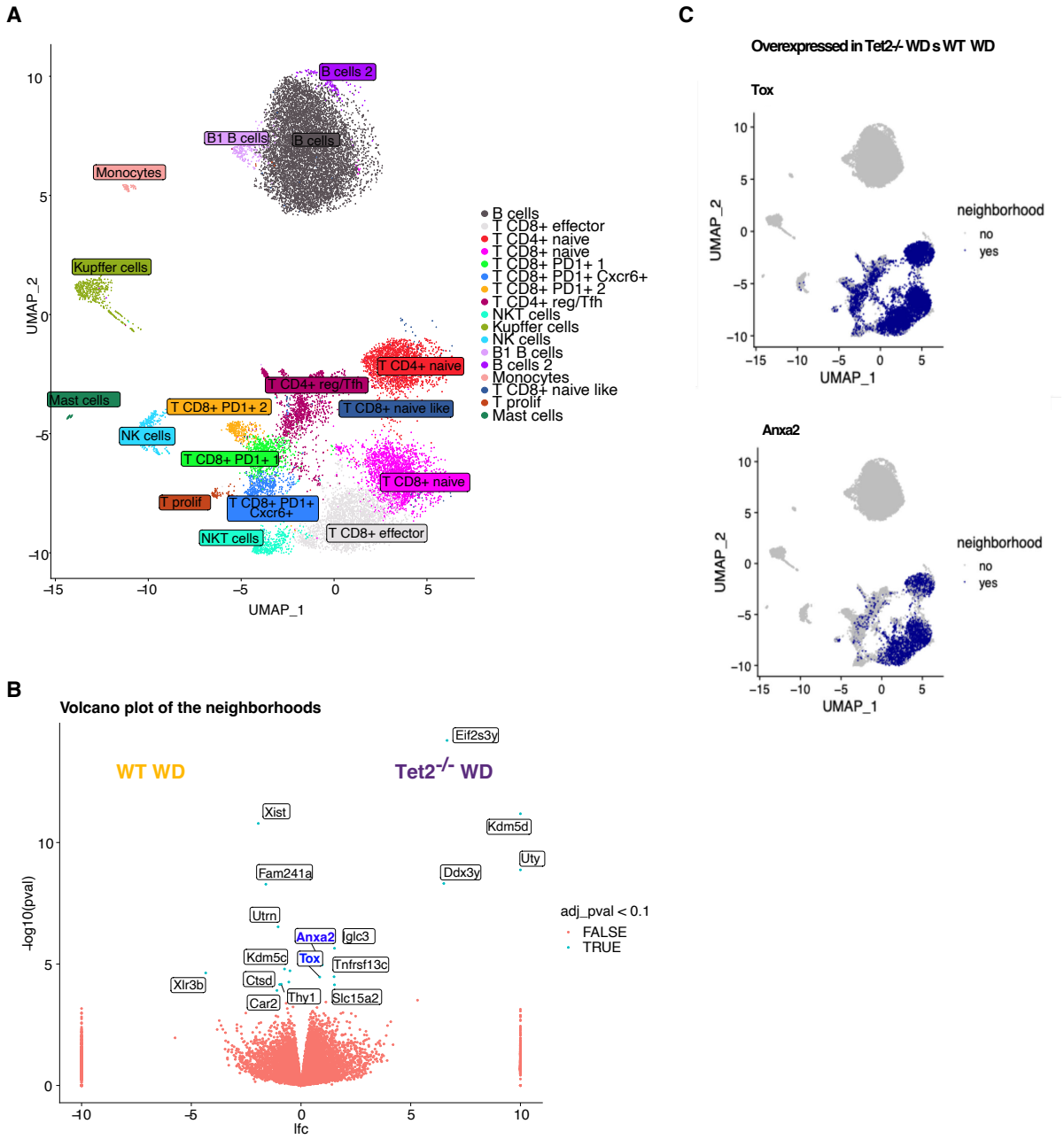


Figure 5.13. scRNA-seq analysis of liver-infiltrating hematopoietic cells revealed gene expression changes in T cells with potential clinical relevance. A) UMAP displaying the 17 clusters identified, and their cell type annotation. **B)** LEMUR analysis showing differentially expressed genes between *Tet2*$^{-/-}$ WD cells compared to WT WD. **C)** UMAP showing in which cell type clusters there is an upregulation of *Tox* and *Anxa2* genes.
(n=4 mice per group). Figures made by Dr. Charles Dussiau.

While this scRNA-seq experiment revealed molecular changes in lymphocytic populations, the myeloid resolution, in terms of the number of sequenced cells, was clearly underpowered. To delve into the molecular programming of myeloid populations, I next performed a bulk RNA-seq experiment of three liver-infiltrating immune cell types: Kupffer cells, Ly6C^{hi} monocytes and PD1^{+}CD8^{+} T cells. Analysis was also performed in cells isolated from the 6-month endpoint.

Initial principal component analysis revealed three clusters correlating with the three analyzed cell types (**Figure 5.14A**). Next, I explored differences within individual cell types, specifically focusing on synergistic changes resulting from combining the WD and *Tet2*$^{-/-}$. In this case, the diet exerted the biggest influence on the transcriptome, segregating ND and WD samples along the PC1 and PC2 components (**Figure 5.14B**). Conversely, the *Tet2* status had a limited impact on the overall transcriptome compared to the diet. These data is consistent with my prior bulk RNA-seq analysis on liver homogenates, where the *Tet2* deletion exhibited considerably less effect on the liver transcriptome than the WD.

To evaluate transcriptomic alterations attributable to *Tet2* deletion and WD, I performed a DESeq2 analysis, followed by GSEA, to understand which pathways were differentially regulated between the groups. Comparative analysis between *Tet2*$^{-/-}$ WD and WT WD cells revealed a number of upregulated and downregulated pathways in the *Tet2* CHIP group (**Figure 5.15**). Of particular interest is the upregulation of inflammatory pathways (IL2 STAT5 signaling, IL6 JAK2 STAT3 signaling, inflammatory response) in PD1^{+}CD8^{+} T cells. This indicates that, at the timepoint of analysis, the WD and *Tet2* CHIP synergized in CD8^{+} T cells to enhance inflammation, potentially influencing disease progression. Moreover, epithelial-mesenchymal transition was consistently upregulated in all hematopoietic cell types in the *Tet2* CHIP group. Further investigation into the genes driving this upregulation will help elucidate the specific processes that are enhanced in the *Tet2* CHIP setting. Another disease-related hallmark which was upregulated in Ly6C^{hi} monocyte and T cells was angiogenesis, which could theoretically have implications for HCC development.

Taken together, RNA-seq of liver-infiltrating immune cells revealed synergistic molecular changes, some of them with clinical relevance. Further investigation of these data is needed to identify potential targets in *Tet2* CHIP-related HCC cases.

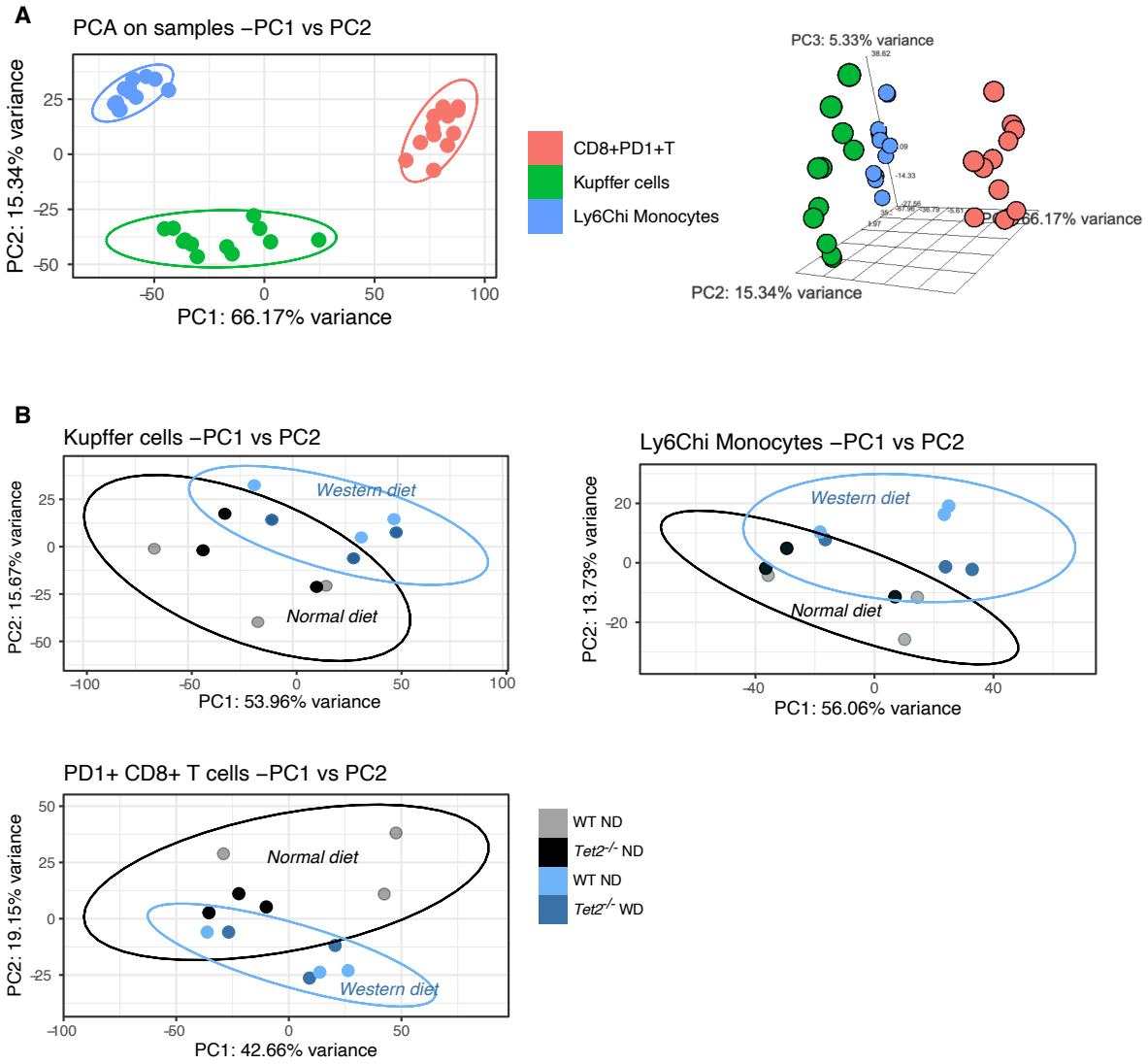


Figure 5.14. Bulk RNA-sequencing of liver-infiltrating hematopoietic cells. A) 2D (left) and 3D (right) PCAs on the three cell types sequenced: Kupffer cells, Ly6C^{hi} monocytes and PD1^{+}CD8^{+} T cells. **B)** 2D PCA analysis within the individual cell types encompassing the four experimental groups: WT normal diet, WT western diet, *Tet2*$^{-/-}$ normal diet, *Tet2*$^{-/-}$ western diet.
(n=3 samples per group per each cell type).

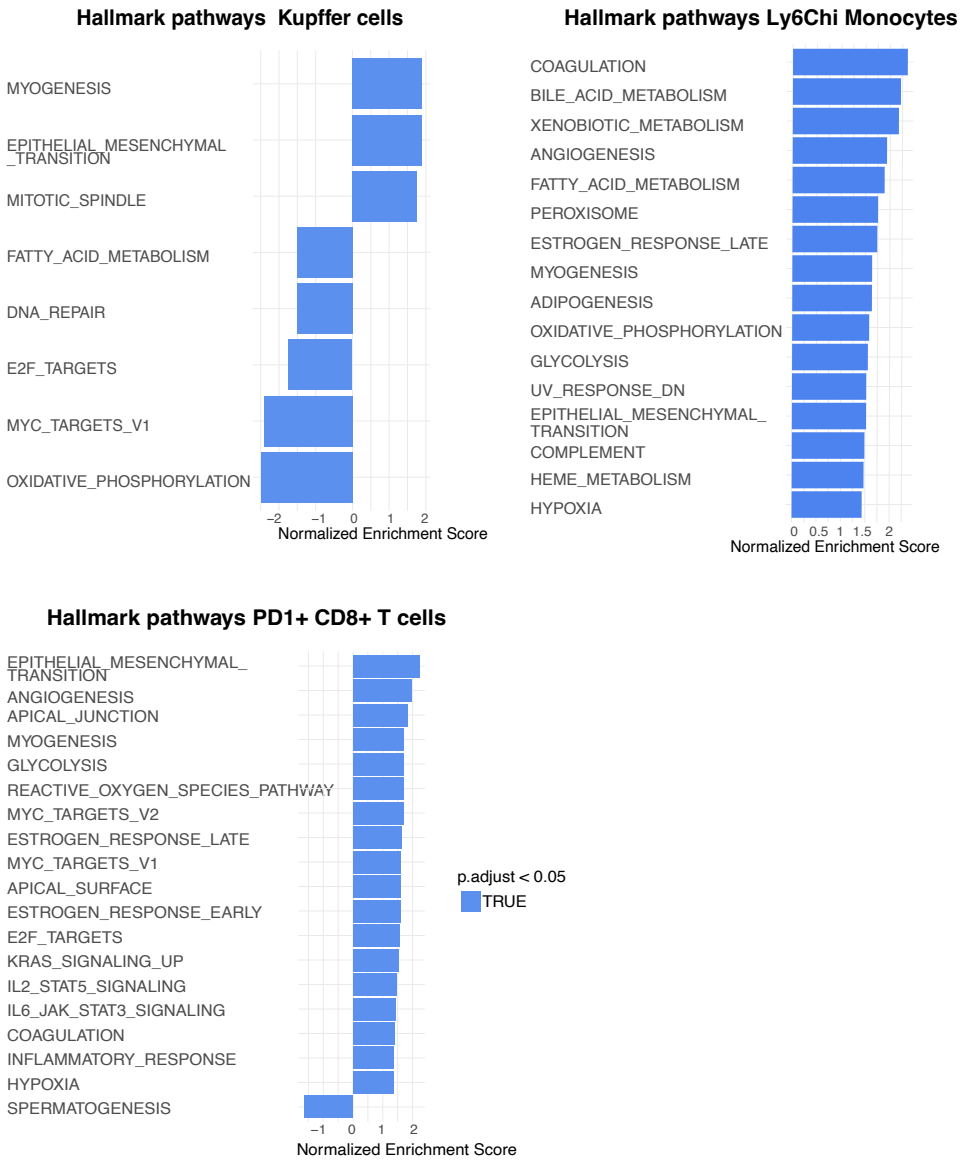


Figure 5.15. Differentially regulated hallmark pathways in *Tet2*$^{-/-}$ cells compared to their WT counterparts. Results of GSEA Hallmark analysis showing enriched gene sets in Kupffer cells, Ly6C^{hi} monocytes and PD1^{+}CD8^{+}T cells in the *Tet2*$^{-/-}$ WD group compared to the WT WD group.

(n=3 samples per group per each cell type, Data were analyzed with GSEA with p-adjusted value of 0.05).

5.3.2.3. Phenotypic analysis at 3-months suggested no clear acceleration of the NAFLD phenotype

One possible explanation for the high incidence and severity of HCC in mice with *Tet2* clonal hematopoiesis is an accelerated disease progression. Therefore, I investigated the degree of liver damage, immune cell infiltration and composition in mice fed for 3 months with a WD, representing an earlier stage characterized by fatty liver and initial signs of NASH, but no HCC development yet.

In terms of liver damage, levels of ALT and AST showed no significant differences between WT and CHIP mice on the Western diet, indicating that at earlier timepoints, the combination of the diet and *Tet2* CHIP does not result in higher levels of serum aminotransferases compared to the diet alone (**Figure 5.16A**). Likewise, the degree of liver immune infiltration was comparable between WT and *Tet2*$^{-/-}$ groups (**Figure 5.16B)**. The presence of PD1^{+}CXCR6^{+}CD8^{+} T cells, a well-established subset in NASH, showed no significant differences between the two groups, as previously observed in the 6-month timepoint (**Figure 5.16C**). Additionally, in line with my 6-month analysis, a higher frequency of myeloid cells, particularly Kupffer cells, was noted in WD mice with *Tet2* clonal hematopoiesis (**Figure 5.16D-E**).

In summary, analysis at 3-months did not reveal any synergistic effect between WD and *Tet2* CHIP. Nevertheless, molecular and functional analyses of liver infiltrating hematopoietic cells at this timepoint will be necessary in order to understand whether *Tet2*$^{-/-}$ cells exhibit disease-relevant molecular and functional programs earlier than the WT counterparts, therefore accelerating the transition from NASH to HCC.

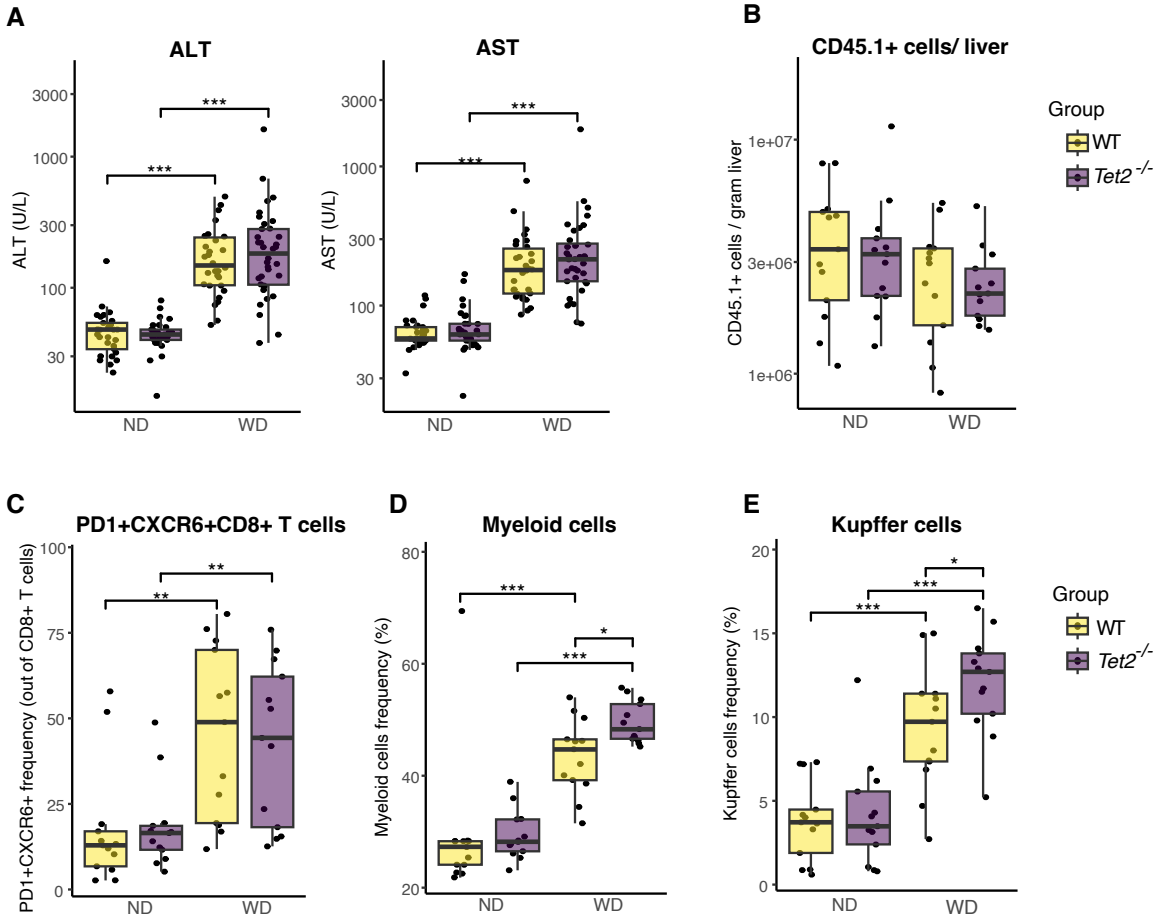


Figure 5.16. Preliminary analysis at an earlier timepoint supported no acceleration of the liver disease phenotype in mice with *Tet2* CHIP. A) Levels of serum aminotransferases ALT and AST. **B)** Absolute number of liver infiltrating CD45.1⁺ cells per grams of liver. Frequency of **C)** PD1⁺CXCR6⁺ cells within the CD8⁺ T population, **D)** myeloid cells and **E)** Kupffer cells. Data collected at 3-months timepoint.

(n=13-36 mice per group; Data were analyzed using a two-way analysis of variance (ANOVA) followed by post-hoc multiple comparisons using the Tukey method. Significant differences between specific groups are denoted by asterisks (*p < 0.05, **p < 0.01, ***p < 0.001), only significant comparisons are indicated).

5.3.2.4. *Tet2* CHIP and WD induced a metabolomic reprogramming in liver-infiltrating hematopoietic cells

Metabolites are known to regulate the activity of several key enzymes involved in chromatin remodeling. For example, alpha-ketoglutarate (aKG) is an important co-factor for TET2 and jumonji domain–containing histone demethylases (Jmjd), whereas the citric acid cycle (TCA) intermediates succinate and fumarate are known TET2 inhibitors. I therefore aimed to explore whether cell-type-specific disease-relevant epigenome programming may be impacted by major metabolic alterations induced by sustained exposure to Western diet.

Given that my mouse model often exhibits heterozygous deletion of *Tet2* in hematopoietic cells, instead of a complete knock out, I hypothesized that the expressed allele would be regulated at the protein level by its metabolic cofactors and inhibitors. Specifically, I investigated 1) metabolite changes due to the WD capable of reprogramming the epigenome in a way that could favor disease progression, both in WT and CHIP settings; 2) alterations in key metabolites with potential impact on TET2 functionality; and 3) whether any synergy can result from partial loss of TET2 and metabolite-induced reprogramming of the epigenetic landscape, so that together they enhance programs involved in disease progression (**Figure 5.17**).

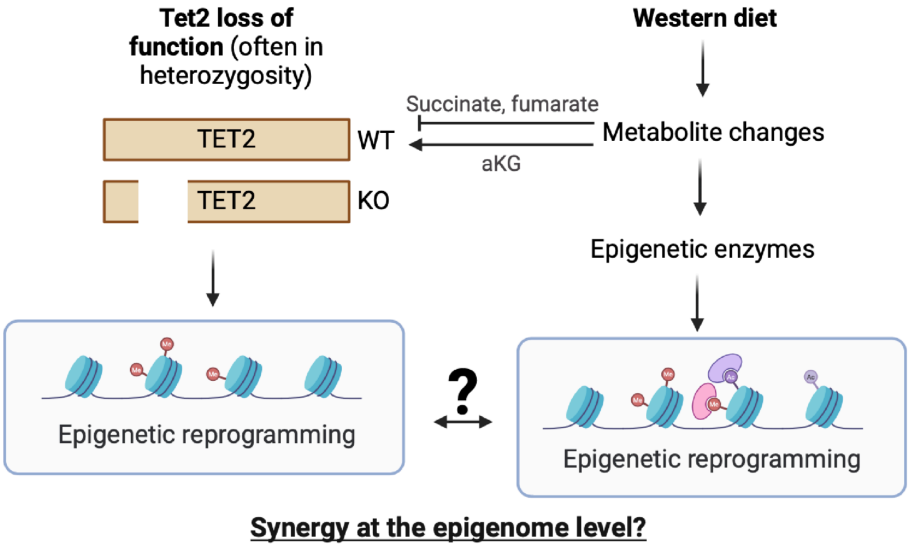


Figure 5.17. Synergistic epigenetic reprogramming as a result of combining Tet2 deletion and metabolic-induced modulation of epigenetic enzymes.

Image created using Biorender.

First, I looked into general metabolic changes resulting from the administration of the WD. Betaine, trymethyl-5-aminovalerate and carnitine levels were significantly decreased in the liver infiltrating immune cell types derived from WD mice (**Figure 5.18**). In contrast, the WD induced an increase of lysophosphatidylcholine (LPCs), such as LPC 18.1. These results align with previous literature associating these metabolites to fatty liver disease and NASH[123–126].

Furthermore, other metabolic changes were caused by the *Tet2* deletion. Whereas WD feeding increased the levels of essential amino acids such as valine, serine, leucine and tryptophan, among others, in Kupffer cells, unaltered amino acid levels were observed in cells with TET2 loss of function (**Figure 5.19**).

Next, I looked into TET2 enzyme cofactors and inhibitors, which revealed no evident significant changes between the groups (**Figure 5.20**). Some samples did not overpass the limit of detection, suggesting that perhaps these metabolites are not abundant enough to draw conclusions regarding their changes upon WD feeding or *Tet2*$^{-/-}$. Overall, metabolites with potential impact on modulating epigenetic enzymes did not seem to alter in WD mice.

In summary, metabolomics analysis revealed interesting changes from which conclusions and new hypotheses can be established, however, no metabolite related to epigenetic enzymes regulation and epigenome reprogramming was supported by this data.

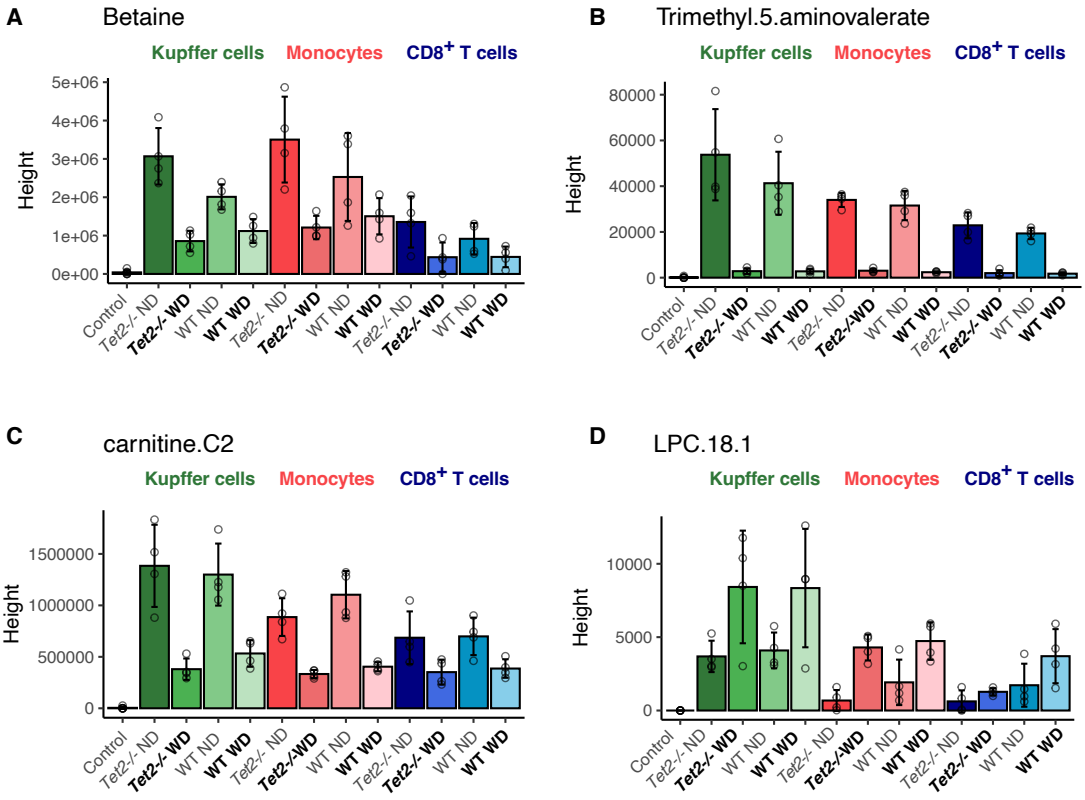


Figure 5.18. Metabolic reprograming caused by Western diet feeding. Levels of **A)** betaine, **B)** trimethyl 5-aminovalerate, **C)** carnitine C2, **D)** Lysophosphatidylcholine (LPC) 18.1, in Kupffer, Ly6C^{hi} monocytes and CD8^{+} T cells isolated from the liver and measured by mass spectrometry.
(n=4 samples per group).

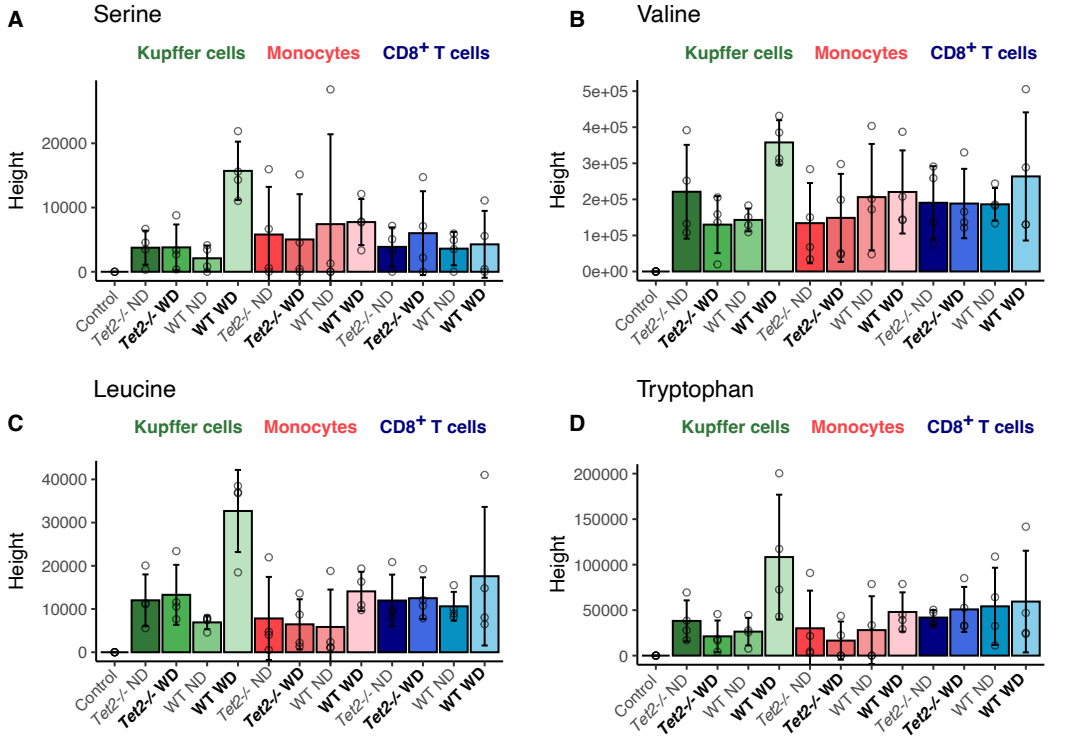


Figure 5.19. Metabolic reprograming caused by Tet2 deletion. Levels of **A)** serine, **B)** valine, **C)** leucine, **D)** tryptophan, in Kupffer, Ly6C^{hi} monocytes and CD8^{+} T cells isolated from the liver and measured by mass spectrometry.
(n=4 samples per group).

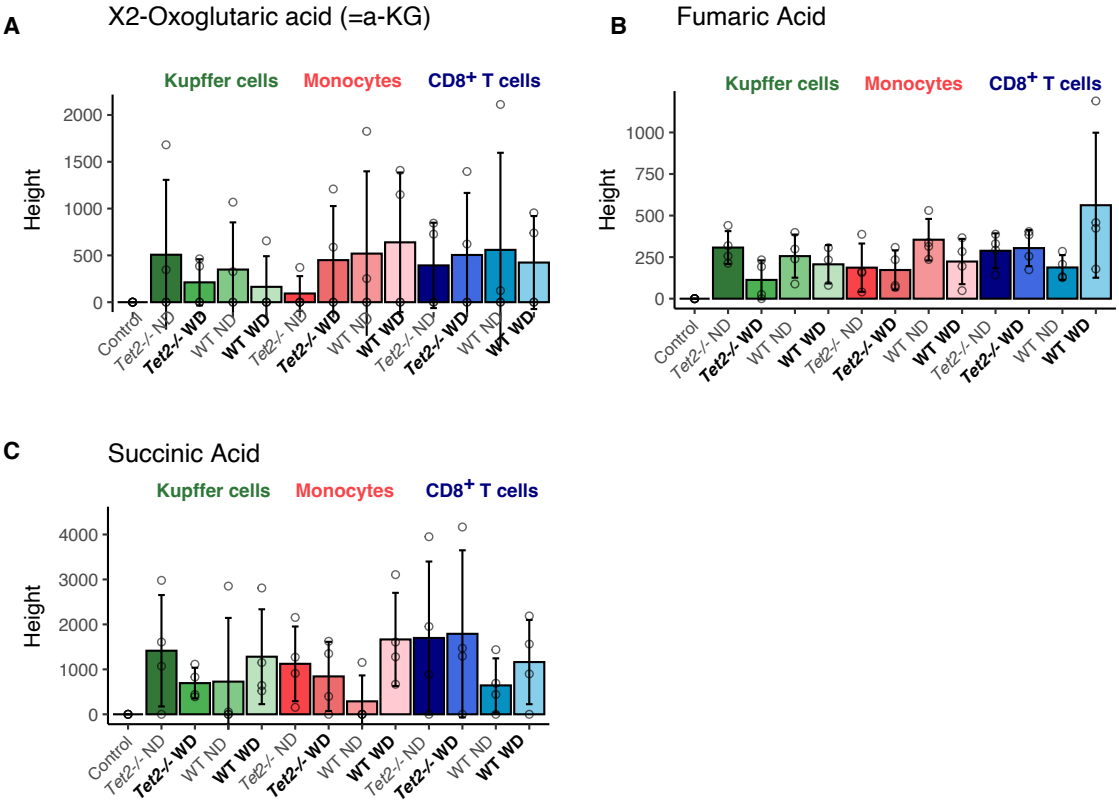


Figure 5.20. TET2 metabolic cofactors did not significantly change upon WD feeding. Levels of **A)** X2-Oxoglutaric acid (a-KG), **B)** Fumaric acid, **C)** Succinic acid, in Kupffer, Ly6C^{hi} monocytes and CD8^{+} T cells isolated from the liver and measured by mass spectrometry.
(n=4 samples per group).

6

Discussion project II

6.1. Clonal hematopoiesis as a risk factor for non-hematologic diseases

Clonal hematopoiesis of indeterminate potential (CHIP) has been linked in clinical cohorts to an increased risk for both hematologic and non-hematologic diseases. While the presence of mutations in hematopoietic cells would be predicted to contribute to hematologic malignancies, such a connection is less clear in the context of other diseases. Initial studies demonstrated an association between CHIP and the development of cardiovascular diseases, including atherosclerosis, thrombosis and stroke[52,53,127]. Apart from hematologic and cardiovascular diseases, the impact of CHIP in other pathologies remains poorly understood. CHIP has been modestly linked to type 2 diabetes[128]. Moreover, other clinical outcomes related to CHIP include chronic obstructive pulmonary disease[129], osteoporosis[130], autoimmune diseases such as antibody-associated vasculitis[131], and COVID19 clinical prognosis[132]. Interestingly, in Alzheimer´s disease, CHIP appears to play a protective role[133]. Recent analyses of clinical datasets from cancer patients suggest an association with CHIP, however, it seems to depend on the type of cancer entity and the specific clonal hematopoiesis mutation. In fact, CHIP seems to have opposite effects on tumor progression depending on the organ in mouse models.

In this project, I investigated the clinical value of *Tet2* CHIP on hepatocellular carcinoma (HCC) development, demonstrating that *Tet2* CHIP can promote the progression from non-alcoholic steatohepatitis (NASH) to HCC (**Figure 6.1**). This finding is consistent with unpublished clinical data analyzed by Dr. Robert Vanner (UHN, Toronto), which revealed a significant enrichment of *TET2* mutations in peripheral blood cells derived from HCC patients, compared to any other type of cancer entity. Although not specifically examined in this thesis,

these clinical data support the association between CHIP and HCC only in the context of *TET2* mutations, with no apparent link observed in individuals with other CHIP mutations like in *DNMT3A*. The identification of *Tet2* clonal hematopoiesis as a potential risk factor for chronic liver disease and liver cancer shown in this thesis aligns with a recent publication from the group of Benjamin Ebert, which proposed an association between *Tet2* CHIP and the progression of chronic non-alcoholic and alcoholic fatty liver disease[134]. Nevertheless, work in this dissertation not only linked *Tet2* CHIP with NAFLD progression, but also its transformation into liver cancer. Over the time span of this thesis, more studies have been published linking CHIP to the progression of other solid cancers, both in human clinical reports[62,135,136], as well as using mouse models[64,65,67]. Collectively, my thesis contributes to recent research generating evidence of CHIP as a risk factor for the development of solid cancers.

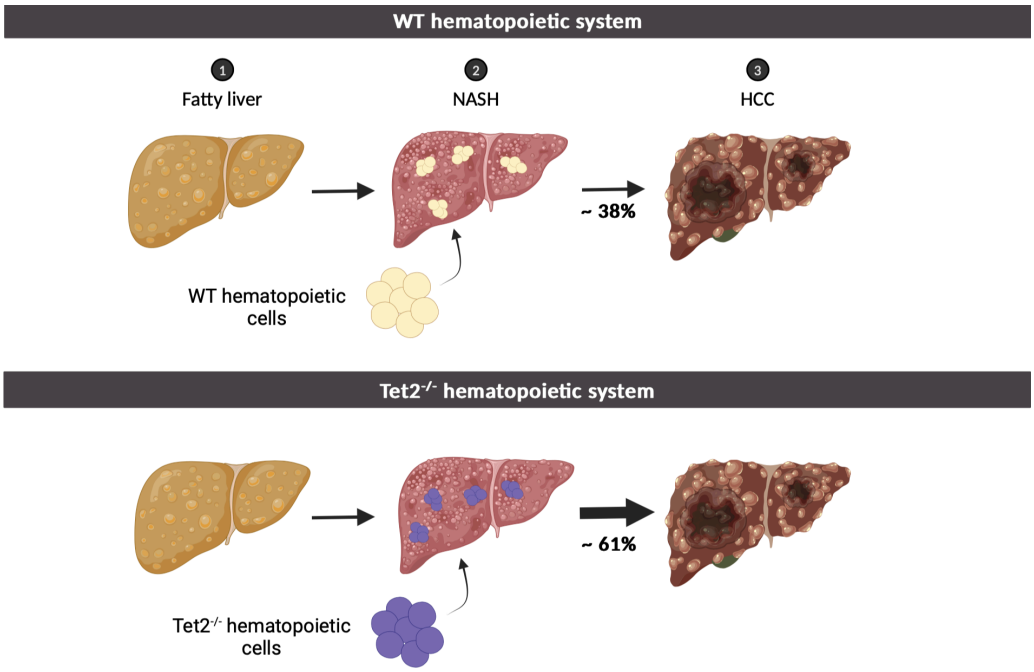


Figure 6.1. Graphical abstract showing the synergistic effect between Tet2 CHIP and the Western diet to favor the transition from NASH to HCC.
Image created using Biorender.

6.2. Selecting an optimal model to investigate the impact of *Tet2* CHIP on liver disease

Numerous models of CHIP and NAFLD-HCC have been described in the literature. In this thesis, I took advantage of a dietary model to induce NAFLD-HCC, consisting of high

levels of fat, cholesterol and fructose, known as the Western diet (WD). This combination has been shown to faithfully recapitulate the evolution of NAFLD observed in humans and is capable of inducing HCC[100]. Research from the Heikenwälder lab (DKFZ) using this type of dietary models has highlighted the pivotal role of hematopoietic cells, including platelets[97], $CD8^+$ T cells[100] and B cells[137], among others, in the evolution of this pathology through induced liver inflammation. Hence, dietary models seemed ideal to study how hematopoietic cells with a *Tet2* deletion could influence NAFLD-HCC outcomes.

In order to model *Tet2* clonal hematopoiesis in mice, I employed a transplantation of *Tet2*-floxed bone marrow cells into lethally irradiated recipient mice. This experimental strategy was chosen for several reasons. Transplantations allow for the modulation of the $Tet2^{-/-}$ VAF, which is important for correlating *Tet2* CHIP VAF to disease prognosis, and reproduce the low VAFs that are observed in humans. Nevertheless, transplantation-based CHIP models present challenges related to side effects from bone marrow irradiation, such as associated inflammation or long-term hematopoietic failures, which theoretically could contribute to disease progression. Thereby, future experiments will need to validate the effect of *Tet2* CHIP on NAFLD-HCC shown in this dissertation in the absence of transplantation using primary $Tet2^{fl/fl}$ mice.

There are other variables differing to how previous studies have model CHIP in mice, which relate to 1) the timepoint of induction and 2) the cell type in which *Tet2* deletion is induced. On one hand, the *Tet2* knock-out was induced after successful hematopoietic reconstitution in the recipient mice instead of pre-transplantation. With regards to point number 2, the *Tet2* deletion was triggered specifically in the adult HSPC compartment (Scl promoter), opposite to previous studies inducing the knock-out in all hematopoietic and vascular cell types during development (Vav promoter). These distinctions are crucial; one the one hand, HSCs with *Tet2* deletion have been shown to exhibit engraftment advantages compared to WT HSCs. Therefore, inducing the knock-out in steady-state conditions helps prevent conferring this advantage to the $Tet2^{-/-}$ group, which could potentially contribute to the progression of hepatocellular carcinoma. On the other hand, inducing $Tet2^{-/-}$ in all hematopoietic and vascular cells early in development may lead to different phenotypes in hematopoietic cells compared to those induced by CHIP mutations in adult settings. Thus, the

experimental design used in this dissertation closely mirrors the process of clonal hematopoiesis in humans.

Assessment of *Tet2* knock-out induction revealed a bias towards heterozygous deletion of the *Tet2* gene, despite the presence of the floxed *Tet2* transgene in both alleles. The rationale behind this preference for heterozygous clones remains elusive. Nonetheless, this observation holds significance as it mirrors the acquisition of heterozygous mutations in adult HSCs observed in human CHIP. Unlike previous investigations with CHIP mouse models, which primarily induced homozygous knock-outs, our study presents a novel approach.

In summary, three key aspects of our *Tet2* CHIP mouse model stand out in comparison to prior studies:

- Induction during steady-state rather than pre-transplantation and in the adult instead of during development.
- Induction exclusively in the HSPC compartment rather than in all hematopoietic and vascular cells.
- Predominance of heterozygous *Tet2* knock-out instead of homozygosity.

Screening for CHIP mutations in humans is commonly done in peripheral blood samples. In my thesis, I characterized the *Tet2*$^{-/-}$ VAF only in the HSCs, where the *Tet2* recombination takes place. A notable gap in our understanding lies in determining the extent to which liver-infiltrating immune cells are *Tet2*$^{-/-}$ or WT. With help from Sena Alptekin and Lina Merg (Division of Experimental Hematology, DKFZ), I am currently evaluating the *Tet2*$^{-/-}$ VAF in various immune cells in peripheral blood, bone marrow and liver, in order to understand whether heterozygous deletion of *Tet2* is cell type- and organ-specific (**Figure 6.2**). Through the use of droplet digital PCR (ddPCR), our aim is to achieve absolute quantification of the proportion of *Tet2*$^{-/-}$ cells in individual mice and correlate it with their disease phenotype. While these analyses introduce new avenues of experimental inquiry, our primary focus at present is to investigate whether *Tet2*$^{-/-}$ cells are preferentially recruited into pathological livers, which specific cell types are involved, and whether the VAF correlates with disease outcome.

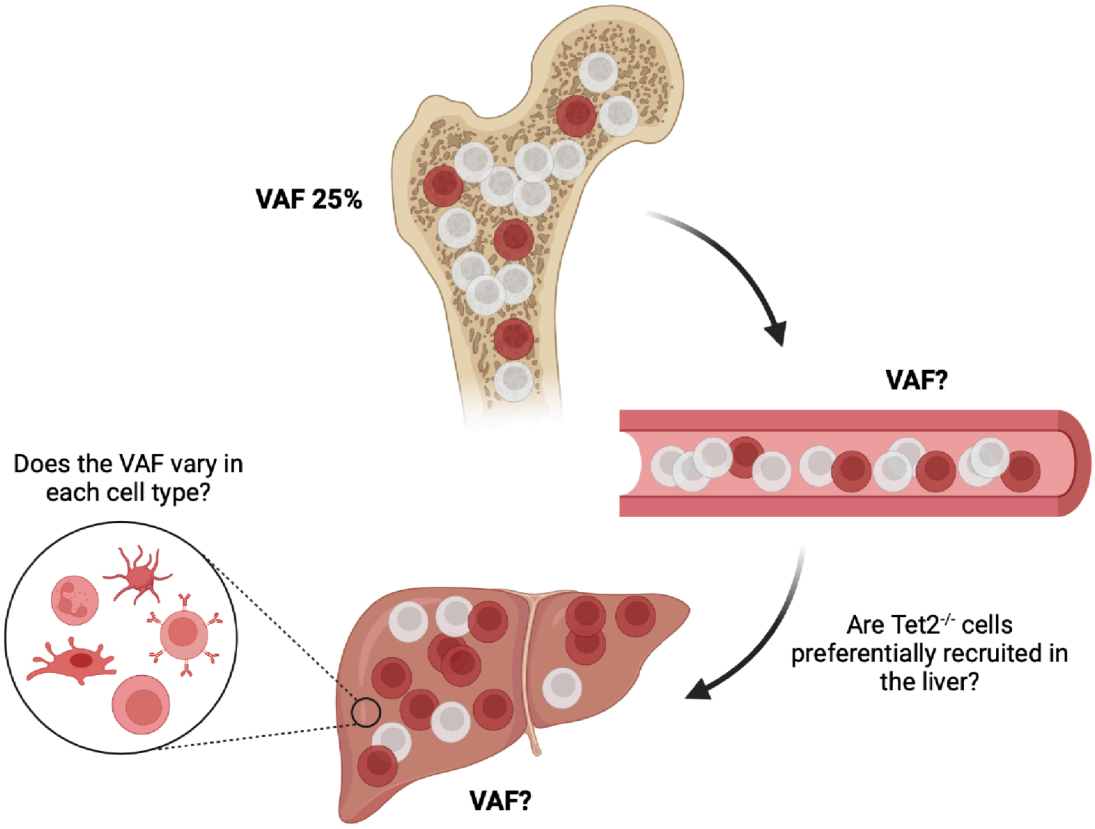


Figure 6.2. Assessing whether *Tet2*$^{-/-}$ VAF is cell-type and organ-specific.
Image created using Biorender.

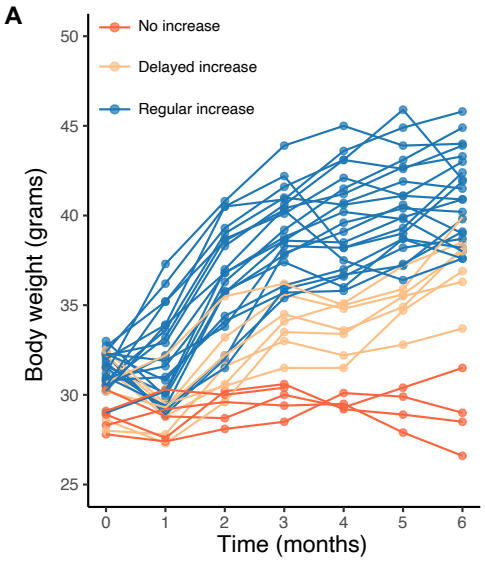
6.3. Heterogeneity in disease progression in mice treated with a Western diet

Previous studies have shown that high-caloric diets, such as CD-HFD and WD, induce HCC in approximately 25% of male mice after a year[138]. In contrast, females rarely reach advanced stages of the NAFLD disease and rarely develop HCC[139]. Other papers have identified a small fraction of non-responder mice which do not exhibit weight gain or develop NAFLD and HCC despite high-caloric feeding. Occasionally, these non-responders can develop liver cancer despite remaining lean, without evidence of NAFLD etiology. A recent publication characterized this subset of mice, demonstrating high levels of biliary damage (cholemia), which upon high-caloric diets, can trigger a rapid development of liver tumors[140].

In this project, I also detected a number of non-responders in all cohorts, some of whom eventually developed liver cancer. Given that this dissertation tries to investigate whether *Tet2*

CHIP contributes to the transition from NAFLD to HCC, mice without NAFLD progression were not included in downstream analyses. In addition to observing non-responders, I noted a high degree of variability in terms of disease kinetics among individual mice. Despite all mice were equally treated with a WD, the rate of body weight increase varied significantly among them, with some mice initiating weight gain months later and others exhibiting a milder, gradual increase (**Figure 6.3A**). The heterogeneity in disease progression has become a challenge in this project, as it is important to select homogenous cohorts to interrogate the risk of progressing from NAFLD to HCC in the presence or absence of *Tet2* CHIP.

So far, only non-responders have been excluded from analyses. However, the establishment of criteria defining mice reaching a comparable stage in NAFLD progression is still needed (**Figure 6.3B**). For instance, selecting mice with similar body weight gain kinetics could help exclude those with delayed or notably milder responses. Another criterion to score NAFLD would be the NAS score, which as shown in this thesis, significantly increases in WD mice, and is able to determine the disease stage. In fact, mice with delayed or moderate increase body weight correlate with low NAS scores in my data (data not shown), therefore demonstrating that the increase in body weight is an essential step to develop subsequent stages of NAFLD and transform to HCC. A third strategy to define homogenous NAFLD cohorts would be to establish the 6-months timepoint analysis not based on the start of the diet, but on the timepoint the mice start to put on weight. In summary, future criteria will be needed in order to investigate the mechanisms underlying *Tet2* clonal hematopoiesis as a risk factor in NAFLD patients to transition to liver cancer.



B

Criteria	
Increase in body weight	≥20% of initial body weight
NAS score	≥5
Months increasing weight	≥6 months

Figure 6.3. Heterogeneity in the NAFLD model as evidenced by heterogeneous increase in body weight over time on WD. A) Monthly body weight measurements, dividing mice between lack of increase in body weight, delayed or regular increase in body weight. **B)** Criteria to stratify mice reaching a specific pathological stage of NAFLD.

6.4. Exploring the mechanisms via which *Tet2* CHIP contributes to NAFLD-HCC progression

Numerous clinical studies have established a link between clonal hematopoiesis and an elevated risk of disease development; however, the underlying mechanisms driving these associations remain poorly understood. The biological implications of CHIP have been mostly characterized in the HSPC compartment, where mutations are acquired in the first place. Research on *Dnmt3a* and *Tet2* mutations demonstrated that they can modify stem cell biology, enhancing their self-renewal potential while compromising healthy hematopoietic differentiation[50,119,141,142]. Functional assays have shown enhanced replating ability of mutant HSCs in vitro, and an engraftment advantage in recipient mice when transplanted alongside competitor cells. Despite generally producing the same phenotypic alterations, recent studies have suggested divergent outcomes in *Tet2* and *Dnmt3a* mutant HSCs, with differences in terms of differentiation biases and molecular mechanisms[143].

While mutant HSCs can result in the development of leukemias, their role in non-hematologic diseases remains less clear. Instead, mutant mature blood cells infiltrating peripheral organs are responsible in this context. Mutant macrophages, neutrophils and

platelets infiltrating peripheral tissues have been associated to CHIP-related diseases, such as cardiovascular conditions, where they induce inflammation and exacerbate disease progression. Mechanistically, platelets showed abnormal aggregation patterns producing plaques, neutrophils generated neutrophil extracellular traps (NET), a process called NETosis, and macrophages exacerbated their production of inflammatory cytokines[52,59,144]. In the context of chronic liver disease, macrophages seem to play a pivotal role in inducing inflammation and exacerbating liver damage and fibrosis[134].

In my doctoral thesis, I employed various methodologies to investigate how the presence of *Tet2*$^{-/-}$ hematopoietic cells could increase the incidence and severity of NAFLD-HCC. Two mechanistic options were considered: the first one assumed that CHIP accelerates the evolution of NAFLD-HCC induced by the Western diet, through previously described sequential events. The alternative suggested that *Tet2* CHIP triggers NAFLD-HCC transition via distinct mechanistic pathways. To interrogate this question, I conducted a kinetics-based assessment of disease progression. Unlike previous research, my data demonstrated no difference between WT and *Tet2*$^{-/-}$ groups in terms of immune cell recruitment, at 3- or 6-months. This suggests that either recruitment levels do not vary in this NAFLD-CHIP model, or enhanced recruitment occurs at earlier timepoints not analyzed in this thesis. Interestingly, the proportion of donor infiltration (% CD45.1^{+} cells) significantly correlated to markers of liver damage such as ALT only in the *Tet2*$^{-/-}$ group, suggesting that the higher the *Tet2*$^{-/-}$ VAF in liver-hematopoietic cells, the more liver damage is induced.

Moreover, assessment of immune cell composition identified a higher proportion of Kupffer cells in the *Tet2*$^{-/-}$ group; however, the significance of this altered composition in disease progression remains unclear. An important next step will involve characterizing immune infiltration at the histological level, where dysfunctional patterns, such as excessive aggregation, or altered spatial localization, can be detected.

Given that absolute immune cell infiltration did not alter in *Tet2*$^{-/-}$ cells, I soughed to explore whether these cells exhibited distinct molecular programs compared to WT cells. As TET2 functions as an epigenetic regulator, its loss likely leads to methylation changes affecting chromatin accessibility, ultimately influencing gene expression and cellular processes. In this

thesis, I tried to deconvolute the consequences of *Tet2*$^{-/-}$ in the epigenome and transcriptome. Analysis has only been performed on the transcriptomic data, which is what I discussed in this dissertation. Previous studies suggested increased inflammation as a potential mechanism in *Tet2*$^{-/-}$ cells, specifically within myeloid cell types[134]. While sequencing of liver homogenates demonstrated significantly higher inflammation in *Tet2*$^{-/-}$ infiltrated livers compared to WT, pro-inflammatory gene expression programs were not detected in *Tet2*$^{-/-}$ myeloid cells. My data set, on the contrary, revealed pro-inflammatory phenotypes in CD8^{+} T cells. A potential hypothesis explaining this data would be that at the 6-months timepoint, all myeloid cells are pro-inflammatory, regardless of the *Tet2* status, and that differences segregating WT and Tet2$^{-/-}$ cells are only detectable at earlier timepoints. This goes in line with Wong et al. publication, which showed pro-inflammatory gene expression Kupffer cells at 3-months after the start of the diet[134]. T cells have delayed infiltration in NAFLD livers compared to the myeloid cell types. Hence, this delayed kinetics could explain why I can detect differences in inflammatory responses in T cells with *Tet2* deletion.

T cells have received less attention in the CHIP field due to higher mutation frequencies observed in myeloid over lymphoid cells; however, mutant T and B cells infiltrating peripheral organs could significantly impact disease progression. In NAFLD-HCC, T cells play a crucial role in later disease stages and are pivotal for transitioning to HCC[100]. My research uncovered a novel role for *Tet2* CHIP T cells in driving inflammatory responses in chronic liver disease—a contribution potentially overlooked in prior studies assessing molecular changes at early timepoints. Therefore, my analysis likely captures a later stage in liver disease progression, potentially more relevant for the transition to liver cancer.

In addition to inflammation, other gene expression changes were identified in liver-infiltrating immune cells. Interestingly, EMT-related and angiogenesis genes were consistently upregulated in *Tet2*$^{-/-}$ cells compared to WT, which suggests a common mechanism shared between hematopoietic cells. However, these changes will need to be validated with other molecular assays, as well as at the functional level. An ongoing analysis focuses on validating specific targets, such as vessel formation, fibrotic markers from the EMT pathway, inflammatory markers, in histological sections.

In this thesis, I also explored the potential synergy between *Tet2* CHIP and diet-induced metabolic alterations in epigenome reprogramming by metabolomics analysis in hematopoietic cells. Although TET2 cofactors such as a-KG, succinate and fumarate did not show pronounced differences between the groups, this analysis revealed other interesting differences resulting from the diet or *Tet2* CHIP. Notably, essential amino acids were increased upon WD in WT hematopoietic cells, but not in *Tet2*$^{-/-}$. The biological meaning of this finding has not been explored in the thesis, however, it could be hypothesized that excessive levels of amino acids are detrimental for immune cells, and that TET2 loss of function somehow protects against this toxicity, supporting cell survival in liver-infiltrating immune cells. Further experiments will need to address this hypothesis.

6.5 Identifying biomarkers for NAFLD-HCC

Advanced liver fibrosis is considered the most frequent risk factor for HCC development[145]. However, around 50% of NAFLD-HCC cases develop without evidence of liver fibrosis. Other studies have revealed additional risk factors, including old age, male sex, mild alcohol intake, diabetes and other metabolic syndromes, obesity, and elevated levels of liver aminotransferases in serum[146]. Also, genetic factors are involved in the pathogenesis of NAFLD-HCC. In reality, it is likely that a combination of factors, both environmental and genetic, influence the risk of HCC in NAFLD patients. Although some studies have proposed prediction models combining a number of the aforementioned factors[147,148], further investigations are needed in order to implement early detection programs for high risk NAFLD patients. In my thesis, I propose *Tet2* CHIP as a novel risk factor for HCC progression, as evidenced by the synergistic increased in HCC incidence and severity of NAFLD when combining *Tet2* CHIP with a Western diet. Targeted sequencing of peripheral blood samples to screen for CHIP mutations would provide a non-invasive opportunity to identify NAFLD patients with high risk of progressing to HCC.

Moreover, early identification of individuals with a high risk of cancer development may facilitate effective cancer prevention using already existing approaches such as intensive dietary/exercise intervention, while new molecular insights into the process of malignant transformation may open up new therapeutic strategies that are focussed on the interplay of

diet-programmed blood cells and the liver. Hence, further analysis from all molecular data generated in this dissertation will ultimately serve as a platform to identify potential therapeutic targets for high risk NAFLD patients.

7

Materials and Methods

7.1 Animal experiments

All animal procedures were approved by the Animal Care and Use Committees of the German Regierungspräsidium Karlsruhe für Tierschutz und Arzneimittelüberwachung (Karlsruhe, Germany) under the TVAs G-41/19 and G-279/19. Mice were maintained in individually ventilated cages under specific pathogen-free (SPF) conditions at the German Cancer Research Center (DKFZ, Heidelberg). All mice were given drinking water and chow *ad libitum.*

Wild-type mice (C57BL/6J) were purchased from Janvier Laboratories. The mouse lines UBC-GFP, KuOrange (KuO), *Rag2*$^{-/-}$, SclCreERT2, *Tet2*$^{fl/fl}$ and C57BL/6 x Ly5.1 were bred in-house. *Tet2*$^{fl/fl}$ mice were crossed with SclCreERT2 to generate *Tet2*$^{fl/fl}$ SclCreERT2 mice. All mice were used as donors or recipients for transplantations experiments.

7.2 Treatments

7.2.1 Tamoxifen

In order to activate the CRE recombinase activity present in the mouse lines SclCreERT2 and *Tet2*$^{fl/fl}$ SclCreERT2, mice were treated with 10mg/mL tamoxifen solution, which was prepared by mixing tamoxifen powder (Sigma; T-5648-5G) with 10% absolute ethanol (Supelco; 1.00983) and 90% sunflower oil (Sigma; S-5007). The solution was dissolved by rotation for 2 hours at room temperature in a roller mixer. Mice were injected intraperitoneally with 200µL tamoxifen solution (2mg), once per day for five consecutive days using a 1mL syringe (SOFT-JECT; SJ-9161406) and a 26-gauge needle (BD; 300300).

7.2.2 Diet

Mice were fed *ad libitum* with 40kcal% fat (non-trans-fat Primex), 22% fructose, and 2% cholesterol (Research Diets, D16022301) for periods of 3-, 6-, 9- or 12- months. Body weight was monitored monthly until the endpoint.

7.3 Bone marrow transplantations

7.3.1 Body irradiation and transplantation

CD45.2^{+} C57BL/6J recipient mice were subjected to whole body irradiation with two rounds of 500 Rad, separated by 4 hours. 24 hours post irradiation, mice were shortly exposed to infrared light to dilate the tail veins, and transplanted via *i.v.* injection with 200µL cell suspension using a 29-gauge insulin syringe (BD; 324827).

7.3.2 Single cell transplantations (Project I)

Mice were transplanted via *i.v.* injection with 200µL RPMI 1640 medium (Sigma; R8758-6X500ML) + 2% FBS (Gibco) containing one LT-HSC (EPCR^{hi}, CD34^{-}, CD150^{+}, CD48^{-}, LSK) derived from a transgenic CD45.1 UBC-GFP donor mouse, together with 1.5x10^{5} WT CD45.1/CD45.2 supportive whole bone marrow cells **(Figure 7.1 A)**. In a second group of experiments, co-transplantations of one UBC-GFP LT-HSC plus one KuO LT-HSC together with 1.5x10^{5} WT CD45.1/CD45.2 supportive whole bone marrow cells were performed **(Figure 7.1 B)**. A third experimental design consisted of co-transplantations of one UBC-GFP LT-HSC plus one KuO LT-HSC together with 1.5x10^{5} *Rag2*$^{-/-}$ supportive whole bone marrow into *Rag2*$^{-/-}$ recipients **(Figure 7.1 C)**.

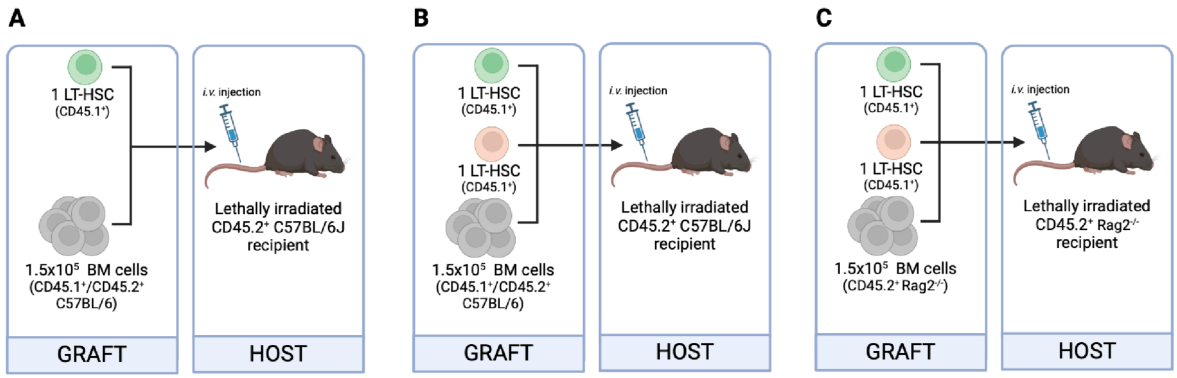


Figure 7.1. Experimental scheme of single cell transplantations. A) Single cell transplantations of single LT-HSCs derived from a UBC-GFP donor mouse. **B)** Co-transplantations of 2 LT-HSCs derived from a UBC-GFP and a KuO mouse. **C)** Same experimental design as B but exchanging the recipient and supportive bone marrow mice to the *Rag2*$^{-/-}$ model.
Image created using Biorender.

7.3.3 Bulk bone marrow transplantations (Project II)

CD45.2 C57BL/6J recipient mice were transplanted with 200µL PBS containing 6x10^{6} whole bone marrow cells derived from either CD45.1 SclCreERT2 or CD45.1 *Tet2*$^{fl/fl}$ SclCreERT2 mice.

7.4 Sample collection

7.4.1 Blood

Peripheral blood was withdrawn from the *vena facialis* using a 23-gauge needle (CHIRANA T.Injecta; CH23100) and collected into EDTA-coated tubes (Sarstedt; 20.1278). A maximum volume of 120µL was collected at a single time. In mouse endpoints of project II, blood was withdrawn by cardiac puncture after an intraperitoneal lethal dose of anesthesia consisting of 20 mg/kg Xylazine (stock 20mg/mL) and 100-300mg/kg Ketamine (stock 100mg/mL). Drugs were obtained from the mouse facility pharmacy at the DKFZ. In this case, I withdrew as much blood as possible. 30µL blood aliquot was used to measure blood cell counts using a Hemavet 950 FS (Drew Scientific) or ScilVet abc-Plus+ veterinary blood cell counting machine (Scil GmbH). The remaining blood was used for flow cytometry analysis or sorting.

7.4.2 Serum

Peripheral blood was withdrawn from the *vena facialis* using a 23-gauge needle (CHIRANA T.Injecta), or cardiac puncture using a 23-gauge needle (CHIRANA T.Injecta; CH23100) attached to a 1mL syringe (SOFT-JECT; SJ-9161406). Blood was collected into serum tubes (Sarstedt; 20.1280) and incubated at room temperature for 30 minutes to allow blood coagulation. Alternatively, blood was left at 4°C for several hours before proceeding to the serum extraction. Then, blood tubes were span down for 20 min at 2000xg at 4°C. Supernatant (serum) was carefully removed and aliquoted into 1.5mL Eppendorf tubes. Serum was sometimes stored at -80°C until needed for analysis. Occasionally, serum was diluted 1:1 in PBS and directly submitted to Zentrallabor at Uniklinikum Heidelberg for serology analysis of cholesterol, ALT, AST and triglycerides levels. Analysis was performed by Dr. Maik Brune.

7.4.3 Bone marrow

Mice were euthanized by cervical dislocation or lethal dose of anesthesia consisting of 20 mg/kg Xylazine (stock 20mg/mL) and 100-300mg/kg Ketamine (stock 100mg/mL), injected intraperitoneally. Bone marrow isolation involved the dissection of the femurs, hips and tibias and when needed the vertebrae, sternum and arms. Soft tissue was cleaned from the bones. In order to generate a bone marrow cell suspension, bones were either crushed with a mortar or flushed with PBS using a 1mL syringe (SOFT-JECT; SJ-9161406) fitted with a 23-gauge needle (CHIRANA T.Injecta; CH23100). The cell suspension was in both cases filtered through 40µm cell strainers (Greiner Bio-One; 542040), span down at 1500rpm at 4 °C for 5 minutes, and the resulting cell pellet was resuspended in an adequate volume of cold PBS + 2% FBS (PAA Laboratories/Sigma Aldrich). 30µL of the cell suspension was used for cell counting using a Hemavet 950 FS (Drew Scientific) or ScilVet abc-Plus+ veterinary blood cell counting machine (Scil GmbH).

7.4.4 Liver

Mice were euthanized with a lethal dose of anesthesia consisting of 20 mg/kg Xylazine (stock 20mg/mL) and 100-300mg/kg Ketamine (stock 100mg/mL), and perfused through the left ventricle with cold PBS using a Safety-Multifly 25G cannula (Sarstedt; 85.1642.201) connected to a 20mL syringe (Terumo; SS+20L1). After perfusion, liver was weighed and cut in several pieces for downstream analysis; a small lobule for histology, 2 small pieces were

snap frozen and stored in -80°C, and the rest was processed for flow cytometry analysis or sorting. The liver part used for flow cytometry was separately weighed. Liver digestion, enrichment of liver-infiltrating immune cells, and antibody staining for flow cytometry analysis was performed by Chaofan Fan (Division of Chronic Inflammation and Cancer, DKFZ).

7.5 Histology

In project II, histological liver sections were processed by Chaofan Fan (Division of Chronic Inflammation and Cancer, DKFZ). Tissues were fixed, cut and stained with H&E.

7.6 EchoMRI

In project II, body composition of normal diet and Western diet mice were analyzed using an EchoMRITM-100V Whole Body Composition Analyzer (Echo Medical Systems, Houston, Texas).

7.7 Flow Cytometry

7.7.1 Isolation of murine LT-HSC cells via FACS

Bone marrow cell suspension was subjected to depletion of mature blood cell lineages incubating with a mix of rat anti-mouse biotin-conjugated lineage markers 4.2µg/mL CD5 (BD; 553019), 4.2µg/mL CD8a (BD; 553029), 2.4µg/mL CD11b (BD; 553309), 2.8µg/mL B220 (BD; 553086), 2.4µg/mL Gr-1 (BD; 553125), 2.6µg/mL Ter-119 (BD; 553672) for 40 min at 4 °C. After incubation, cells were washed once with PBS + 2% FBS, span down at 1500 rpm at 4°C for 5 min, resuspended in 800µl PBS + 2% FBS and mixed with 800µL Biotin Binder Dynabeads (Thermo Fisher; 11415D), which were previously washed (2 washes with PBS + 2% FBS). Beads were added at a concentration of 1mL beads /1x10^8 cells. Cells-beads mix was incubated for 45 min at 4°C with constant rotation. After that, the lineage-positive cells were depleted using a magnetic particle concentrator (Dynal MPC-6, Invitrogen), and the resulting Lineage negative-enriched fraction was washed once with PBS + 2% FBS, and stained with the panel of

antibodies indicated in **Tables 7.6, 7.7, 7.10**. during 30 minutes at 4°C. After the incubation, stained cells were washed once with PBS + 2% FBS, resuspended in a final concentration of 2mL PBS + 2% FBS and filtered through a FACS tube with cell strainer snap cap (Corning; 352235) before the sort. All Project I sorting experiments were performed using a BD FacsAria I flow cytometer (BD Bioscience) with a 100µm nozzle and single cell purity. Single EPCR^{hi} LT-HSCs were sorted into round-bottom 96-well cell culture plates (Greiner bio-one; 650180) with 100µL RPMI + 2% FBS with a cooling system. After the sort, 100µL of supportive total bone marrow at a concentration of 1.5x10^6 cells/mL was added on top of the sorted HSC using a multichannel pipette, reaching a final volume of 200µL per well. Cell suspension was pipetted up and down and immediately taken up using a 29-gauge insulin syringe (BD; 324827).

For in vitro HSC clonal expansion experiments (Project II), single LT-HSCs were sorted into round bottom 96-well cell culture plates (Greiner bio-one; 650180) containing 150µL HSC expansion medium (**Table 7.1**). BD FacsAria I or II flow cytometers (BD Bioscience) were used for these experiments, with 100µm nozzle and single cell purity settings.

Table 7.1. HSC expansion medium.

StemSpan SFEM (STEMCELL Technologies; 09650) medium supplemented with:

Component	Final concentration	Stock concentration	Supplier, Catalog number
Penicillin/Streptavidin	1%		Sigma (P4458-100ML)
L-Glutamine	1%		ThermoFisher (25030024)
rh Flt3 ligand	10ng/µL	100ng/µL	PeproTech (300-19-100)
rm SCF	50ng/µL	100ng/µL	PeproTech (250-03-100)
rm TPO	10ng/µL	100ng/µL	PeproTech (AF-315-14-100)
rm IL3	5ng/µL	100ng/µL	PeproTech (213-13-50)
rm IL7	10ng/µL	100ng/µL	PeproTech (217-17-10)
rm IL11	10ng/µL	100ng/µL	PeproTech (220-11-100)

rm: recombinant murine
rh: recombinant human

7.7.2 Isolation of liver-infiltrating immune cells by FACS

After liver digestion and immune cell enrichment, cells were resuspended in 200µL MACS buffer and filtered through a FACS tube with cell strainer snap cap (Corning; 352235) before the sort. 5µL CountBright™ Absolute Counting Beads (ThermoFisher; C36950) were added to each sample just before sorting in order to calculate absolute cell counts. These experiments were performed in BD FacsAria I, BD Fusion I, or BD Fusion II cytometers.

7.7.3 Isolation of liver-infiltrating immune cells by FACS for bulk RNA sequencing

For bulk RNA-sequencing experiments, sorter settings were 100µm nozzle and 4-way purity precision. A maximum of 16,000 liver-infiltrating CD45.1$^+$ donor Kupffer cells (CD11b$^+$ F4/80$^+$), PD1$^+$CD8$^+$ T cells and Ly6C^{high} monocytes (CD11b$^+$ Ly6C^{high}) were sorted in DNA LoBind 1.5mL tubes (Eppendorf; 0030108051). Cells were sorted directly into 50µL Extraction buffer (Arcturus™ PicoPure™ RNA isolation kit; 12204-01) and directly frozen at -80°C until RNA isolation.

7.7.4 Isolation of liver-infiltrating immune cells by FACS for scRNA sequencing

For single cell RNA-sequencing, sorter settings were 100µm nozzle and 4-way purity precision. 20,000 liver-infiltrating CD45.1$^+$ cells were sorted into DNA LoBind 1.5mL tubes (Eppendorf; 0030108051). Cells were sorted into 200µL of StemSpan SFEM (STEMCELL Technologies; 09650) and directly processed using the 10X Genomics scRNA-sequencing platform.

7.7.5 Isolation of liver-infiltrating immune cells by FACS for low input metabolomics

For metabolomic experiments, sheath fluid was exchange to 0.2% NaCl, and settings were 70 µm nozzle and 4-way purity. Skirted twin-tec LoBind clear PCR 96-well plate (Eppendorf; 0030129512) were used for sample collection, filled with 25µL extraction solution (100% Acetonitrile-LC-MS grade+ 0.1% 13C internal standard). Plate wells were covered with a PCR lid to avoid evaporation before, during and after the sort. 5,000 liver-infiltrating CD45.1+ donor Kupffer cells (CD11b$^+$ F4/80$^+$), CD8$^+$ T cells and Ly6C^{high} monocytes (CD11b$^+$

Ly6C^{high}) were sorted into individual wells. In addition to the samples, 3 debris controls (in which an equal number of droplets containing a very low light-scattering-signal is sorted) and 3 negative controls (without sorting cells) were sorted. After the sort, plates were stored at -80°C and shipped to the laboratory of Prof. Dr. Nina Cabezas-Wallscheid (Max-Planck Institute of Immunobiology and Epigenetics, Freiburg) to proceed with the metabolomics analysis.

7.7.6 Antibody-based staining of peripheral blood cells

Peripheral blood was stained using monoclonal antibodies recognizing cell-specific surface proteins. For white blood cell staining, 30-50µL of peripheral blood was incubated with 100µL antibody mix prepared in PBS + 2% FBS. Platelet and erythrocyte staining consisted of 3µL peripheral blood and 27µL antibody mix. Cells were incubated for 30-45 min at 4°C in the dark. Blood samples stained with antibodies against white blood cell epitopes were subject to an erythrocyte lysis step using a self-made ACK lysis buffer (**Table 7.2**). Blood cells were incubated with 1mL ACK lysis buffer for 10min at room temperature in the dark. After the lysis, cells were washed once with PBS + 2% FBS, span down at 1500rpm for 5min in a table top centrifuge, and resuspended in 100µL (white blood cell staining) and 400µL (platelet and erythrocyte staining) PBS + 2% FBS. All samples were filtered prior to flow cytometry analysis. In case of platelet and erythrocyte staining, this lysis step was not performed, so cells were directly washed and resuspended in a final volume of PBS + 2% FBS.

Table 7.2. ACK lysis buffer recipe.

Component	Amount	Concentration	Supplier, Catalog number
Ammonium chloride (mw: 53.49 g/mol)	8.02 g	0.15M	Roth (5470.1)
Potassium bicarbonate (mw: 100.12 g/mol)	1 g	0.01M	Roth (X887.1)
Disodium EDTA (mw: 372.24 g/mol)	0.0372 g	0.0001M	Sigma-Aldrich (ED2SS-1KG)
H_20	1L		
Adjust pH to 7.2-7.4			

7.7.7 Antibody-based staining of bone marrow cells

Bone marrow cell suspensions were stained using monoclonal antibodies recognizing cell-specific surface proteins. Cells were incubated with an antibody mix prepared in PBS + 2% FBS at a concentration of 10µL antibody mix/ $1x10^6$ cells. Cells were incubated for 30min at 4°C in the dark. Stained samples were subjected to an erythrocyte lysis step using a self-made 1mL ACK lysis buffer during 3min at room temperature. After the lysis, cells were washed once with PBS + 2% FBS, span down at 1500 rpm for 5 min in a table top centrifuge, and resuspended in 20 µl PBS + 2% FBS/ $1x10^6$ cells. All samples were filtered prior to flow cytometry analysis.

7.7.8 Flow cytometry analysis

After antibody-based staining, cells were subjected to flow cytometry analysis using a LSRFortessa cytometer (Becton Dickinson), equipped with 350 nm, 405 nm, 488 nm, 561 nm and 641 nm excitation lasers. Antibody panels were manually compensated using OneComp eBeads (eBioscience; 01-1111-41) stained with single antibodies. Data analysis was performed using Flowjo (Tree Star).

7.8 In vitro single HSC expansion and colony PCR

After sorting of single LT-HSCs into 96-well plates containing expansion medium, plates were incubated for ten days in a normoxic cell culture incubator (37°C, 5% CO_2). Wells with successful cell growth (HSC colony) were marked. Plates were span down at 1500 rpm for 5 min at 4°C, supernatant was discarded, and marked HSC colonies were resuspended in lysis buffer (Qiagen; 102-T) with 5% proteinase K (Qiagen; 19131) and transfer into PCR 8-strip tubes (Biozym; 710970). Cell suspensions were incubated in a thermocycler machine at 56°C for 2 hours, followed by 95°C for 30 min to inactivate the proteinase K. Lysates were stored at 4°C. To assess the Cre-mediated recombination efficiency of the *Tet2* floxed gene in the individual colonies, lysates were used for genotyping PCR. Each PCR reaction contained 10 µL PCR Red Master mix (Genaxxon; M3029.0500), 0.2µM of primer 1, 0.2µM of primer 2 and 0.2µM primer 3 (primer stocks: 10µM), 6.5µL H_20 and 2µL lysate (**Table 7.3**). Primer sequences and PCR program are shown in **Table 7.4** and **Table 7.5.**

Table 7.3. PCR reaction for assessing *Tet2* recombination.

	1x	Concentration
PCR Red Master mix 2X	10µL	1X
Primer 1 (10µM)	0.4µL	0.2µM
Primer 2 (10µM)	0.4µL	0.2µM
Primer 3 (10µM)	0.4µL	0.2µM
H_20	6.5µL	
DNA (lysate)	2µL	
Final volume	20µL	

Table 7.4. *Tet2* genotyping primer sequences. Primer sequences taken from Moran Crusio et al.[50]

Name	Sequence
Tet2 Primer 1	TAGAGGGAGGGGGCATAAGT
Tet2 Primer 2	AAGAATTGCTACAGGCCTGC
Tet2 Primer 3	TTCTTTAGCCCTTGCTGAGC

Table 7.5. Touchdown PCR program for *Tet2* recombination genotyping.

Step	Temperature	Time	Cycles
Initial denaturation	94	2 min	
Denaturation	94	20 sec	10
Annealing	65 (-0.5°C per cycle)	15 sec	
Extension	68	10 sec	
Denaturation	94	15 sec	28
Annealing	60	15 sec	
Extension	72	10 sec	
Final extension	72	2 min	
	4	∞	

7.9 RNA-sequencing

7.9.1 Bulk RNA-sequencing of liver-infiltrating hematopoietic cells

RNA was isolated using a PicoPure™ RNA Isolation Kit (Applied Biosystems; KIT0204), according to manufacturer´s instructions. The optional DNase treatment step was included in the protocol using a RNase-Free DNase Set (Qiagen; 79254). RNA elution was performed in DNA LoBind 1.5mL microcentrifuge tube (Eppendorf; 0030108051) with 20-30µL DNase/RNase free H_2O, depending on the sorted cell input. RNA concentration and quality were validated using the RNA 6000 Pico Kit for 2100 Bioanalyzer Systems (Agilent Technologies; 5067-1513). 1ng of the isolated RNA was used to generate libraries for sequencing using the NEBNext Single Cell/Low Input RNA Library Prep Kit for Illumina (NEB; E6420L) according to the manufacturer´s instructions. 36 libraries were multiplexed using different combination of NEBNext oligos from the NEBNext Multiplex Oligos for Illumina (Dual Index Primers Set 1, NEB; E7600S) The average fragment size of the final libraries was assessed using a High Sensitivity DNA (Agilent Technologies; 5067-4626), and the DNA concentration with a Qubit dsDNA High Sensitivity (HS) kit (Invitrogen; Q33230). A 10nM equimolar multiplex containing all the libraries was prepared and sequenced in a NovaSeq 6000 patterned flowcell with a paired 100bp sequencing read length at the DKFZ NGS Core Facility. Bioinformatic analysis was performed using the DESeq2 script published by Love, M.I., Huber, W., Anders, S[149].

7.9.2 Bulk RNA-sequencing of liver homogenates

Pieces of liver were snap frozen and stored at -80°C until continuing with the homogenization. Then, 10mg of liver tissue was cut with help of a scalper on top of a petri dish in direct contact with ice to constantly maintain the integrity of the tissue. The 10mg of liver tissue were transferred to Precellys tubes containing 350uL Buffer RLT (Qiagen; 79216) + 1:100 β-ME (ThermoFisher; 31350010) and homogenized using a Precellys Evolution Touch Homogenizer (Bertin Technology) at 5000 rpm, 4°C for 2 min. Afterwards, samples were immediately cooled down by placing them in ice. After homogenization, lysates were transferred to 1.5mL tubes, and span down for 3 minutes at maximum speed. Supernatant was carefully transferred to new 1.5mL tubes. Total RNA was isolated according to the manufacturer's protocol using RNeasy Mini Kit (Qiagen; 74104). The final RNA concentration

was quantified using a Nanodrop analyzer (Thermo Scientific). RNA quality was determined using the RNA 6000 Pico Kit for 2100 Bioanalyzer Systems (Agilent Technologies; 5067-1513). DNA libraries were prepared by the DKFZ NGS Core Facility, and sequenced in a NovaSeq 6000 patterned flowcell with a paired 100bp sequencing read length. Bioinformatic analysis was performed using the DESeq2 script published by Love, M.I., Huber, W., Anders, S[149].

7.9.3 Single cell RNA-sequencing of liver-infiltrating hematopoietic cells

Following the digestion and enrichment of liver-infiltrating immune cells, individual samples underwent cell multiplexing using the 3' CellPlex Kit for Cell Multiplexing (10X Genomics; PN-1000261). A total of $2x10^6$ cells were utilized as input for the CellPlex protocol, which was followed by antibody staining using PE CD45.1 and DAPI in PBS + 10% FBS. $CD45.1^+$ live cells were sorted into DNA LoBind 1.5mL tubes (Eppendorf; 0030108051) with four samples multiplexed into the same tube. Each sample consisted of 7,000 cells, resulting in a combined total of 28,000 cells. After the sort, collection tube was span down in a table top centrifuge for 5min at 400g. Supernatant was carefully removed leaving 60µL of cell-containing medium. 5µL volume was taken out for cell counting and cell viability assessment in a Cytosmart, and the rest of the sample was loaded into a Chromium Next GEM Chip G. Samples were processed using the Chromium Next GEM Single Cell 3' Reagent Kits v3.1 Dual Index (10X Genomics) according to the manufacturer´s instructions. The average fragment size of the final libraries was assessed using a High Sensitivity DNA (Agilent Technologies; 5067-4626), and the DNA concentration was measured with a Qubit dsDNA High Sensitivity (HS) kit (Invitrogen; Q33230). Bioinformatic analysis was performed by Dr. Charles Dussiau (Milsom and Zaugg labs).

7.10 Data visualization and statistical analysis

Data visualization and statistical tests were performed using R. The statistical test, sample size (n) and statistical significance are summarized at the end of each figure legend. All figures in this thesis were designed using Affinity Designer software. Images created with Biorender are mentioned in the corresponding figure legend. This thesis was written in Microsoft word.

Table 7.6. Antibody panel for the isolation of GFP$^+$ EPCR^{hi} LT-HSCs.

Antigen	Fluorophore	Clone	Supplier, Catalog number
CD4	AF700	GK1.5	eBioscience (56-0041-82)
CD8	AF700	53-6.7	eBioscience (56-0081-82)
B220	AF700	RA3-6B2	eBioscience (56-0452-82)
CD11b	AF700	M1/70	eBioscience (56-0112-82)
Gr-1	AF700	RB6-BC5	eBioscience (56-5931-82)
Ter119	AF700	TER-119	Biolegend (116220)
cKit (CD117)	BV711	2B8	Biolegend (105835)
Sca1 (Ly-6A/E)	APC-Cy7	D7	BD Biosciences (560654)
CD150	PE-Cy5	TC15-12F12.2	Biolegend (115912)
CD48	PE-Cy7	HM48-1	Biolegend (103424)
CD34	eFluor450	RAM34	eBioscience (48-0341-82)
EPCR	PE	eBio1560	eBioscience (12-2012-82)
	GFP$^+$ cells		

Table 7.7. Antibody panel for the isolation of KuO$^+$ EPCR^{hi} LT-HSCs.

Antigen	Fluorophore	Clone	Supplier, Catalog number
CD4	PE-Cy7	GK1.5	eBioscience (25-0041-82)
CD8	PE-Cy7	53-6.7	eBioscience (25-0081-82)
B220	PE-Cy7	RA3-6B2	eBioscience (25-0452-82)
CD11b	PE-Cy7	M1/70	eBioscience (25-0112-82)
Gr-1	PE-Cy7	RB6-BC5	eBioscience (25-5931)
Ter119	PE-Cy7	TER-119	eBioscience (25-5921-82)
cKit (CD117)	BV711	2B8	Biolegend (105835)
Sca1 (Ly-6A/E)	APC-Cy7	D7	BD Biosciences (560654)
CD150	APC	TC15-12F12.2	Biolegend (115910)
CD48	BUV395	HM48-1	BD (740236)
CD34	eFluor450	RAM34	eBioscience (48-0341-82)
EPCR	PerCP-eF710	eBio1560	eBioscience (46-2012-80)
	KuO$^+$ cells		

Table 7.8. Antibody panel for stem and progenitor cell staining (1).

Antigen	Fluorophore	Clone	Supplier, Catalog number
CD4	APC	GK1.5	eBioscience (17-0041-82)
CD8	APC	53-6.7	eBioscience (17-0081-82)
B220	APC	RA3-6B2	eBioscience (17-0452)
CD11b	APC	M1/70	eBioscience (17-0112-82)
Gr-1	APC	RB6-BC5	eBioscience (17-5931-82)
Ter119	APC	TER-119	eBioscience (17-5921-82)
cKit (CD117)	BV711	2B8	Biolegend (105835)
Sca1 (Ly-6A/E)	APC-Cy7	D7	BD Biosciences (560654)
CD150	PE-Cy5	TC15-12F12.2	Biolegend (115912)
CD48	PE-Cy7	HM48-1	Biolegend (103424)
CD34	eFluor450	RAM34	eBioscience (48-0341-82)
CD45.1	PE	A20	eBioscience (12-0453)
CD45.2	AL700	104	eBioscience (56-0454-82)
	GFP^+ cells		

Table 7.9 Antibody panel for stem and progenitor cell staining (2).

Antigen	Fluorophore	Clone	Supplier, Catalog number
CD4	PE-Cy7	GK1.5	eBioscience (25-0041-82)
CD8	PE-Cy7	53-6.7	eBioscience (25-0081-82)
B220	PE-Cy7	RA3-6B2	eBioscience (25-0452-82)
CD11b	PE-Cy7	M1/70	eBioscience (25-0112-82)
Gr-1	PE-Cy7	RB6-BC5	eBioscience (25-5931)
Ter119	PE-Cy7	TER-119	eBioscience (25-5921-82)
cKit (CD117)	BV711	2B8	Biolegend (105835)
Sca1 (Ly-6A/E)	APC-Cy7	D7	BD Biosciences (560654)
CD150	APC	TC15-12F12.2	Biolegend (115910)

CD48	BUV395	HM48-1	BD (740236)
CD34	eFluor450	RAM34	eBioscience (48-0341-82)
CD45.1	AL700	A20	Biolegend (110724)
´	GFP^+ cells		
	KuO^+ cells		

Table 7.10. Antibody panel for stem and progenitor cell staining (3).

Antigen	Fluorophore	Clone	Supplier, Catalog number
CD4	eFluor450	GK1.5	eBioscience (48-0042-82)
CD8	eFluor450	53-6.7	eBioscience (48-0081-82)
B220	eFluor450	RA3-6B2	eBioscience (48-0452)
CD11b	eFluor450	M1/70	eBioscience (48-0112-82)
Gr-1	eFluor450	RB6-BC5	eBioscience (48-5931-82)
Ter119	eFluor450	TER-119	eBioscience (48-5921)
cKit (CD117)	BV711	2B8	Biolegend (105835)
Sca1 (Ly-6A/E)	APC-Cy7	D7	BD Biosciences (560654)
CD150	PE-Cy5	TC15-12F12.2	Biolegend (115912)
CD48	PE-Cy7	HM48-1	Biolegend (103424)
CD34	FITC	RAM34	eBioscience (11-0341-82)
CD45.1	PE	A20	eBioscience (12-0453)
CD45.2	AF700	104	eBioscience (56-0454-82)

Table 7.11. Antibody panel for committed progenitors staining (1).

Antigen	Fluorophore	Clone	Supplier, Catalog number
CD4	PE-Cy7	GK1.5	eBioscience (25-0041-82)
CD8	PE-Cy7	53-6.7	eBioscience (25-0081-82)
B220	PE-Cy7	RA3-6B2	eBioscience (25-0452-82)
CD11b	PE-Cy7	M1/70	eBioscience (25-0112-82)
Gr-1	PE-Cy7	RB6-BC5	eBioscience (25-5931)

Ter119	PE-Cy7	TER-119	eBioscience (25-5921-82)
cKit (CD117)	BV711	2B8	Biolegend (105835)
Sca1 (Ly-6A/E)	APC-Cy7	D7	BD Biosciences (560654)
CD16/32	APC	93	eBioscience (17-0161-82)
CD34	eFluor450	RAM34	eBioscience (48-0341-82)
CD127	PE	A7R34	eBioscience (12-1273)
CD45.1	PE-Cy5	A20	eBioscience (15-0453-82)
CD45.2	AF700	104	eBioscience (56-0454-82)
	GFP^+ cells		

Table 7.12. Antibody panel for committed progenitors staining (2).

Antigen	Fluorophore	Clone	Supplier, Catalog number
CD4	APC	GK1.5	eBioscience (17-0041-82)
CD8	APC	53-6.7	eBioscience (17-0081-82)
B220	APC	RA3-6B2	eBioscience (17-0452)
CD11b	APC	M1/70	eBioscience (17-0112-82)
Gr-1	APC	RB6-BC5	eBioscience (17-5931-82)
Ter119	APC	TER-119	eBioscience (17-5921-82)
cKit (CD117)	BV711	2B8	Biolegend (105835)
Sca1 (Ly-6A/E)	APC-Cy7	D7	BD Biosciences (560654)
CD16/32	BUV737	2.4G2	BD Biosciences (565272)
CD127	PE-Cy7	A7R34	BD Biosciences (560733)
CD34	eFluor450	RAM34	eBioscience (48-0341-82)
CD45.1	AL700	A20	Biolegend (110724)
	GFP^+ cells		
	KuO^+ cells		

Table 7.13. Antibody panel for committed progenitors staining (3).

Antigen	Fluorophore	Clone	Supplier, Catalog number
CD4	eFluor450	GK1.5	eBioscience (48-0042-82)
CD8	eFluor450	53-6.7	eBioscience (48-0081-82)
B220	eFluor450	RA3-6B2	eBioscience (48-0452)
CD11b	eFluor450	M1/70	eBioscience (48-0112-82)
Gr-1	eFluor450	RB6-BC5	eBioscience (48-5931-82)
Ter119	eFluor450	TER-119	eBioscience (48-5921)
cKit (CD117)	BV711	2B8	Biolegend (105835)
Sca1 (Ly-6A/E)	APC-Cy7	D7	BD Biosciences (560654)
CD16/32	APC	93	BD Biosciences (565272)
CD34	FITC	RAM34	eBiosciences (11-0341-82)
CD127	PE-Cy7	SB/199	BD Biosciences (560733)
CD55	PE	RIKO-3	Biolegend (131803)
CD45.1	PE-Cy5	A20	Biolegend (15-0453-82)
CD45.2	AL700	104	eBioscience (56-0454-82)

Table 7.14. Antibody panel for mature white blood cells staining (1).

Antigen	Fluorophore	Clone	Supplier, Catalog number
CD4	PE-Cy5	GK1.5	eBioscience (15-0041-82)
CD8	PE-Cy7	53-6.7	eBioscience (25-0081-82)
B220	APC-Cy7	RA3-6B2	eBioscience (47-0452)
CD11b	APC	M1/70	eBioscience (17-0112-82)
Gr-1	PE	RB6-8C5	Invitrogen (12-5931-82)
CD45.1	PacificBlue	A20	Biolegend (110722)
CD45.2	AL700	104	eBioscience (56-0454-82)
	GFP^+ cells		

Table 7.15. Antibody panel for mature white blood cells staining (2).

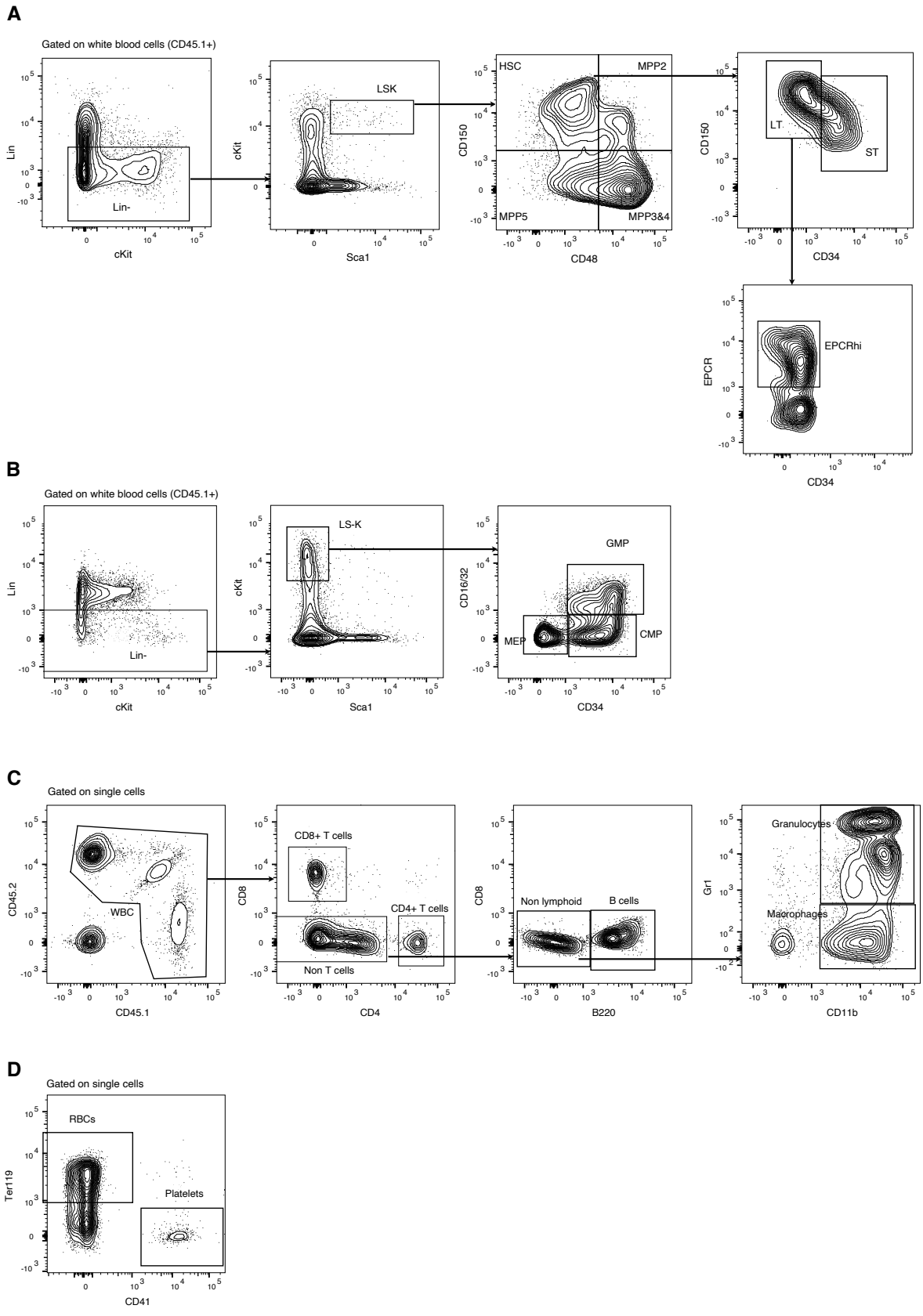
Antigen	Fluorophore	Clone	Supplier, Catalog number
CD4	BUV805	GK1.5	BD Biosciences (564922)
CD8	BUV395	53-6.7	BD Biosciences (563786)
B220	APC-Cy7	RA3-6B2	eBioscience (47-0452)
CD11b	APC	M1/70	eBioscience (17-0112-82)
Gr-1	PE-Cy7	RB6-8C5	eBioscience (25-5931)
CD45.1	PacificBlue	A20	Biolegend (110722)
	GFP^+ cells		
	KuO^+ cells		

Table 7.16. Antibody panel for mature erythrocyte and platelet staining.

Antigen	Fluorophore	Clone	Supplier, Catalog number
Ter119	APC	TER-119	eBioscience (17-5921-82)
CD41	PE-Cy7	MWReg30	eBioscience (25-0411)

Table 7.17. Antibody panel for liver-infiltrating white blood cell staining.

Antigen	Fluorophore	Clone	Supplier, Catalog number
CD11b	BV650	M1/70	BD Biosciences (562721)
CD8	PacificBlue	53-6.7	BD Biosciences (558106)
PD1	PE-Dazzle	RMP1-30	Biolegend (109115)
CXCR6	APC	SA051D1	Biolegend (151105)
Ly6C	PerCP-Cy5.5	HK1.4	eBioscience (45-5932-82)
F4/80	PE-Cy7	BM8	eBioscience (25-4801-82)
CD45.1	FITC	A20	eBioscience (11-0453-82)
Zombie Aqua	BV510		


A
Gated on white blood cells (CD45.1+)
Lin
cKit
Lin-
cKit
Sca1
LSK
CD150
CD48
HSC
MPP2
MPP5
MPP3&4
CD150
CD34
LT
ST
EPCR
CD34
EPCRhi
B
Gated on white blood cells (CD45.1+)
Lin
cKit
Lin-
cKit
Sca1
LS-K
CD16/32
CD34
GMP
MEP
CMP
C
Gated on single cells
CD45.2
CD45.1
WBC
CD8
CD4
CD8+ T cells
CD4+ T cells
Non T cells
CD8
B220
Non lymphoid
B cells
Gr1
CD11b
Granulocytes
Macrophages
D
Gated on single cells
Ter119
CD41
RBCs
Platelets

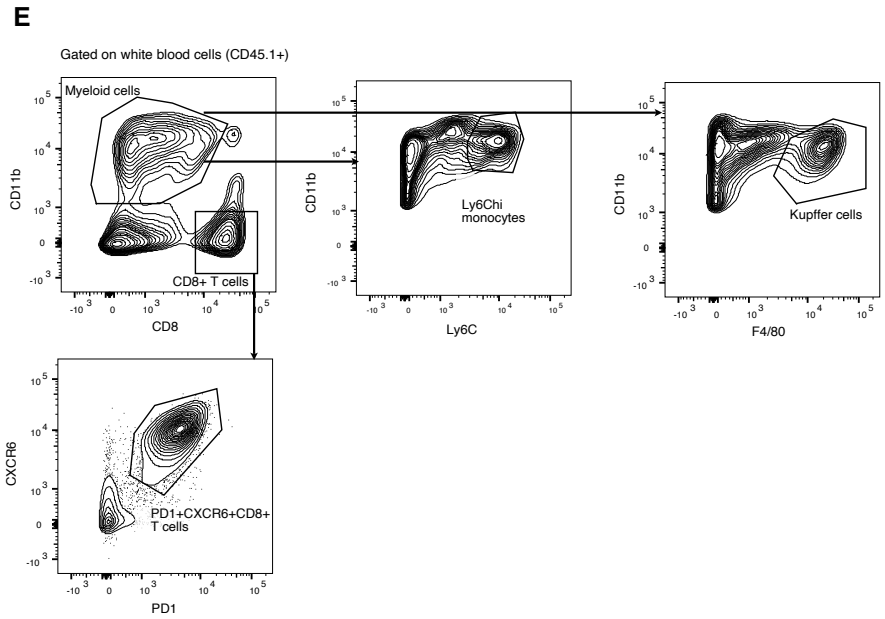


Figure 7.2. Gating strategies for the analysis and isolation of hematopoietic cells. A) Gating strategy for the isolation of a highly pure population of LT-HSCs, or analysis or the stem and progenitor cell compartment. **B)** gating strategy for the analysis of committed progenitors GMP, CMP, MEP. **C)** Gating strategy for the analysis of the mature cell compartment (B cells, T cells, myeloid cells). **D)** Gating strategy for the analysis of platelets and red blood cells**. E)** Gating strategy for the analysis and isolation of liver-infiltrating immune cells (Kupffer cells, Ly6C^{hi} monocytes, CD8^{+} T cells).

References

1. Orkin, S. H. & Zon, L. I. Hematopoiesis: An Evolving Paradigm for Stem Cell Biology. *Cell* **132**, 631–644 (2008).
2. Nombela-Arrieta, C. & Manz, M. G. Quantification and three-dimensional microanatomical organization of the bone marrow. *Blood Adv.* **1**, 407–416 (2017).
3. Seita, J. & Weissman, I. L. Hematopoietic stem cell: Self-renewal versus differentiation. *Wiley Interdisciplinary Reviews: Systems Biology and Medicine* (2010) doi:10.1002/wsbm.86.
4. Morrison, S. J. & Weissman, I. L. The long-term repopulating subset of hematopoietic stem cells is deterministic and isolatable by phenotype. *Immunity* **1**, 661–673 (1994).
5. Akashi, K., Traver, D., Miyamoto, T. & Weissman, I. L. A clonogenic common myeloid progenitor that gives rise to all myeloid lineages. *Nature* **404**, 193–197 (2000).
6. Na Nakorn, T., Traver, D., Weissman, I. L. & Akashi, K. Myeloerythroid-restricted progenitors are sufficient to confer radioprotection and provide the majority of day 8 CFU-S. *J. Clin. Invest.* **109**, 1579–1585 (2002).
7. Kondo, M., Weissman, I. L. & Akashi, K. Identification of clonogenic common lymphoid progenitors in mouse bone marrow. *Cell* **91**, 661–672 (1997).
8. Mercier, F. E. & Scadden, D. T. Not All Created Equal: Lineage Hard-Wiring in the Production of Blood. *Cell* **163**, 1568–1570 (2015).
9. Macaulay, I. C. *et al.* Single-Cell RNA-Sequencing Reveals a Continuous Spectrum of Differentiation in Hematopoietic Cells. *Cell Rep.* **14**, 966–977 (2016).
10. Haas, S., Trumpp, A. & Milsom, M. D. Causes and Consequences of Hematopoietic Stem Cell Heterogeneity. *Cell Stem Cell* **22**, 627–638 (2018).
11. SIMINOVITCH, L., MCCULLOCH, E. A. & TILL, J. E. THE DISTRIBUTION OF COLONY-FORMING CELLS AMONG SPLEEN COLONIES. *J. Cell. Comp. Physiol.* **62**, 327–336 (1963).
12. BECKER, A. J., McCULLOCH, E. A. & TILL, J. E. Cytological demonstration of the clonal nature of spleen colonies derived from transplanted mouse marrow cells. *Nature* **197**, 452–454 (1963).
13. Adolfsson, J. *et al.* Upregulation of Flt3 expression within the bone marrow Lin(-)Sca1(+)c-kit(+) stem cell compartment is accompanied by loss of self-renewal capacity. *Immunity* **15**, 659–669 (2001).
14. Kiel, M. J. *et al.* SLAM family receptors distinguish hematopoietic stem and progenitor cells and reveal endothelial niches for stem cells. *Cell* **121**, 1109–1121 (2005).
15. Goodell, M. A., Brose, K., Paradis, G., Conner, A. S. & Mulligan, R. C. Isolation and

functional properties of murine hematopoietic stem cells that are replicating in vivo. *J. Exp. Med.* **183**, 1797–1806 (1996).

16. Rabe, J. L. *et al.* CD34 and EPCR coordinately enrich functional murine hematopoietic stem cells under normal and inflammatory conditions. *Exp. Hematol.* **81**, 1-15.e6 (2020).

17. Harrison, D. E. Competitive repopulation: a new assay for long-term stem cell functional capacity. *Blood* **55**, 77–81 (1980).

18. Purton, L. E. & Scadden, D. T. Limiting Factors in Murine Hematopoietic Stem Cell Assays. *Cell Stem Cell* **1**, 263–270 (2007).

19. Wilkinson, A. C., Igarashi, K. J. & Nakauchi, H. Haematopoietic stem cell self-renewal in vivo and ex vivo. *Nat. Rev. Genet.* **21**, 541–554 (2020).

20. Osawa, M., Hanada, K., Hamada, H. & Nakauchi, H. Long-term lymphohematopoietic reconstitution by a single CD34-low/negative hematopoietic stem cell. *Science* **273**, 242–245 (1996).

21. Gerrits, A. *et al.* Cellular barcoding tool for clonal analysis in the hematopoietic system. *Blood* (2010) doi:10.1182/blood-2009-06-229757.

22. Lu, R., Neff, N. F., Quake, S. R. & Weissman, I. L. Tracking single hematopoietic stem cells in vivo using high-throughput sequencing in conjunction with viral genetic barcoding. *Nat. Biotechnol.* (2011) doi:10.1038/nbt.1977.

23. Naik, S. H. *et al.* Diverse and heritable lineage imprinting of early haematopoietic progenitors. *Nature* (2013) doi:10.1038/nature12013.

24. Sun, J. *et al.* Clonal dynamics of native haematopoiesis. *Nature* (2014) doi:10.1038/nature13824.

25. Rodriguez-Fraticelli, A. E. *et al.* Clonal analysis of lineage fate in native haematopoiesis. *Nature* (2018) doi:10.1038/nature25168.

26. Busch, K. *et al.* Fundamental properties of unperturbed haematopoiesis from stem cells in vivo. *Nature* (2015) doi:10.1038/nature14242.

27. Ganuza, M. *et al.* The global clonal complexity of the murine blood system declines throughout life and after serial transplantation. *Blood* (2019) doi:10.1182/blood/2018-09-873059.

28. Pei, W. *et al.* Resolving Fates and Single-Cell Transcriptomes of Hematopoietic Stem Cell Clones by PolyloxExpress Barcoding. *Cell Stem Cell* **27**, 383-395.e8 (2020).

29. Bowling, S. *et al.* An Engineered CRISPR-Cas9 Mouse Line for Simultaneous Readout of Lineage Histories and Gene Expression Profiles in Single Cells. *Cell* **181**, 1410-1422.e27 (2020).

30. Konturek-Ciesla, A. & Bryder, D. Stem Cells, Hematopoiesis and Lineage Tracing: Transplantation-Centric Views and Beyond. *Front. cell Dev. Biol.* **10**, 903528 (2022).

31. Morita, Y., Ema, H. & Nakauchi, H. Heterogeneity and hierarchy within the most primitive hematopoietic stem cell compartment. *J. Exp. Med.* **207**, 1173–1182 (2010).

32. Muller-Sieburg, C. E., Cho, R. H., Karlsson, L., Huang, J. F. & Sieburg, H. B. Myeloid-biased hematopoietic stem cells have extensive self-renewal capacity but generate diminished lymphoid progeny with impaired IL-7 responsiveness. *Blood* (2004) doi:10.1182/blood-2003-10-3448.

33. Yamamoto, R. *et al.* Clonal analysis unveils self-renewing lineage-restricted progenitors generated directly from hematopoietic stem cells. *Cell* (2013) doi:10.1016/j.cell.2013.08.007.

34. Dykstra, B. *et al.* Long-Term Propagation of Distinct Hematopoietic Differentiation Programs In Vivo. *Cell Stem Cell* (2007) doi:10.1016/j.stem.2007.05.015.

35. Sanjuan-Pla, A. *et al.* Platelet-biased stem cells reside at the apex of the haematopoietic stem-cell hierarchy. *Nature* **502**, 232–236 (2013).

36. Carrelha, J. *et al.* Hierarchically related lineage-restricted fates of multipotent haematopoietic stem cells. *Nature* (2018) doi:10.1038/nature25455.

37. Velten, L. *et al.* Human haematopoietic stem cell lineage commitment is a continuous process. *Nat. Cell Biol.* **19**, 271–281 (2017).

38. Nestorowa, S. *et al.* A single-cell resolution map of mouse hematopoietic stem and progenitor cell differentiation. *Blood* **128**, e20-31 (2016).

39. Grover, A. *et al.* Single-cell RNA sequencing reveals molecular and functional platelet bias of aged haematopoietic stem cells. *Nat. Commun.* **7**, 11075 (2016).

40. Meng, Y. *et al.* Epigenetic programming defines haematopoietic stem cell fate restriction. *Nat. Cell Biol.* **25**, 812–822 (2023).

41. Vijg, J. & Dong, X. Pathogenic Mechanisms of Somatic Mutation and Genome Mosaicism in Aging. *Cell* **182**, 12–23 (2020).

42. Yizhak, K. *et al.* RNA sequence analysis reveals macroscopic somatic clonal expansion across normal tissues. *Science* **364**, (2019).

43. Genovese, G. *et al.* Clonal Hematopoiesis and Blood-Cancer Risk Inferred from Blood DNA Sequence. *N. Engl. J. Med.* (2014) doi:10.1056/nejmoa1409405.

44. Jaiswal, S. *et al.* Age-related clonal hematopoiesis associated with adverse outcomes. *N. Engl. J. Med.* (2014) doi:10.1056/NEJMoa1408617.

45. Xie, M. *et al.* Age-related mutations associated with clonal hematopoietic expansion and malignancies. *Nat. Med.* (2014) doi:10.1038/nm.3733.

46. DeZern, A. E., Malcovati, L. & Ebert, B. L. CHIP, CCUS, and Other Acronyms: Definition, Implications, and Impact on Practice. *Am. Soc. Clin. Oncol. Educ. book. Am. Soc. Clin. Oncol. Annu. Meet.* **39**, 400–410 (2019).

47. Tahiliani, M. *et al.* Conversion of 5-methylcytosine to 5-hydroxymethylcytosine in mammalian DNA by MLL partner TET1. *Science* **324**, 930–935 (2009).

48. Delhommeau, F. *et al.* Mutation in TET2 in myeloid cancers. *N. Engl. J. Med.* **360**, 2289–2301 (2009).

49. Abdel-Wahab, O. *et al.* Genetic characterization of TET1, TET2, and TET3 alterations in myeloid malignancies. *Blood* **114**, 144–147 (2009).

50. Moran-Crusio, K. *et al.* Tet2 loss leads to increased hematopoietic stem cell self-renewal and myeloid transformation. *Cancer Cell* **20**, 11–24 (2011).

51. Ko, M. *et al.* Ten-Eleven-Translocation 2 (TET2) negatively regulates homeostasis and differentiation of hematopoietic stem cells in mice. *Proc. Natl. Acad. Sci.* **108**, 14566–14571 (2011).

52. Fuster, J. J. *et al.* Clonal hematopoiesis associated with TET2 deficiency accelerates atherosclerosis development in mice. *Science (80-.).* (2017) doi:10.1126/science.aag1381.

53. Jaiswal, S. *et al.* Clonal Hematopoiesis and risk of atherosclerotic cardiovascular disease. *N. Engl. J. Med.* (2017) doi:10.1056/NEJMoa1701719.

54. Abelson, S. *et al.* Prediction of acute myeloid leukaemia risk in healthy individuals. *Nature* **559**, 400–404 (2018).

55. Takahashi, K. *et al.* Preleukaemic clonal haemopoiesis and risk of therapy-related myeloid neoplasms: a case-control study. *Lancet. Oncol.* **18**, 100–111 (2017).

56. Coombs, C. C. *et al.* Therapy-Related Clonal Hematopoiesis in Patients with Non-hematologic Cancers Is Common and Associated with Adverse Clinical Outcomes. *Cell Stem Cell* **21**, 374-382.e4 (2017).

57. Sperling, A. S., Gibson, C. J. & Ebert, B. L. The genetics of myelodysplastic syndrome: from clonal haematopoiesis to secondary leukaemia. *Nat. Rev. Cancer* **17**, 5–19 (2017).

58. Sano, S. *et al.* CRISPR-Mediated Gene Editing to Assess the Roles of Tet2 and Dnmt3a in Clonal Hematopoiesis and Cardiovascular Disease. *Circ. Res.* **123**, 335–341 (2018).

59. Wolach, O. *et al.* Increased neutrophil extracellular trap formation promotes thrombosis in myeloproliferative neoplasms. *Sci. Transl. Med.* **10**, (2018).

60. Jaiswal, S. & Libby, P. Clonal haematopoiesis: connecting ageing and inflammation in cardiovascular disease. *Nature Reviews Cardiology* (2020) doi:10.1038/s41569-019-0247-5.

61. Bolton, K. L. *et al.* Cancer therapy shapes the fitness landscape of clonal hematopoiesis. *Nat. Genet.* **52**, 1219–1226 (2020).

62. Kar, S. P. *et al.* Genome-wide analyses of 200,453 individuals yield new insights into the causes and consequences of clonal hematopoiesis. *Nat. Genet.* **54**, 1155–1166 (2022).

63. Kleppe, M. *et al.* Somatic mutations in leukocytes infiltrating primary breast cancers. *NPJ breast cancer* **1**, 15005 (2015).

64. Nguyen, Y. T. M. *et al.* Tet2 deficiency in immune cells exacerbates tumor progression by increasing angiogenesis in a lung cancer model. *Cancer Sci.* **112**, 4931–4943 (2021).

65. Pan, W. *et al.* The DNA Methylcytosine Dioxygenase Tet2 Sustains Immunosuppressive Function of Tumor-Infiltrating Myeloid Cells to Promote Melanoma Progression. *Immunity* **47**, 284-297.e5 (2017).

66. Feng, Y. *et al.* Dnmt3a Mutations in the Hematopoietic System Promote Colitis-Associated Colon Cancer: A Model of Clonal Hematopoiesis in Solid Tumors. *Blood* **138**, 2161 (2021).

67. Feng, Y. *et al.* Hematopoietic-specific heterozygous loss of Dnmt3a exacerbates colitis-associated colon cancer. *J. Exp. Med.* **220**, (2023).

68. Rumgay, H. *et al.* Global, regional and national burden of primary liver cancer by subtype. *Eur. J. Cancer* **161**, 108–118 (2022).

69. El-Serag, H. B. Epidemiology of viral hepatitis and hepatocellular carcinoma. *Gastroenterology* **142**, 1264-1273.e1 (2012).

70. Shiels, M. S. & O'Brien, T. R. Recent Decline in Hepatocellular Carcinoma Rates in the United States. *Gastroenterology* **158**, 1503-1505.e2 (2020).

71. Russo, F. P. *et al.* Hepatocellular Carcinoma in Chronic Viral Hepatitis: Where Do We Stand? *Int. J. Mol. Sci.* **23**, (2022).

72. Suresh, D., Srinivas, A. N. & Kumar, D. P. Etiology of Hepatocellular Carcinoma: Special Focus on Fatty Liver Disease. *Front. Oncol.* **10**, 601710 (2020).

73. Younossi, Z. M. *et al.* Global epidemiology of nonalcoholic fatty liver disease-Meta-analytic assessment of prevalence, incidence, and outcomes. *Hepatology* **64**, 73–84 (2016).

74. Anstee, Q. M., Reeves, H. L., Kotsiliti, E., Govaere, O. & Heikenwalder, M. From NASH to HCC: current concepts and future challenges. *Nature Reviews Gastroenterology and Hepatology* vol. 16 411–428 (2019).

75. Shao, G. *et al.* The Pathogenesis of HCC Driven by NASH and the Preventive and Therapeutic Effects of Natural Products. *Front. Pharmacol.* **13**, 944088 (2022).

76. Rolo, A. P., Teodoro, J. S. & Palmeira, C. M. Role of oxidative stress in the pathogenesis of nonalcoholic steatohepatitis. *Free Radic. Biol. Med.* **52**, 59–69 (2012).

77. Kordes, C., Bock, H. H., Reichert, D., May, P. & Häussinger, D. Hepatic stellate cells: current state and open questions. **402**, 1021–1032 (2021).

78. Angulo, P. *et al.* Liver Fibrosis, but No Other Histologic Features, Is Associated With Long-term Outcomes of Patients With Nonalcoholic Fatty Liver Disease. *Gastroenterology* **149**, 389–97.e10 (2015).

79. Febbraio, M. A. *et al.* Preclinical Models for Studying NASH-Driven HCC: How Useful

Are They? *Cell Metabolism* (2019) doi:10.1016/j.cmet.2018.10.012.

80. Nakagawa, H. *et al.* ER Stress Cooperates with Hypernutrition to Trigger TNF-Dependent Spontaneous HCC Development. *Cancer Cell* **26**, 331–343 (2014).

81. Schierwagen, R. *et al.* Seven weeks of Western diet in apolipoprotein-E-deficient mice induce metabolic syndrome and non-alcoholic steatohepatitis with liver fibrosis. *Sci. Rep.* **5**, (2015).

82. Machado, M. V. *et al.* Mouse Models of Diet-Induced Nonalcoholic Steatohepatitis Reproduce the Heterogeneity of the Human Disease. *PLoS One* **10**, e0127991 (2015).

83. Wolf, M. J. *et al.* Metabolic activation of intrahepatic CD8+ T cells and NKT cells causes nonalcoholic steatohepatitis and liver cancer via cross-talk with hepatocytes. *Cancer Cell* (2014) doi:10.1016/j.ccell.2014.09.003.

84. Dowman, J. K. *et al.* Development of Hepatocellular Carcinoma in a Murine Model of Nonalcoholic Steatohepatitis Induced by Use of a High-Fat/Fructose Diet and Sedentary Lifestyle. *Am. J. Pathol.* **184**, 1550–1561 (2014).

85. Fujii, M. *et al.* A murine model for non-alcoholic steatohepatitis showing evidence of association between diabetes and hepatocellular carcinoma. *Med. Mol. Morphol.* **46**, 141–152 (2013).

86. Kishida, N. *et al.* Development of a novel mouse model of hepatocellular carcinoma with nonalcoholic steatohepatitis using a high-fat, choline-deficient diet and intraperitoneal injection of diethylnitrosamine. *BMC Gastroenterol.* **16**, (2016).

87. Suriano, F. *et al.* Novel insights into the genetically obese (ob/ob) and diabetic (db/db) mice: two sides of the same coin. *Microbiome* **9**, 147 (2021).

88. Lebeaupin, C. *et al.* Endoplasmic reticulum stress signalling and the pathogenesis of non-alcoholic fatty liver disease. *J. Hepatol.* **69**, 927–947 (2018).

89. Asgharpour, A. *et al.* A diet-induced animal model of non-alcoholic fatty liver disease and hepatocellular cancer. *J. Hepatol.* **65**, 579–588 (2016).

90. Xiong, X. *et al.* Landscape of Intercellular Crosstalk in Healthy and NASH Liver Revealed by Single-Cell Secretome Gene Analysis. *Mol. Cell* **75**, 644-660.e5 (2019).

91. Zang, S. *et al.* Neutrophils Play a Crucial Role in the Early Stage of Nonalcoholic Steatohepatitis via Neutrophil Elastase in Mice. *Cell Biochem. Biophys.* **73**, 479–487 (2015).

92. van der Windt, D. J. *et al.* Neutrophil extracellular traps promote inflammation and development of hepatocellular carcinoma in nonalcoholic steatohepatitis. *Hepatology* **68**, 1347–1360 (2018).

93. Krenkel, O. & Tacke, F. Liver macrophages in tissue homeostasis and disease. *Nat. Rev. Immunol.* **17**, 306–321 (2017).

94. Tran, S. *et al.* Impaired Kupffer Cell Self-Renewal Alters the Liver Response to Lipid

Overload during Non-alcoholic Steatohepatitis. *Immunity* **53**, 627-640.e5 (2020).

95. Deczkowska, A. *et al.* XCR1(+) type 1 conventional dendritic cells drive liver pathology in non-alcoholic steatohepatitis. *Nat. Med.* **27**, 1043–1054 (2021).

96. Semple, J. W., Italiano, J. E. J. & Freedman, J. Platelets and the immune continuum. *Nat. Rev. Immunol.* **11**, 264–274 (2011).

97. Malehmir, M. *et al.* Platelet GPIba is a mediator and potential interventional target for NASH and subsequent liver cancer. in *35. Jahrestagung der Deutschen Arbeitsgemeinschaft zum Studium der Leber* (2019). doi:10.1055/s-0038-1677172.

98. Fujita, K. *et al.* Effectiveness of antiplatelet drugs against experimental non-alcoholic fatty liver disease. *Gut* **57**, 1583–1591 (2008).

99. Bruzzì, S. *et al.* B2-Lymphocyte responses to oxidative stress-derived antigens contribute to the evolution of nonalcoholic fatty liver disease (NAFLD). *Free Radic. Biol. Med.* **124**, 249–259 (2018).

100. Pfister, D. *et al.* NASH limits anti-tumour surveillance in immunotherapy-treated HCC. *Nature* (2021) doi:10.1038/s41586-021-03362-0.

101. Huby, T. & Gautier, E. L. Immune cell-mediated features of non-alcoholic steatohepatitis. *Nat. Rev. Immunol.* **22**, 429–443 (2022).

102. Yamamoto, R. *et al.* Large-Scale Clonal Analysis Resolves Aging of the Mouse Hematopoietic Stem Cell Compartment. *Cell Stem Cell* **22**, 600-607.e4 (2018).

103. Benz, C. *et al.* Hematopoietic stem cell subtypes expand differentially during development and display distinct lymphopoietic programs. *Cell Stem Cell* (2012) doi:10.1016/j.stem.2012.02.007.

104. Ema, H., Morita, Y. & Suda, T. Heterogeneity and hierarchy of hematopoietic stem cells. *Exp. Hematol.* **42**, 74-82.e2 (2014).

105. Rodriguez-Fraticelli, A. E. *et al.* Single-cell lineage tracing unveils a role for TCF15 in haematopoiesis. *Nature* **583**, 585–589 (2020).

106. Scala, S. & Aiuti, A. In vivo dynamics of human hematopoietic stem cells: novel concepts and future directions . *Blood Adv.* **3**, 1916–1924 (2019).

107. Wilson, A. *et al.* Hematopoietic Stem Cells Reversibly Switch from Dormancy to Self-Renewal during Homeostasis and Repair. *Cell* (2008) doi:10.1016/j.cell.2008.10.048.

108. Bogeska, R. *et al.* Inflammatory exposure drives long-lived impairment of hematopoietic stem cell self-renewal activity and accelerated aging. *Cell Stem Cell* **29**, 1273-1284.e8 (2022).

109. Hinge, A. *et al.* Asymmetrically Segregated Mitochondria Provide Cellular Memory of Hematopoietic Stem Cell Replicative History and Drive HSC Attrition. *Cell Stem Cell* **26**, 420-430.e6 (2020).

110. Beerman, I. *et al.* Proliferation-Dependent Alterations of the DNA Methylation Landscape Underlie Hematopoietic Stem Cell Aging. *Cell Stem Cell* **12**, 413–425 (2013).

111. Beerman, I. *et al.* Functionally distinct hematopoietic stem cells modulate hematopoietic lineage potential during aging by a mechanism of clonal expansion. *Proc. Natl. Acad. Sci.* **107**, 5465–5470 (2010).

112. Challen, G. A., Boles, N. C., Chambers, S. M. & Goodell, M. A. Distinct hematopoietic stem cell subtypes are differentially regulated by TGF-beta1. *Cell Stem Cell* **6**, 265–278 (2010).

113. Yu, V. W. C. *et al.* Epigenetic Memory Underlies Cell-Autonomous Heterogeneous Behavior of Hematopoietic Stem Cells. *Cell* **168**, 944–945 (2017).

114. Nguyen, L. *et al.* Functional compensation between hematopoietic stem cell clones in vivo. *EMBO Rep.* **19**, (2018).

115. Brewer, C., Chu, E., Chin, M. & Lu, R. Transplantation Dose Alters the Differentiation Program of Hematopoietic Stem Cells. *Cell Rep.* **15**, 1848–1857 (2016).

116. Fu, S. *et al.* Molecular Biomarkers in Drug-Induced Liver Injury: Challenges and Future Perspectives. *Front. Pharmacol.* **10**, 1667 (2019).

117. Thandra, K. C. *et al.* Epidemiology of non-alcoholic fatty liver disease and risk of hepatocellular carcinoma progression. *Clin. Exp. Hepatol.* **6**, 289–294 (2020).

118. Luci, C., Bourinet, M., Leclère, P. S., Anty, R. & Gual, P. Chronic Inflammation in Non-Alcoholic Steatohepatitis: Molecular Mechanisms and Therapeutic Strategies. *Front. Endocrinol. (Lausanne).* **11**, 597648 (2020).

119. Li, Z. *et al.* Deletion of Tet2 in mice leads to dysregulated hematopoietic stem cells and subsequent development of myeloid malignancies. *Blood* **118**, 4509–4518 (2011).

120. Wen, Y., Lambrecht, J., Ju, C. & Tacke, F. Hepatic macrophages in liver homeostasis and diseases-diversity, plasticity and therapeutic opportunities. *Cell. Mol. Immunol.* **18**, 45–56 (2021).

121. Wang, X. *et al.* TOX promotes the exhaustion of antitumor CD8(+) T cells by preventing PD1 degradation in hepatocellular carcinoma. *J. Hepatol.* **71**, 731–741 (2019).

122. Qiu, L.-W. *et al.* Annexin A2 promotion of hepatocellular carcinoma tumorigenesis via the immune microenvironment. *World J. Gastroenterol.* **26**, 2126–2137 (2020).

123. Haikonen, R., Kärkkäinen, O., Koistinen, V. & Hanhineva, K. Diet- and microbiota-related metabolite, 5-aminovaleric acid betaine (5-AVAB), in health and disease. *Trends Endocrinol. Metab.* **33**, 463–480 (2022).

124. Kakisaka, K. *et al.* Mechanisms of lysophosphatidylcholine-induced hepatocyte lipoapoptosis. *Am. J. Physiol. Gastrointest. Liver Physiol.* **302**, G77-84 (2012).

125. Li, N. & Zhao, H. Role of Carnitine in Non-alcoholic Fatty Liver Disease and Other

Related Diseases: An Update. *Front. Med.* **8**, 689042 (2021).

126. Sookoian, S. *et al.* Nonalcoholic steatohepatitis is associated with a state of betaine-insufficiency. *Liver Int. Off. J. Int. Assoc. Study Liver* **37**, 611–619 (2017).

127. Bick, A. G. *et al.* Genetic Interleukin 6 Signaling Deficiency Attenuates Cardiovascular Risk in Clonal Hematopoiesis. *Circulation* **141**, 124–131 (2020).

128. Kim, M. J. *et al.* Clonal hematopoiesis as a novel risk factor for type 2 diabetes mellitus in patients with hypercholesterolemia. *Front. public Heal.* **11**, 1181879 (2023).

129. Miller, P. G. *et al.* Association of clonal hematopoiesis with chronic obstructive pulmonary disease. *Blood* **139**, 357–368 (2022).

130. Kim, P. G. *et al.* Dnmt3a-mutated clonal hematopoiesis promotes osteoporosis. *J. Exp. Med.* **218**, (2021).

131. Arends, C. M. *et al.* Clonal hematopoiesis in patients with anti-neutrophil cytoplasmic antibody-associated vasculitis. *Haematologica* vol. 105 e264–e267 (2020).

132. Saiki, R. *et al.* Clonal Hematopoiesis Is Associated with Severe COVID-19 Enhancing Inflammatory Responses in Myeloid Cells. *Blood* **142**, 1321 (2023).

133. Bouzid, H. *et al.* Clonal hematopoiesis is associated with protection from Alzheimer's disease. *Nat. Med.* **29**, 1662–1670 (2023).

134. Wong, W. J. *et al.* Clonal haematopoiesis and risk of chronic liver disease. *Nature* **616**, 747–754 (2023).

135. Tian, R. *et al.* Clonal Hematopoiesis and Risk of Incident Lung Cancer. *J. Clin. Oncol. Off. J. Am. Soc. Clin. Oncol.* **41**, 1423–1433 (2023).

136. Kessler, M. D. *et al.* Common and rare variant associations with clonal haematopoiesis phenotypes. *Nature* **612**, 301–309 (2022).

137. Kotsiliti, E. *et al.* Intestinal B cells license metabolic T-cell activation in NASH microbiota/antigen-independently and contribute to fibrosis by IgA-FcR signalling. *J. Hepatol.* **79**, 296–313 (2023).

138. Fang, J., Celton-Morizur, S. & Desdouets, C. NAFLD-Related HCC: Focus on the Latest Relevant Preclinical Models. *Cancers (Basel).* **15**, (2023).

139. Nevola, R. *et al.* Gender Differences in the Pathogenesis and Risk Factors of Hepatocellular Carcinoma. *Biology (Basel).* **12**, (2023).

140. Gallage, S. *et al.* Spontaneous Cholemia in C57BL/6 Mice Predisposes to Liver Cancer in NASH. *Cell. Mol. Gastroenterol. Hepatol.* **13**, 875–878 (2022).

141. Challen, G. A. *et al.* Dnmt3a and Dnmt3b have overlapping and distinct functions in hematopoietic stem cells. *Cell Stem Cell* **15**, 350–364 (2014).

142. Challen, G. A. *et al.* Dnmt3a is essential for hematopoietic stem cell differentiation. *Nat. Genet.* **44**, 23–31 (2011).

143. Ostrander, E. L. *et al.* Divergent Effects of Dnmt3a and Tet2 Mutations on Hematopoietic Progenitor Cell Fitness. *Stem cell reports* **14**, 551–560 (2020).

144. Wang, B. *et al.* Loss of Tet2 affects platelet function but not coagulation in mice. *Blood Sci. (Baltimore, Md.)* **2**, 129–136 (2020).

145. Younossi, Z. M. & Henry, L. Epidemiology of non-alcoholic fatty liver disease and hepatocellular carcinoma. *JHEP reports Innov. Hepatol.* **3**, 100305 (2021).

146. Ueno, M., Takeda, H., Takai, A. & Seno, H. Risk factors and diagnostic biomarkers for nonalcoholic fatty liver disease-associated hepatocellular carcinoma: Current evidence and future perspectives. *World J. Gastroenterol.* **28**, 3410–3421 (2022).

147. Lee, J. S. *et al.* Liver Stiffness-Based Risk Prediction Model for Hepatocellular Carcinoma in Patients with Nonalcoholic Fatty Liver Disease. *Cancers (Basel).* **13**, (2021).

148. Ioannou, G. N., Green, P., Kerr, K. F. & Berry, K. Models estimating risk of hepatocellular carcinoma in patients with alcohol or NAFLD-related cirrhosis for risk stratification. *J. Hepatol.* **71**, 523–533 (2019).

149. Love, M. I., Huber, W. & Anders, S. Moderated estimation of fold change and dispersion for RNA-seq data with DESeq2. *Genome Biol.* **15**, 550 (2014).

List of Figures

Figure 1.1. Models of hematopoiesis. 2
Figure 1.2. Approaches to study HSC functionality 5
Figure 1.3. HSC lineage biases. 7
Figure 1.4. Clonal hematopoiesis of indeterminate potential (CHIP). 8
Figure 1.5. Association between CHIP and the development of hematological malignancies. 10
Figure 1.6. Associations between CHIP and cardiovascular diseases. 11
Figure 1.7. Incidence and mortality rates of highest ranked cancer types. 13
Figure 1.8. Stages of non-alcoholic fatty liver disease. 14
Figure 1.9. Role of hematopoietic cells in the development of NAFLD-induced HCC. 18
Figure 3.1. Experimental design for serial single cell transplantations to interrogate fundamental properties of HSCs. 23
Figure 3.2. Chimerism analysis of single cell transplantations based on their final lineage output. 24
Figure 3.3. Single cell reconstitution outcomes. 26
Figure 3.4. Comparison between classical and new model describing the functional heterogeneity within the HSC pool. 27
Figure 3.5. Paired analysis of transplantation outcomes between parent and daughter HSCs. 29
Figure 3.6. Daughter HSCs acquire faster kinetics compared to the parent, correlating with changes in their lineage bias. 31
Figure 3.7. Daughter HSCs displayed faster reconstitution kinetics and reduced functional potency than their parent HSC. 32
Figure 3.8. Mathematical modelling of single cell transplantation outcomes 34
Figure 3.9. Single HSC functional outcome is determined by the activity of the neighboring HSCs. 36
Figure 3.10. Experimental scheme for single cell transplants using *Rag2*$^{-/-}$ supportive BM and recipients. 36

Figure 3.11. Slow and fast reconstituting kinetics were still present when transplanting single HSCs with lymphoid-deficient supportive bone marrow cells. 37
Figure 3.12. HSC lineage biases are modulated by the presence of *Rag2*$^{-/-}$ HSCs with impaired lymphoid differentiation. 38
Figure 3.13. HSC outcomes with WT or *Rag2*$^{-/-}$ supportive BM environment. 39
Figure 4.1. Reconstitution kinetics correlates with final lineage outputs. 43
Figure 4.2. Discrete or continuum transitions from slow- to fast-reconstituting clones. 44
Figure 4.3. Schematic of the changes in potency with HSC division. 46
Figure 4.4. Cell-extrinsic mechanisms influencing HSC functional outcome. 49
Figure 5.1. Experimental scheme for assessing the impact of *Tet2* CHIP on diet-induced hepatocellular carcinoma. 51
Figure 5.2. Induction of *Tet2* deletion in adult HSCs selects for heterozygosity. 52
Figure 5.3. Development of obesity and hepatomegaly as a result of treating mice with a high caloric Western diet. 54
Figure 5.4. Histopathological analysis of liver sections to assess NAFLD stage. 56
Figure 5.5. Serum levels of liver damage biomarkers. 57
Figure 5.6. *Tet2* CHIP increased the incidence of hepatocellular carcinoma in WD-treated mice. 58
Figure 5.7. Bulk RNA sequencing of liver homogenates. 60
Figure 5.8. Increased expression of fibrosis-related genes in *Tet2* CHIP livers. 61
Figure 5.9. Inflammatory and metabolic pathways were differentially expressed in *Tet2* CHIP compared to their WT counterparts. 63
Figure 5.10. Erythroid differentiation was impacted in *Tet2* CHIP mice. 65
Figure 5.11. Influx of bone marrow-derived immune cells to the liver upon WD. 67
Figure 5.12. Similar immune cell composition in WD livers with or without CHIP. 69
Figure 5.13. scRNA-seq analysis of liver-infiltrating hematopoietic cells revealed gene expression changes in T cells with potential clinical relevance. 71
Figure 5.14. Bulk RNA sequencing of liver-infiltrating hematopoietic cells. 73
Figure 5.15. Differentially regulated hallmark pathways in *Tet2*$^{-/-}$ cells compared to their WT counterparts. 74
Figure 5.16. Preliminary analysis at an earlier timepoint supported no acceleration of the liver disease phenotype in mice with *Tet2* CHIP. 76

Figure 5.17. Synergistic epigenetic reprogramming as a result of combining Tet2 deletion and metabolic-induced modulation of epigenetic enzymes. 77
Figure 5.18. Metabolic reprograming caused by Western diet feeding. 79
Figure 5.19. Metabolic reprograming caused by Tet2 deletion. 80
Figure 5.20. TET2 metabolic cofactors did not significantly change upon WD feeding. 80
Figure 6.1. Graphical abstract showing the synergistic effect between Tet2 CHIP and the Western diet to favor the transition from NASH to HCC. 82
Figure 6.2. Assessing whether *Tet2*$^{-/-}$ VAF is cell-type and organ-specific. 85
Figure 6.3. Heterogeneity in the NAFLD model as evidenced by heterogeneous increase in body weight over time on WD. 87
Figure 7.1. Experimental scheme of single cell transplantations. 94
Figure 7.2. Gating strategies for the analysis and isolation of hematopoietic cells. 111

List of Tables

Table 1.1 Preclinical models of NASH-induced HCC. 16
Table 7.1. HSC expansion medium 97
Table 7.2. ACK lysis buffer recipe 99
Table 7.3. PCR reaction for assessing *Tet2* recombination 101
Table 7.4. *Tet2* genotyping primer sequences. 101
Table 7.5. Touchdown PCR program for *Tet2* recombination genotyping 101
Table 7.6. Antibody panel for the isolation of GFP^{+} $EPCR^{hi}$ LT-HSCs 104
Table 7.7. Antibody panel for the isolation of KuO^{+} $EPCR^{hi}$ LT-HSCs 104
Table 7.8. Antibody panel for stem and progenitor cell staining (1) 105
Table 7.9 Antibody panel for stem and progenitor cell staining (2) 105
Table 7.10. Antibody panel for stem and progenitor cell staining (3) 106
Table 7.11. Antibody panel for committed progenitors staining (1) 106
Table 7.12. Antibody panel for committed progenitors staining (2) 107
Table 7.13. Antibody panel for committed progenitors staining (3) 108
Table 7.14. Antibody panel for mature white blood cells staining (1) 108
Table 7.15. Antibody panel for mature white blood cells staining (2) 109
Table 7.16. Antibody panel for mature erythrocyte and platelet staining 109
Table 7.17. Antibody panel for liver-infiltrating white blood cell staining 109

List of Abbreviations

	Abbreviation	Definition
A	ACK	Ammonium-chloride-potassium
	a-KG	Alpha-ketoglutarate
	ALT	Alanine aminotransferase
	AML	Acute myeloid leukemia
	APC	Allophycocyanin
	APC-Cy7	Allophycocyanin cyanine 7
	AST	Aspartate aminotransferase
B	B6	C57BL/6J mouse line
	bp	Base pair
	BM	Bone marrow
C	CD	Cluster of differentiation
	CD-HFD	Choline-deficient high-fat diet
	CH	Clonal hematopoiesis
	CHIP	Clonal hematopoiesis of indeterminate potential
	CLP	Common lymphoid progenitor
	CMP	Common myeloid progenitor
D	DAPI	4′.6-diamidino-2-phenylindole
	DC	Dendritic cell
	DNMT3A	DNA methyltransferase 3 alpha
E	ECM	Extracellular matrix
	EDTA	Ethyline diamine tetra acetic acid
	EPCR	Endothelial protein C receptor
	EPO	Erythropoietin
F	FACS	Fluorescent-activated cell sorting
	FBS	Fetal bovine serum
	FITC	Fluorescein isothiocyanate
G	GFP	Green fluorescent protein
	GMP	Granulocyte-monocyte progenitor
	GSEA	Gene set enrichment analysis
	GT	Gene therapy
H	HCC	Hepatocellular carcinoma
	HFD	High-fat diet
	hi	high
	HSC	Hematopoietic stem cell
	HSCT	Hematopoietic stem cell transplantation
	HSPC	Hematopoietic stem and progenitor cell
	H&E	Hematoxylin and Eosin

I	IMDM	Iscove´s modified Dulbecco´s medium
	IL	Interleukin
	i.p.	Intraperitoneal
	i.v.	intravenous
J	JAK2	Janus-kinase 2
K	KO	Knock out
	KuO	Kusabira Orange
L	LEMUR	Latent Embedding Multivariate Regression
	Lin	Lineage
	LMPP	Lymphoid-myeloid common progenitors
	LSK	Lineage$^-$ Sca$^+$ cKit$^+$
	LT-HSC	Long-term hematopoietic stem cell
M	MEP	Megakaryocyte-erythroid progenitor
	MDS	Myelodysplastic syndrome
	MPN	Myeloproliferative neoplasm
	MPP	Multipotent progenitor
N	NAFL	Non-alcoholic fatty liver
	NAFLD	Non-alcoholic fatty liver disease
	NAS	NAFLD Assessment Score
	NASH	Non-alcoholic steatohepatitis
	NET	Neutrophil extracellular traps
	ND	Normal diet
P	PB	Peripheral blood
	PBS	Phosphate-buffered saline
	PC	Principal component
	PCA	Principal component analysis
	PCR	Polymerase chain reaction
	PE	Phycoerythrin
	PE-Cy5	Phycoerythrin cyanine 5
	PE-Cy7	Phycoerythrin cyanine 7
	PLT	Platelet
R	RAG2	Recombination activating gene 2 protein
	RBC	Red blood cell
	ROS	Reactive oxygen species
	rpm	Rotations per minute
	RPMI	Roswell Park Memorial Institute
	RT	Room temperature
S	SCF	Stem cell factor
	scRNA-seq	Single cell RNA sequencing
	SPF	Specific pathogen free
	ST-HSC	Short-term hematopoietic stem cell

T	TCA	Citric acid cycle
	TET2	Ten-eleven translocation 2
	$Tet2^{-/-}$	Tet2 knock-out
	TPO	Thrombopoietin
V	VAF	Variant allele fraction
	Vwf	Von Willebrand factor
W	WBC	White blood cells
	WD	Western diet
	WT	Wild type

Conference Talks and Poster Presentations

Conference talks

Impact of clonal hematopoiesis of indeterminate potential (CHIP) on the evolution of hepatocellular carcinoma
Esther Rodríguez Correa. *iBLOOD kick-off meeting*, Heidelberg, 04/2022

Serial single cell transplantations demonstrate a defined hierarchy of HSC subtypes correlating with loss of reconstitution potential
Esther Rodríguez Correa, Natasha Anstee, Tamar Nizharadze, Congxin Li, Melanie Ball, Julia Knoch, Jeyan Jayarajan, Megan Druce, Foteini Fotopoulou, Ian Ghezzi, Marleen Büchler-Schäff, Susanne Lux, Dhyani Shah, Thomas Höfer, Michael Milsom. *International Society for Experimental Hematology (ISEH) annual meeting*, Edinburgh, 09/2022

Clonal hematopoiesis as a mechanistic driver of diet-induced liver cancer
Esther Rodríguez Correa. *FSP-A Retreat*, Schöntal, 04/2023

Poster presentations

Serial single cell transplantations demonstrate a defined hierarchy of HSC subtypes correlating with loss of reconstitution potential
Esther Rodríguez Correa, Natasha Anstee, Tamar Nizharadze, Congxin Li, Melanie Ball, Julia Knoch, Jeyan Jayarajan, Megan Druce, Foteini Fotopoulou, Ian Ghezzi, Marleen Büchler-Schäff, Susanne Lux, Dhyani Shah, Thomas Höfer, Michael Milsom. *International Society for Experimental Hematology (ISEH)*, Edinburgh, 09/2022

Clonal hematopoiesis as a mechanistic driver of diet-induced liver cancer
Esther Rodríguez Correa, Chaofan Fan, Melanie Ball, Dhyani Shah, Lina Merg, Ian Ghezzi, Jeyan Jayarajan, Foteini Fotopoulou, Susanne Lux, Julia knoch, Charles Dussiau, Mengjie Qiu, Maik Brune, Elisa Donato, Theo Aurich, Helene Foissner, Robert Vanner, Andreas Trumpp, Mathias Heikenwälder, Michael Milsom. *DfGA annual meeting*, Jena, 06/2023

Apparent hematopoietic stem cell lineage biases are mediated by cell extrinsic feedback mechanisms
Esther Rodríguez Correa, Florian Grünschläger, Tamar Nizharadze, Natasha Anstee, Melanie Ball, Jeyan Jayarajan, Julia Knoch, Megan Druce, Ian Ghezzi, Foteini Fotopoulou, Marleen Büchler-Schäff, Susanne Lux, Theo Aurich, Daniel Hübschmamnn, Thomas Höfer, Simon Haas, Michael Milsom. *International Society for Experimental Hematology (ISEH) annual meeting*, New York, 08/2023

Apparent hematopoietic stem cell lineage biases are mediated by cell extrinsic feedback mechanisms
Esther Rodríguez Correa, Florian Grünschläger, Tamar Nizharadze, Natasha Anstee, Melanie Ball, Jeyan Jayarajan, Julia Knoch, Megan Druce, Ian Ghezzi, Foteini Fotopoulou, Marleen Büchler-Schäff, Susanne Lux, Theo Aurich, Daniel Hübschmamnn, Thomas Höfer, Simon Haas, Michael Milsom. *Stem cell conference Heidelberg*, 09/2023

Clonal hematopoiesis as a mechanistic driver of diet-induced liver cancer
Esther Rodríguez Correa, Chaofan Fan, Melanie Ball, Dhyani Shah, Lina Merg, Ian Ghezzi, Jeyan Jayarajan, Foteini Fotopoulou, Susanne Lux, Julia knoch, Charles Dussiau, Mengjie Qiu, Maik Brune, Elisa Donato, Theo Aurich, Helene Foissner, Robert Vanner, Andreas Trumpp, Mathias Heikenwälder, Michael Milsom. *PhD poster presentation*, Heidelberg, 11/2023

Manuscripts

Clonal reconstitution kinetics are predictive of hematopoietic stem cell potency and contribute towards apparent lineage biased output.
Esther Rodríguez Correa, *et al*. (manuscript in preparation)

Inflammatory exposure drives long-lived impairment of hematopoietic stem cell self-renewal activity and accelerated aging. *Cell Stem Cell* **29**, 1273-1284.e8 (2022).
Bogeska R, Mikecin AM, Kaschutnig P, Fawaz M, Büchler-Schäff M, Le D, Ganuza M, Vollmer A, Paffenholz SV, Asada N, Rodriguez-Correa E, Frauhammer F, Buettner F, Ball M, Knoch J, Stäble S, Walter D, Petri A, Carreño-Gonzalez MJ, Wagner V, Brors B, Haas S, Lipka DB, Essers MAG, Weru V, Holland-Letz T, Mallm JP, Rippe K, Krämer S, Schlesner M, McKinney Freeman S, Florian MC, King KY, Frenette PS, Rieger MA, Milsom MD.

Contributions

The work in this PhD thesis was supervised by **Dr. Michael Milsom** in the Division of Experimental Hematology at the DKFZ and HI-STEM.

Both projects presented in this thesis involved close collaborations with the groups of **Prof. Dr. Thomas Höfer** (Division of Theoretical Systems Biology, DKFZ) and **Prof. Dr. Mathias Heikenwälder** (Division of Chronic Inflammation and Cancer, DKFZ and Division of Immune signatures of chronic inflammatory human diseases driving cancer, The M3 Research Center)

Melanie Ball (Experimental Hematology, DKFZ) and **Julia Knoch** (Experimental Hematology, DKFZ) provided technical support for mouse experiments, such as mouse breeding, mouse treatments, mouse sample collection and downstream processing.

Experimental support during mouse endpoints and mouse model validation in project II was provided by **Lina Merg** (Master student, Experimental Hematology, DKFZ), **Dhyani Shah** (Master student, Experimental Hematology, DKFZ) and **Sophia Okeke** (MD student, Experimental Hematology, DKFZ).

Technical help during endpoint analysis of mouse cohorts was provided by former and current members of the Experimental Hematology division (**Fenia Fotopoulou, Ian Ghezzi, Sena Alptekin, Lena Bognar, Dr. Jeyan Jayarajan, Dr. Megan Druce, Dr. Susanne Lux, Dr. Marleen Büchler-Schäff, Theo Aurich, Dr. Matea Mikecin**).

Dr. Natasha Anstee (Division of Experimental Hematology, DKFZ) initiated the single cell transplantation project, performing 53 out of 278 primary single cell transplantations. She also wrote both TVAs for the experimental work carried out in my thesis.

Mathematical modeling in project I was performed by **Tamar Nizharadze** (Division of Theoretical Systems Biology, DKFZ)

Chaofan Fan (Division of Chronic Inflammation and Cancer, DKFZ) carried out liver histopathological analyses, as well as processed the mouse livers for the isolation of liver-infiltrating hematopoietic cells in all endpoints performed in project II.

Analysis of mouse serum in project II was done by **Dr. Maik Brune** at Zentrallabor (Uniklinikum Heidelberg)

scRNA-seq analysis in project II was performed by **Dr. Charles Dussiau** (Division of Experimental Hematology, DKFZ). Libraries were prepared together with **Dr. Susanne Lux**.

Libraries for bulk RNA-seq of liver-infiltrating hematopoietic cells were prepared with help from **Dr. Elisa Donato** (Prof. Andreas Trumpp lab, Division, DKFZ)

Metabolomics analysis was, in part, done at the Max Planck Institute of Immunology and Epigenetics by **Jasmin Rettkowski** and **Julian Mess** (Prof. Dr Nina Cabezas-Wallscheid lab) and the mass spectrometry facility.

Flow Cytometry Core facility at the DKFZ provided technical assistance for flow cytometry analysis.

All animal care takers from the **DKFZ Animal Facility** provided support with daily monitoring of experimental mice and body irradiation.

DKFZ NGS Facility generated libraries for RNA-seq of liver homogenates and provided technical recommendations.

This thesis was proof-read in parts by **Dr. Michael Milsom**, **Dr. Natasha Anstee** and **Fenia Fotopoulou**.

Acknowledgments

The work in this dissertation would not have been possible without the valuable inputs from many people.

First, I would like to thank my direct supervisor **Dr. Mick Milsom**, for giving me the opportunity to work on such amazing projects. I am extremely thankful for your mentorship over the past five years as both master´s and PhD student. You are a role model for me as a scientist, I always try to learn from you the way of driving scientific questions and running a lab. I attribute much of the development and achievements I have experienced during this journey to you, and I will always be grateful for that. I hope to keep your mentorship and friendship in the future.

Thanks to my thesis advisory committee, **Prof. Dr. Thomas Höfer**, **Prof. Dr. David Kent** and **Dr. Caroline Pabst** for your valuable feedback during the TAC meetings. I would also like to thank **Prof. Dr. Lazaro Centanin** and **Prof. Dr. med. Irmela Jeremias**, for taking time to be part of my defense committee.

Thanks to **Prof. Dr. Andreas Trumpp**, for being the inspiring driving force behind such great working place, HI-STEM.

A very special thanks goes to my dear friend **Melanie Ball**. I am immensely glad to have known you and to have you as a friend. I admire your work ethic and multitasking skills. You are that person that could be Scilveting, calculating and aliquoting at the same time, while listening to funny German podcasts. Thanks for supporting me with all my experiments, and for making them easier and more enjoyable.

Another thanks goes to **Julia Knoch**, especially for your support during the big single cell transplantation experiments. Thank you for sharing the responsibility and pressure with me, for staying until very late at the barrier making sure everything will succeed. I wish you had stayed longer in the lab, but I am very grateful for the chance to work with you.

A very special thanks to my office mate and friend, **Fenia Fotopoulou**. I am so grateful you decided to join the lab at our selection round and I could share this whole journey with you. Thank you for your friendship and for the fun days in and out the office. I believe you were a turning point in the lab for me and the force that brought together this amazing constellation of friends. It makes me so happy to know that besides moving to the other side of the planet, I would have you so close by.

Another special thanks to my friend **Ian Ghezzi**. Already in the selection round I felt you would be a big plus for our group, and I am so happy you chose us. Thank you for your support in the lab and for bringing so much joy and fun moments to the group. No pressure, but I am quite hopeful you decide to move across the Atlantic ;)

I would also like to thank **Lina Merg** and **Sena Alptekin**, for joining the CHIP project with that enthusiasm and for supporting me. I am immensely grateful to work with you and happy that this project is and will be taken care by such talented scientists. I am so happy to have you as friends. I would have loved to have had you in the lab from the beginning of my PhD to share more time with you.

Thanks to little **Dhyani Shah**, for your great work during your master´s thesis. I had such a great time with you during experiments and out of the lab.

I want to thank **Theo Aurich**, for being my friend, for your scientific enthusiasm and for making this lab even better.
Another thanks to my other office mate **Dr. Charles Dussiau**, for your support with the bioinformatic analysis. I am very happy I got the opportunity to work with you.

I am also incredibly grateful for the support and great time in the lab I had with **Lena**, **Tash**, **Jeyan**, **Megan**, **Marleen**, **Susi**, **Matea**, **Ruzhi**, **Robin**, **Helene**, **Viktoria**, **Sophia**. Thank you all for your help during the past years. Thanks to **Dr. Elisa Donato** for helping out with library preparation and being always patient with all of us. Another thanks to **Dagmar Wolf** and **Erika Krückel** for your assistance with lots of difficult burocratic things.

A huge thanks to **Chaofan Fan**, for closely collaborating with me on the liver CHIP project. I really appreciate your hard work and how easy it was always working with you. Another thanks to **Tamar Nizharadze** for your collaborative spirit and supporting the single cell transplantation project.

A big thanks to my partner in crime **Lars**. I am immensely happy I got to share professional passion and personal journey with you. Thank you for supporting me, for listening to my presentations so many times despite having nothing to do with your projects, you are so ready for a hematology postdoc if you wish. I am very much looking forward to all exciting things we are about to experience this year, and to our future.

Gracias a mis padres **Inma** e **Julio** y mi hermano **Javier** por apoyarme en todas mis decisiones. Me siento muy agradecida de teneros como familia. Esta tesis y este esfuerzo de 4 años está dedicado a vosotros, por oportunidades ilimitadas, el apoyo y el cariño que se necesitan para tener éxito. Aunque esté un poco lejos, yo siempre os siento muy cerca.